

BomDetec – Wide Area Surveillance and Suicide Bomber Detection at >10M

Phase I Preliminary Design Review (PDR) Report

in response to:

Prototypes and Technology for Improvised Explosives Device Detection (PTIEDD)
Broad Agency Announcement 05-05 (BAA 05-03)

for the:

Homeland Security Advanced Research Projects Agency of
Department of Homeland Security

submitted by:

**The Bernard M. Gordon Center for Subsurface Sensing and Imaging Systems
(Gordon-CenSSIS)**
A National Science Foundation Engineering Research Center, at

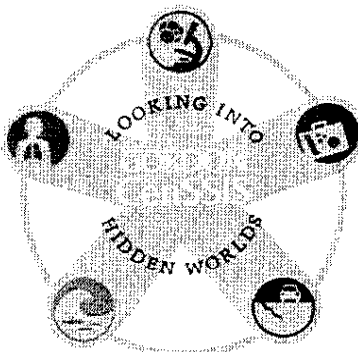
Northeastern University (lead)

with:

Academic Partner
Rensselaer Polytechnic Institute

and:

Industrial Partners
**American Science & Engineering,
Personal Protection Technologies,
Raytheon Company, and
Siemens Corporate R&D**



Stearns Center, Suite 302
360 Huntington Avenue
Boston, MA 02115-5000

This page intentionally left blank.



Table of Contents

1	PROGRAM OVERVIEW	1
1.1	SUMMARY OF PHASE I ACCOMPLISHMENTS	2
1.2	PROPOSED PHASE II CONFIGURATION	3
1.3	PHASE I CONCLUSIONS	3
2	CONCEPT OF OPERATIONS	4
2.1	SCOPE	4
2.2	VIDEO	4
2.3	BASIC OPERATING SCENARIOS	4
2.4	SENSOR PLACEMENT	6
2.5	INTELLIGENT VIDEO (ONLY) USER INTERACTION	7
2.6	OPERATOR WORKFLOW AND PROCESSING RATE CONSIDERATIONS	8
2.6.1	Phase 1	8
2.6.2	Phase 2	8
2.6.3	Phase 3	8
2.7	FURTHER DESCRIPTION OF OPERATOR TASKS	10
2.8	OTHER EXPECTED SENSOR CONFIGURATIONS FOR PHASE I	11
2.8.1	Radar	11
2.8.2	X-ray	11
2.8.3	Terahertz	12
2.9	VALIDATION TEST FOR PHASE II	12
3	SENSOR REVIEWS	13
3.1	RADAR SENSOR	13
3.1.1	Introduction	13
3.1.2	Computer Modeling	14
3.1.3	Testing Equipment	28
3.1.4	Test Procedure	32
3.1.5	Radar Detection Methods	35
3.1.6	Experimental Results	38
3.1.7	Recommendations	47
3.1.8	Conclusions	49
3.1.9	Bibliography	50
3.2	TERAHERTZ SENSOR	54
3.2.1	Summary	54
3.2.2	Theory of operation	55
3.2.3	Capability and purpose	56
3.2.4	Activity highlights in Phase I	56
3.2.5	Building THz spectrum library	56
3.2.6	Summary of phase I accomplishment of Terahertz sensor	66
3.3	BACKSCATTER X-RAY SENSOR	67
3.3.1	Executive Summary	67
3.3.2	What are Backscatter x-rays	67
3.3.3	Backscatter x-ray Imaging	70
3.3.4	How an x-ray Beam becomes an Image	71
3.3.5	Long Distance Viewing (LDV) Hoop – LDV x-ray Hoop Description	78
3.3.6	Theory of Operation	78

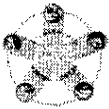


3.3.7	Sensor Statement of Work	81
3.3.8	Sensor Hardware Interface	92
3.3.9	Sensor Software Interface.....	93
3.3.10	Conclusions.....	97
4	HARDWARE INTEGRATION.....	98
4.1	EXECUTIVE SUMMARY	98
4.2	PURPOSE OF PROGRAM	99
4.3	AS&E PROJECT SCOPE.....	99
4.3.1	Hardware Integration Design.....	99
4.3.2	Systems Integration Design	100
4.4	SENSOR HARDWARE SYNOPSIS.....	101
4.4.1	Hardware Integration	101
4.4.2	SENSOR – Intelligent Video.....	102
4.4.3	SENSOR – Long Distance Radar	102
4.4.4	SENSOR – Backscatter Imaging.....	103
4.4.5	SENSOR – Terahertz Spectroscopy.....	103
4.5	SENSOR HARDWARE PLATFORM INTEGRATION	104
4.5.1	Host Vehicle Centralized Sensor Platform	104
4.5.2	ZBV - Exterior Layout.....	105
4.5.3	ZBV - Interior Space and Components Layout	105
4.5.4	ZBV - Proposed Sensor Equipment Locations.....	106
4.5.5	ZBV - Proposed Sensor Pattern Coverage	106
4.5.6	ZBV - Weight Budget.....	106
4.5.7	ZBV - Power Budget.....	107
4.5.8	ZBV - Power Distribution Block Diagram	107
4.5.9	ZBV – Physical / Environmental Characteristics	108
4.5.10	ZBV – Container Vibration Analysis.....	109
4.5.11	ZBV – Proposed Operator’s Console.....	110
4.5.12	Hardware Objects Power / Thermal Conditions	111
4.5.13	Component Safety Labeling Published Health and Safety Compliances	111
4.6	HARDWARE INTEGRATION SUMMARY.....	112
4.6.1	Evaluation.....	112
4.6.2	Results.....	112
4.7	SENSOR SYSTEMS INTEGRATION	112
4.7.1	Systems Design includes the following:.....	112
4.7.2	Systems Integration.....	113
4.7.3	System Analysis Problem Definition	113
4.7.4	System Level Validation Plan.....	121
5	DATA INTEGRATION, SYSTEM CONTROL AND DATA PRESENTATION ..	122
5.1	INTRODUCTION.....	122
5.2	GOALS	122
5.3	APPROACH	123
5.4	CHALLENGES AND ROADBLOCKS.....	124
5.4.1	How to construct a multi-modality, multi-sensor system	124
5.4.2	Providing automated wide-area surveillance	124
5.4.3	Determining a platform to meet the system requirement	124
5.4.4	Managing resources.....	125
5.4.5	Evaluating the many algorithms and models	125
5.4.6	Achieving real-time, robust, high-accuracy performance.....	125



5.5	SYSTEM DESIGN RESULTS	125
5.5.1	Reference Model	125
5.5.2	Sensor Communication Model	126
5.5.3	Communication Through Network.....	126
5.5.4	Data Format.....	127
5.5.5	Data Fusion	127
5.5.6	Database Schema & Sequence Diagrams.....	128
5.6	RESOURCE MANAGEMENT CONCEPT DEVELOPMENT	128
5.6.1	Active Sensing and the Importance of Resource Management.....	128
5.6.2	Resource Management Process.....	129
5.7	DEFINING TESTS OF SYSTEM FEASIBILITY	130
5.7.1	Software System (including SiteIQ Platform) Simulation	130
5.7.2	Algorithm Testing	131
5.8	TEST RESULTS	132
5.8.1	SiteIQ was verified to provide a highly flexible configuration	132
5.8.2	Simulations Results for Real-Time Solution, especially regarding Sensor Scheduling	133
5.8.3	Simulation Results: Convergence of Threat Levels	133
5.8.4	Pedestrian Detection Results: ROC Curve	134
5.8.5	Pedestrian through-put Results based on Operator Workflow Analysis	136
5.8.6	CONOPS Demo/Simulation Results	137
5.8.7	Tracking results - Overview.....	137
5.8.8	Tracking Analysis – close range.....	138
5.8.9	Tracking Analysis – Long range.....	139
5.8.10	The Need for Multiple-View Localization.....	140
5.8.11	3D Localization Testing.....	140
5.8.12	Distance (Depth) Measurement - Results.....	142
5.8.13	Is the Distance (Depth) Measurement Accurate Enough?.....	142
5.9	CONCLUSIONS	143
5.9.1	High-level Intelligent Video Conclusions.....	144
5.9.2	Multi-modality Conclusions.....	144
5.9.3	Conclusions on SiteIQ as Integration Platform	144
5.9.4	Pedestrian through-put based on Operator Workflow Analysis	144
5.9.5	Resource Management Conclusions	145
5.9.6	Pedestrian Detection Conclusions	145
5.9.7	Tracking at mid/long range (>30m).....	145
5.9.8	Need for multi-focal length cameras.....	145
5.9.9	3D Localization Conclusions	146
5.9.10	Achieving real-time, robust, high-accuracy performance	146
5.10	ANNEXES	146
5.10.1	ANNEX A - Data and Command Definitions	146
5.10.2	ANNEX B - Database Schema and Sequence Diagram.....	150
5.10.3	ANNEX C – Resource Management: A Dynamic Multi-Modality Sensor Control and Data Fusion Framework for Target Classification	155
6	BOMDETEC PHASE I CONCLUSION.....	162

This page intentionally left blank.



1 Program Overview

Body-worn explosive devices are a growing and important threat to both civilians and the military. Being small, these improvised explosive devices (IEDs) are hidden under the clothing of suicide bombers. Since they are often built out of non-standard parts, these explosives are hard to detect, especially at a safe distance. It is important to develop a sensor suite that can detect whether a person is wearing such an explosive device at a distance sufficient to prevent entrance into populated or strategically important areas.

The premise for the BomDetec program is that if one can detect metal and/or explosive chemicals at stand off distances of ~50M, one can associate this with a potential suicide bomber in time to mitigate the threat. At the outset of the program it was recognized, that there is no single sensor that can identify metal and chemical explosives at distances sufficient for reliable mitigation. In other words, there is “no silver bullet.” At the beginning of the program (Phase I), a suite of sensors, in principle capable of detecting metal and/or chemical explosives, was selected. During Phase I the performance of each sensor was evaluated to determine its state of the art performance. These performance results will be presented below.

Concurrently in Phase I the BomDetec program created a concept for an integrated hardware and software platform to control the suite of sensors and to acquire, interpret and display the data from the sensors. This display data was optimized so that an operator could easily identify potential suicide bombers. Additionally, the BomDetec software platform was designed to be flexible so other sensors could be easily incorporated. The hardware and software elements of the system will be presented in their respective sections of this Phase I report.

Summary of the proposed BomDetec system

As the BomDetec system was proposed and awarded, four technologies were to be synthesized into a surveillance vehicle/van system for suicide bomber detection. (At this point the vehicle used in the design is the Z Backscatter Van, known as **ZBV**, currently produced by AS&E). Possible “bombers” would be identified and continuously tracked starting at a distances of ~ 50M. The system was proposed to be organized by an intelligent video and data handling system, which would identify and track every person in (and entering) the surveillance zone. It would provide a ground-based coordinate system and motion-compensated tracking coordinates for the other sensors. The video system would also alert and provide tracking coordinates for any of the detection sensors when a person comes in range. An operator would be able to intervene and direct a Pan Tilt Zoom (PTZ) camera for zoomed images and to focus sensors for surveillance of a specific person. The tracking system would then associate the sensor data to that person throughout the surveillance zone. In addition to intelligent video, three additional sensors would be incorporated into the proposed initial design to identify metal, conformation and explosives in the surveillance zone. Millimeter Wave Radar (MMWRadar) would survey the area and provide a signature to identify people wearing threatening metallic objects such as hidden pipe bombs at distances up to ~ 50M. At a closer distance (~10M) x-ray backscatter would be capable of imaging both metal conformation and the presence of explosive materials (proper density). At still closer distances (~3M), Terahertz (THz) radiation would sense and spectroscopically identify explosives on a person. The radar would continue to improve its information as the person approaches, as would the x-ray. At some point the data would exceed a threshold, and the system would identify the person as a “Potential Bomber”. Each modality has a role, and each provides specific information. Together they would provide a reliable stand-off, real time suicide bomber identification system. As documented in this report it will be seen that much of the above Concept of Operations (ConOps) remains the same, but the measured effectiveness of the initial MMW/Radar sensor has changed our approach for defining the signatures of the most distant metallic targets. A detailed discussion of the BomDetec ConOps is provided below.



Technical Approach

The program is composed of three phases. This document is the Report for the Phase I Preliminary Design Review (PDR). For Phase I (6 months), we chose a suite of four initial sensors: intelligent video, backscatter x-ray, Millimeter Wave Radar (MMWRadar), and Terahertz Wave (THz). Each sensor was evaluated independently. The initial design for sensor data integration and fusion was conducted and a sequence of system operations developed. This resulted in the system configuration and design discussed in this report.

The next phase, Phase II (12 months), will improve the performance of the initial sensors in the system configuration and operation. Other sensors may be added to augment the capabilities of the initial suite. The sensor hardware and associated software (control, analysis and GUI) will be integrated into a bread board unit. The breadboard will be tested in laboratory and field conditions, and the results evaluated, to improve the system operation and performance. Phase II will end in a CDR.

Phase III (6 months) will build and deliver a prototype BomDetec Van. The sensors chosen in Phase II will be integrated into AS&E's ZBV. The GUI, control, and data handling systems will be upgraded, improving performance and ease-of-use. The BomDetec Van will pass through a cycle of "test, evaluate and improve". The prototype van performance will be characterized. The Program Goal is to deliver a BomDetec Van that will (with low false alarm rate) reliably identify all potential Suicide Bombers at distances >10M.

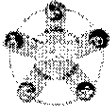
1.1 Summary of Phase I Accomplishments

Concepts for flexible hardware and software platforms for the detection of suicide bombers were developed. The hardware platform (American Science & Engineering ZBV) was re-engineered to hold multiple sensors considering their space, power, thermal, and mechanical requirements. Similarly, the integrative software platform (Siemens Corporate Research) was designed and engineered considering the control, acquisition, interpretation and presentation of the BomDetec sensor data. Both the hardware and software elements of the system were conceptually designed and engineered to accommodate additional and/or different sensors. Full details for the hardware and software elements of the system concept are provided below.

Each sensor in the set of proposed sensors was evaluated. The video cameras were obtained and were evaluated in conjunction with the software platform. The cameras met or exceeded our understanding of their performance and the performance proposed in the BomDetec Phase I proposal. As documented below the MMWave Radar experiments did not clearly differentiate between people, people with an empty suicide vest and people with a suicide vest complete with simulated pipe bombs. The results of our MMWave Radar experiments and the literature have caused us to re-think how Radar in a revised form could contribute to the BomDetec program. The x-ray backscatter experiments and simulation can identify metal and provide conformational information about the metal on suicide bombers at distances of ~10M. The Terahertz sensor was shown to detect and identify chemical explosives at distances of ~3M. Terahertz continues to show promise of chemical explosives at greater distance.

In their respective sections each Phase I sensor is described along with its testing protocol and performance. The hardware and software platforms are also detailed.

The system design concepts are ready to be implemented in Phase II of the program.



1.2 Proposed Phase II Configuration

One of the deliverables for this Phase I report is the proposed sensor configuration for the BomDetec Phase II breadboard. The following table outlines each sensor's function and Phase II role in the breadboard.

Sensor	Function	Phase II Role
Intelligent Video	tracking	tracking
Radar	metal	continue research
X-ray	metal	metal/shape
Terahertz	chemical	chemical identification
Spectroscopic FLIR (possible new sensor)	chemical	test chemical identification

Initial testing of a Spectroscopic FLIR (8 μ m – 12 μ m) indicates promising potential for the detection of chemical explosives in trace quantities. New promising sensors such as the FLIR and the flexibility of the hardware and software platforms, will allow BomDetec to propose the best compliment of sensors to detect suicide bombers, as the program moves forward.

1.3 Phase I Conclusions

BomDetec Phase I has resulted in a design for a flexible multi-sensor system for suicide bomber detection. The system was built around an initial suite of sensors, but sensors can be easily added and removed from this suite. The hardware platform, software platform and the suite of sensors are ready to be made into a breadboard as the deliverable of BomDetec, Phase II.

This page intentionally left blank.



2 Concept of Operations (Siemens, (b) (6))

2.1 Scope

This document proposes an operating scenario for HSARPA BomDetec Phase-I given the then (late 2006) current understanding of the expected configuration and capabilities of the sensors.

Note: Sensor information described in this document is based on the then (late 2006) current understanding of the sensors as presented by the participating groups. Also note that Phase II sensors may be different and may not have the same limitations as in Phase I.

2.2 Video

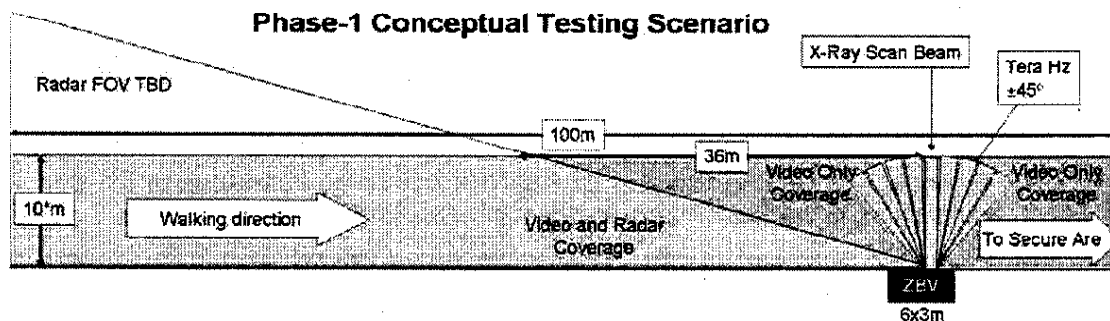
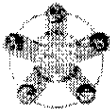
The video system consists of a selection of fixed lens cameras and PTZ cameras. A fixed lens camera provides a continuous and uninterrupted video stream observing everything within its field of view, however fixed lens cameras suffer from a tradeoff between resolution and coverage. PTZ cameras are capable of switching their attention from one part of the scene to another, thus providing high resolution images at a very wide field of view - however not simultaneously. In addition, a PTZ camera requires time to change its viewing direction, zoom focus and therefore its video stream could be interrupted.

The video system will detect new persons arriving at the scene, track them and send the track information to the data fusion module which is responsible to collect all information, assist the operator and other sensor systems by providing them with direction, timing and possibly speed and approximate range information about objects of interest.

2.3 Basic Operating Scenarios

Figure 2-1(a) shows the proposed basic operating scenario. In this scenario the ZBV is placed on the side of a walkway, presumably leading to a protected area. People who walk along this path must walk past the side of the ZBV allowing the x-ray sensor a short time-window in which it can scan them. The Radar is pointed directly at the approach to the secure area to obtain metal information as soon as possible. Since the Terahertz sensor must be close to the scanned object, the time-window from the x-ray scanning and the Terahertz scanning is very small. We therefore suggest that for Phase-I the Terahertz sensor will be allowed to probe persons (that have been detected with metal or otherwise marked by the operator) either slightly before the x-ray, together with the x-ray or after the x-ray. It is assumed that the x-ray and the Terahertz do not interfere with each other. Figure 2-1(b) shows the proposed video set up. One camera (camera-1) is dedicated to the radar. This camera is a fixed lens camera co-located with the radar and covers the same or slightly larger field of view as the radar's. By being co-located we ensure that every object that is visible to the camera is also visible to the radar without occlusion. To ensure maintenance of continuous radar data on each person, the radar will be constantly sequenced over the radar field of view (FOV). In this way a person will be tracked from the moment he enters the FOV until he leaves it. This allows data to be collected over a period of time and from different aspect angles.

Three additional cameras are fixed lens cameras, each with a field of view of 60 degrees or slightly more, pointed 60 degrees apart. These cameras will provide moderate resolution video over a 180-degree field of view. These cameras will provide the input for the main video tracking component.



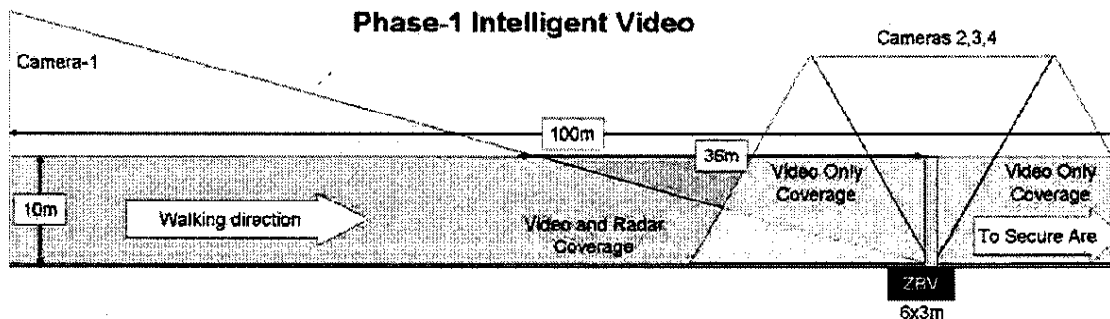
Notes:

1. Radar field of view is TBD and is mechanically steered.
2. X-Ray backscatter is firmly attached to the ZEV. In order to get the best picture people must walk perpendicular to the beam. Video can provide the required speed estimation to the X-Ray backscatter. This is a hard constraint of the current system.
3. Radar has an average window of up to TBD meters to select which persons should be scanned by the X-Ray.
4. Video will cover the area from 100m ahead to 50m beyond the van.
5. Tera-Hz probing will be done together or shortly before or after the X-Ray scan. Tera-Hz is capable of mechanical steering.
6. Except for the PTZ cameras, and perhaps the Thz, there are no mechanically steerable components.

*10m at most for phase-1

Dimensions are to scale

(a)



Notes:

1. Camera: 1 is co-located and dedicated to the radar. Its field of view overlaps or slightly exceeds the radar's field of view. This camera detects new people and tracks every person at the Radar's FOV and continuously and repeatedly schedules radar beams to probe each person in the Radar's view, thus collecting multiple measurements (possibly from different angles) or each person. In addition, The operator can click at a person to schedule Radar probing of the specific person. Since the camera and the radar are co-located, direction, and occlusion will precisely match.
2. Cameras: 2-4 are located at the roof and cover a complete 180° field of view
3. Two to four Ptz camera will be located at the corners of the Van

Dimensions are to scale

(b)

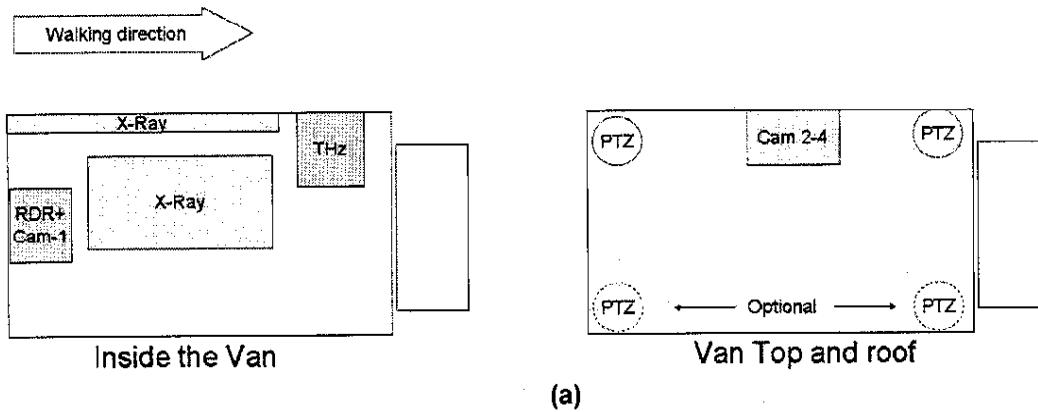
Figure 2-1. Basic operating scenario: (a) Radar, x-ray, and Terahertz sensor configuration, (b) Intelligent video configuration



2.4 Sensor Placement

Figure 2-2 shows the proposed sensor placement for Phase I. The x-ray is already placed in the ZBV and cannot be moved (at least in Phase I). The radar which is approximately shoebox-sized, and the radar's camera (which is firmly attached to it and calibrated) will be placed at the back of the ZBV pointing backwards, viewing the road via a window transparent for visible and millimeter electromagnetic radiation. Alternatively, the Radar could be mounted outside the ZBV (at the back or on the roof). This option affects the ability to transport the ZBV by air, and therefore will be cleared during Phase I. The Terahertz is placed near to the x-ray at waist level viewing the same direction as the x-ray (closest proximity to the ZBV, assuming there could be enough place for it inside the ZBV). The three 60-degree cameras will be placed as high as possible, on the top of the ZBV in a special compartment, finally the PTZ camera will be placed inside the ZBV, below the fixed lens cameras to prevent locking their view.

Sensor placement



Sensor placement

Notes:

1. X-Ray stays in its current location
2. Radar and Cam-1 view the incoming traffic through a window at the back of the Van.
3. Thz is placed at waist level.
4. Cams 2-4 are placed at the top of the van to have as clear view as possible.
5. PTZ's are placed below Cam-2-4 (either in the van or at the roof top) not to occlude the view of cameras 2-4.

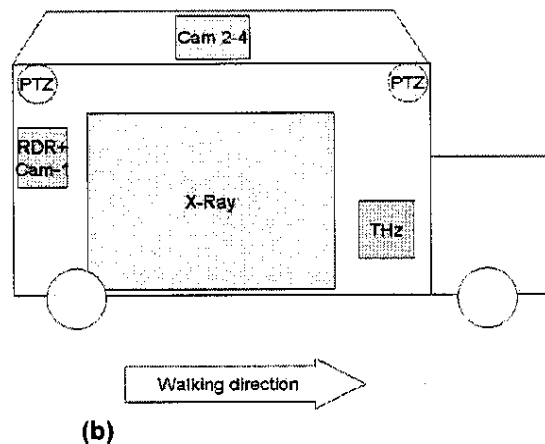
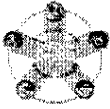


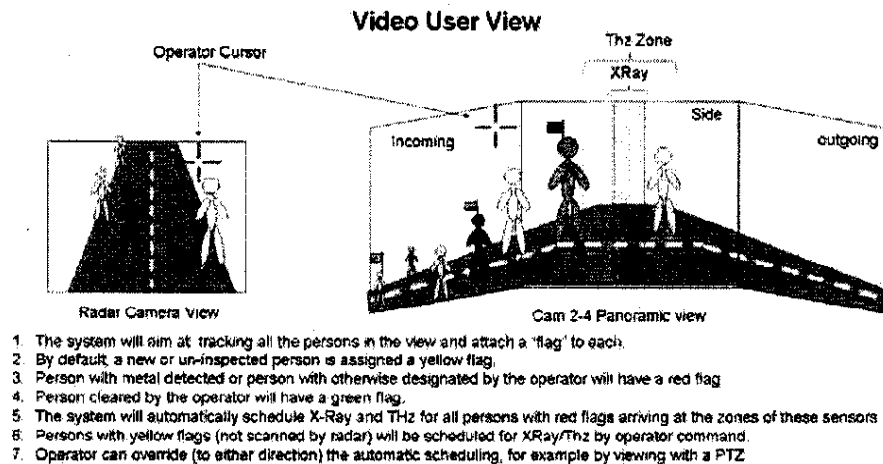
Figure 2-2. Sensor placement within the ZBV: (a) Top view (b) side view



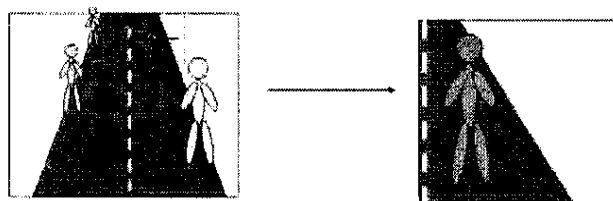
2.5 Intelligent video (only) User Interaction

Ideally, the system could work autonomously by first using video to detect and track people and to hand-off to the radar to detect metal presence. The system will track the persons that carry metal and direct the x-ray and Terahertz sensors to scan these persons when they come into range. This is how we plan the system to work - however, we believe it is essential to have a person-in-the loop to monitor the system at each stage, e.g., to change classification and to schedule radar, x-ray and Terahertz scanning. Figure 2-3 shows a skeleton of user interface for the intelligent video (only). Using the Camera Radar-View, the operator will be able to view all persons within the field of view of the radar. A cursor will allow the operator to point to a particular person and either (i) query information regarding this person that is already inside the system, (ii) schedule/cancel radar beams for this particular person. Finally the operator will be able to enter information to be associated with the person.

The Panoramic view will stitch together the views of cameras 2-4 into a single panoramic view. This view will also clearly mark the field of view of the x-ray and the Terahertz sensors. The operator will be able to query information and enter information - same as in the radar view, and to schedule/cancel x-ray and Terahertz scanning of a particular person. The operator will also be able to point at each person, either on the radar-view or on the panoramic view, and direct a PTZ camera to get a closer look and to track the person.



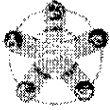
(a)
PTZ usage



- PTZ are operator initiated (only) and have two functions in the system:
1. Get a larger view of a person at the classification stage
 2. Track persons with Red flag, possibly also when they leave the view of cameras 2-4

(b)

Figure 2-3. User Intelligent video view: (a) Fixed lens camera view (b) PTZ usage diagram



2.6 Operator Workflow and Processing Rate Considerations

To place the role of the operator into context, it is necessary to consider the tasks required and the workload encountered by a single operator for the simplest scenario – one pedestrian walking at a constant 2 m/sec. The workload can be broken down into three phases and the operator's actions can be classified as falling into one of three categories: Perception, Analysis or Decision and is shown in Figure 2-4.

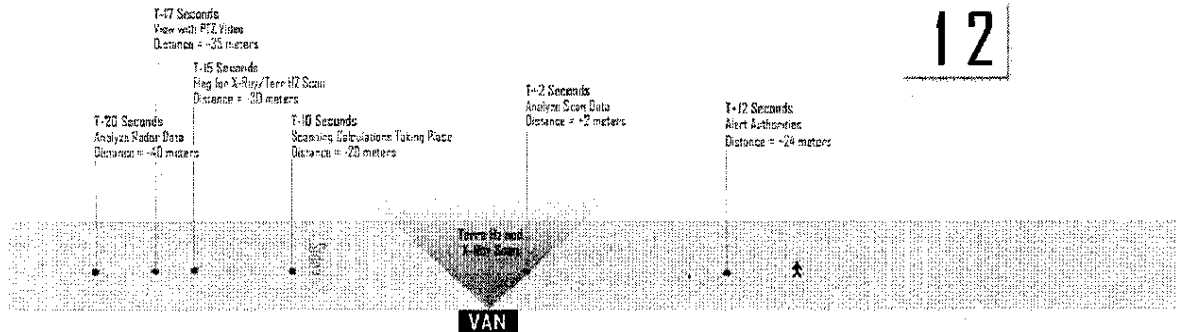


Figure 2-4

2.6.1 Phase 1

Perception. Using the technical information specified earlier in this document, Fixed Video may begin automatic tracking of the pedestrian and presenting live video to the operator approximately 48 m from the point perpendicular with the van (D-48). The operator is then able to make an initial assessment of the pedestrian's behavior and appearance.

Analysis. Two seconds later (D-44) the pedestrian is automatically scanned by radar and that information presented to the operator two seconds after that (D-40). The operator must now review the radar data in order to determine whether the pedestrian is a threat.

Decision. The operator decides that the pedestrian remains a potential threat and takes the overt action to identify and select the pedestrian's image in the PTZ video (D-35).

Perception and Analysis. The operator now views a close-up image of the pedestrian generated by the PTZ video and compares it to the bomber profile (D-30).

Decision. The operator decides that the pedestrian remains a threat and "flags" him/her as suspicious for scanning by x-ray/Terahertz (D-20).

2.6.2 Phase 2

System completes calculations required before x-ray/Terahertz scan (D-20 through D-0)

System scans pedestrian using x-ray and Terahertz. (D-0)

2.6.3 Phase 3

Perception. x-ray and Terahertz scanning data is integrated and presented to the operator (D+2).

Analysis. The operator compares integrated scanning data to bomber profile (D+4).

Decision. The operator decides that the pedestrian is a threat and generates an alert (D+24).



Operators, therefore, have multiple tasks and a substantial workload that must be accomplished under time pressure. The overall task is similar to that of TSA personnel in US airports with the notable exception that airport "pedestrians" are stationary and will wait until screening is complete. An overview of the task organization is shown in Figure 2-5.

Time	Distance to Van	System Action	Operator Action
		Modes: Scan Present Fusion	Modes: Perception Analysis Decision
T-24 sec	D-48 meters	Fixed Video tracks new Pedestrian	Observes behavior, appearance
T-22 sec	D-44 meters	Pedestrian scanned by Radar	
T-20 sec	D-40 meters	Radar derived threat info presented	Operator analyzes radar info If not a threat, Operator can switch to next pedestrian
T-17 sec	D-35 meters	PTZ Video acquires Pedestrian and presents close-up view to Operator	Operator decides to zoom in with PTZ Video Operator identifies & selects Pedestrian in fixed video feed If not a threat, Operator can switch to next pedestrian
T-15 sec	D-30 meters		Compares close-up image of Pedestrian and with bomber profile "Flags" Pedestrian as suspicious for scanning by X-Ray / THZ
T-10 sec	D-20 meters	Prepares for X-Ray / THz scan using motion data from Video	During this time window Operator can switch to Phase 1 Or Phase 3, or view close-up of PTZ Video
T-0 sec	D-0 meters	X-Ray / THz scan	
T+01 sec	D+02 meters	All data integrated & threat visualization presented	
T+02 sec	D+04 meters		Operator compares Fused information to Bomber profile
T+12 sec	D+24 meters		Operator decides Pedestrian is a threat and generates alert

Figure 2-5

Single Operator Scenario

To ensure that a single operator has the time to complete each task in each phase, the minimum distance between pedestrians must be approximately 36 seconds or 72 meters. This is based on the simplest scenario described above. To determine how effective a single operator will be over time, however, requires a more thorough understanding of how vigilance decreases over time. Assuming a perfectly vigilant operator, the maximum number of pedestrians that can be screened by a single operator in one hour is approximately 100. As the space between pedestrians decreases, the level of automation and/or the number of operators must increase to keep pace.

Two Operator Scenario

Theoretically, a minimum distance between pedestrians ranging between 14 and 36 seconds (28-72 meters) can be handled by two operators. Operator 1 would be responsible for all tasks in Phase 1, while Operator 2 would be responsible for all Phase 3 tasks (since Phase 2 tasks are entirely automated). Keeping a minimum distance of 14 seconds between pedestrians and assuming perfectly vigilant operators, the maximum number of pedestrians that can be screened in one hour is approximately 250.



Multi-Operator Scenario

As the distance between pedestrians decrease to less than 14 seconds (28 meters) it becomes no longer possible for a single Phase 1 operator to effectively screen each person. Therefore, a workflow in which there are multiple Phase 1 and Phase 2 operators working in parallel must be explored. It is expected that some further level of automation of the tasks in Phase 1 and Phase 3 might also be accomplished to alleviate the increase operator workload in this scenario. Given the number of variables in this case, we are not able to suggest the maximum number of pedestrians that might be screened in one hour without experimental evidence demonstrating how best to divide operator workflow and further discussion of automation.

2.7 Further Description of Operator Tasks

The operator will observe the wide-angle video, map and animation:

- Seeing pedestrians come and go, while knowing the system is filtering with sensors
- Occasionally initializing tracking of pedestrians missed by the video tracking system
- Overriding system control of the sensor to have the suspect measured, if the operator spots a suspicious behavior.

In case the system identifies a suspect, the operator can:

- Observe PTZ video and other sensor data pertaining to the suspect
- Have more sensor action on the suspect as needed
- Make a decision (mitigate or dismiss).

The effect of our system is that the operator:

- Is not overwhelmed
- Stays alert to constant motion on the screen.

During Automated Operation, the BomDetec system automatically detects and tracks the pedestrians using video tracking through the wide-angle camera as they enter the scene. The system performs automatic and dynamic sensor allocation on the tracked objects.

- Occasionally the operator may identify a suspicious behavior and override sensor control
- PTZ video camera will be assigned to this object to provide a dedicated video stream for the operator.

System performs data analysis and fusion of sensor data and dismisses most of pedestrians as normal

- Operator will not look at the sensor data

If system decides a pedestrian exceeds threat threshold

- Organized sensor data will be presented to the operator in a dedicated display
- PTZ video camera will be assigned to this object to provide a dedicated video stream for the operator

An early concept of the operator's view of the overall environment is illustrated in Figure 2-6.

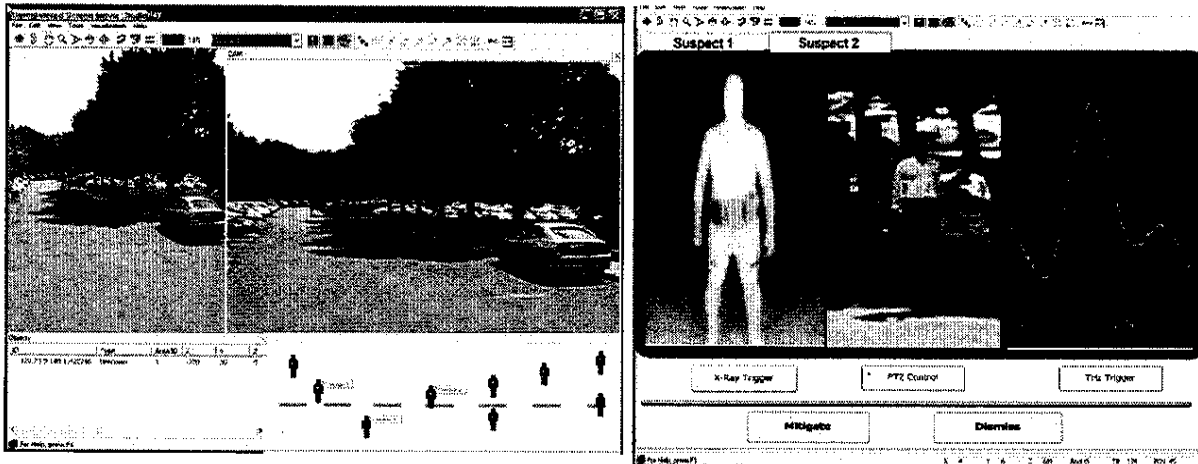


Figure 2-6. An early concept of the operator's view

If no pedestrian exceeds the threshold, the system will choose either randomly or in a defined method the sensor data to display

2.8 Other Expected Sensor Configurations for Phase I

2.8.1 Radar

The Raytheon radar tested as a *prototype* radar for Phase I is a FMCW radar working in the automotive approved millimeter-band (76-77GHz). This radar did not distinguish threats from safe targets, as described in the radar sensor section 3.1.

The radar to be used in Phase II must be redesigned from scratch, incorporating at a minimum a much larger aperture, simultaneous dual polarization measurement capability, and in-phase and quadrature signal detection to provide both amplitude and phase information. The anticipated radar wide-aperture antenna will move mechanically. The exact details of the mechanical steering will be defined during as part of the continuing radar design development work on Phase I. The range resolution is expected to be less than 10 cm. A switching network will also have to be designed to allow the radar to transmit approximately 40 beams each second, receiving sequentially across each receiving antenna element. Assuming 20 transmitting antenna, this corresponds to scanning the field of view of a human torso approximately twice per second. The anticipated radar beamwidth will be 0.06 degree with a illuminated spot width of 0.05 meter at a range of 50 meters, and hence will focus on variations skin surface geometry.

2.8.2 X-ray

The *prototype* x-ray sensor is firmly attached to the side wall of the ZBV and can only create a *clear* image of an object passes close to the sensor (about 10 meters). The object trajectory should be perpendicular to the scanning beam. This limits the deployment of the x-ray sensor to scenarios where people walk past the side of the ZBV. The x-ray is capable of scanning people walking at a normal speed; however the scan cannot image people that are occluded by other people. We must therefore assume that the crowd density is relatively low (it is unlikely that people will walk single file, unless forced to do so).



2.8.3 Terahertz

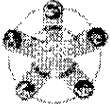
The Terahertz sensor will be attached to the sidewall of ZBV and send out a Terahertz beam to the target to obtain spectroscopic information of explosive materials. The target distance will be in a range of 10m. Time delay of probe pulses will be adjusted to compensate the time of flight of returning THz pulses from the target. The direction of the Terahertz beam will be steered by mechanical scanner. Two axial scanners allows to steer the beam both horizontal and vertical directions. The mechanical scanner is a combination of a rotational stage and a mirror. The Terahertz beam can be sent within an angle range of ± 45 degrees. This angle range allows Terahertz sensor to track a target at 7m away from the side of the street on which ZBV is parked to walk along the street for 14 m. Since typical human walking speed is 1m/s, this tracking range gives a time window of more than 10 seconds if crowd density is not too high. In Phase I, a single axis scanner (horizontal axis) will be tested for the proof-of-concept.

2.9 Validation Test for Phase II

(b) (4)



This page intentionally left blank.



3 Sensor Reviews

3.1 Radar Sensor (NEU, Carey Rappaport)

3.1.1 Introduction

The aim of this project on radar is to examine the feasibility of using millimeter-wave (MMW) radar to detect body-borne IEDs at distances up to 50 meters both through simulation and experimentation. MMW frequencies are especially useful for this in that the beamwidth of a radar signal varies proportionally with the wavelength of an antenna's transmitted signal. Thus, MMW radar offers a much smaller beam width than lower frequency radars. The simulation program used to model scattered near-fields was a modified MATLAB program for both transverse magnetic (TM) and transverse electric (TE) cases in a two-dimensional computational geometry. The radar made available for testing, provided by Raytheon, operates at 77GHz. At a wavelength of 3.89mm, this radar provides, at a testing distance of 10.1 meters, an adequate approximation of a human-torso-sized beam width at 50 meters. Tests were performed at this distance using stationary objects and human subjects with and without body-borne IED simulates.

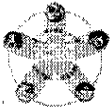
The testing hypothesis is that, inasmuch as body-borne IEDs are constructed of an array of vertically-oriented, cylindrical, metal pipes, a radar system that directs electromagnetic waves of the same polarization as the orientation of the pipes should detect a higher scattered return of waves from an individual wearing an IED than an individual not wearing an IED.

3.1.1.1 Weapons Detection Technology and Research

Suicide bombers carry two distinct materials with them: explosives and shrapnel-producing materials that are typically conductive. There is no existing long-range standoff detection system for these materials. X-ray technologies exist that can see both metal and explosive materials under clothing. But these x-ray machines are only feasible for short-range applications. Of course metal detectors and other similar portal devices exist, but these are also useless for long-range detection, which, given the nature of suicide bombings, is necessary. Some experiments have been done examining passive MMW Radar at frequencies of 26 to 40 GHz, where a variety of handguns were actively illuminated in search of strong reflections at signature frequencies, though little is said of the waveform used and ranges of only 5 m were achieved. There is no shortage of other weapons detection detectors based upon passive radiation resonance signatures. However, such technologies have not been applied to that of a pipe-bomb constructed, body-borne IED and have only been tested at extremely close ranges [7], [8], [9].

The majority of promising research seems to be in the area of imaging, where active radar is scanned across targets and the collected returns converted into a two-dimensional image of the target. In this manner, one can see a variety of objects. Depending upon the frequency used, one may even observe explosive materials such as TNT or other plastic explosives. One such system proposed by Kuznetsov is the microwave system for secret standoff inspection of people (MS-SRIP). Operating in the 2 – 8 GHz range and stepped at 125 MHz, this system can achieve 1 cm resolution at ranges up to 10m. The MS-SRIP system uses electrical length characteristics to determine dielectric constants of explosives. MS-SRIP appears in the presented figures only to have been tested at close ranges, but the actual target range was not reported. The proposed application was for the system to be concealed in a hallway, which would make it similar to a portal system like a metal detector [10].

Other detection schemes have been based on MMW imaging using mechanical scanning, electronic scanning, or a plane array of MMW sensors. Tests were performed with one such passive microwave camera array operating at 94 GHz over a distance of 12 m from the target with unsatisfying results in the



overall image [11]. Results from different MMW imaging experiments have been more promising. An experiment by Pacific Northwest Laboratory (PNL) employed active MMW radar operating from 93 to 99 GHz. The system mechanically scanned every 1.5mm over a 1 m square aperture, recording at 1024 frequency points for every measurement in much the same way as the testing radar described in Chapter 3. The results were impressive as handguns were easily visible on mannequins and under clothing, but the practicality of such a system is questionable given the amount of time it takes to scan so rigorously. Additionally, the target was a mere 0.5 m away from the radar. PNL continued their imaging work using a mechanically-scanned 128 antenna array operating at 35GHz at 0.38 m from the target to detect concealed handguns. The processing components of this system utilize SAR image-reconstruction algorithms to generate 3-D images. PNL has also explored imaging at 100-112 GHz and, at very close ranges, at 350 GHz [12], [13].

Imaging results at 1.56 THz and 350GHz are presented in Dickinson's paper with a mechanically-scanned full beam. A proposed spot scan THz beam was also proposed in the same paper. The system was able to produce a rather grainy image of a concealed metal tie-wrap gun and a close-up of a 0.45 caliber handgun, but the distance to either target was not specified and imaging times were 1-2 minutes per frame. Also, the terahertz spot beam they proposed expands to a focusing diameter of 60 cm at standoff distances of 30 m, which is not much of an improvement from current testing conditions and not optimum for scanning a body at large distances [14].

Perhaps the most impressive MMW radar imaging system was that developed by Smiths Detection in Cork, Ireland. This MMW radar imager/detector for stand-off detection was tested at 20m with the anticipation of achieving ranges up to 50m. The system employs a line-scan method made possible by two rotating mirrors in order to image an entire area. The device has been tested using both a 77 GHz FMCW radar and a 94 GHz Gunn oscillator. Exact resolutions remain unreported though the authors did say the field of view was approximately 4 m square at a range of 20 m. Specifications of the radar itself or its beam width characteristics are also not reported. However, if all results hold true, this is the only other successful research in the area of long-range detection of suicide bombers [15].

3.1.2 Computer Modeling

3.1.2.1 Finite-Difference Frequency-Domain (FDFD)

For complex target geometries, where electromagnetic scattering cannot be predicted easily using analytical methods, predictions as to a target's scattering behaviors must be made numerically via computer simulation. There are several methods by which this can be accomplished, specifically finite-difference time-domain (FDTD), finite element analysis, moment methods, or finite-difference frequency-domain (FDFD). FDFD is one of the simpler and more efficient methods of simulation but has significant computer memory requirements due to the large matrix divisions it must perform. Unlike FDTD, every point in the computational space is calculated simultaneously. Like FDTD, FDFD utilizes the finite difference forms of Faraday's and Ampere's laws to solve for electric field [33], [34]. References [35] thru [48] describe further the implementation of FDFD analysis for various applications.

FDFD was used in this research in that an FDFD simulation had already been developed for the same application, albeit at a lower frequency and more elementary geometry, which we will see later.

3.1.2.1.1 FDFD Formulation for TM Waves

Initial modeling was done using the transverse magnetic (TM) formulation, where all electric field is oriented normal to the cross-section of interest, so that there is no H_z component. In this formulation, we may take Faraday's and Ampere's laws as:



$$(j\omega\epsilon + \sigma)E_z = \frac{\partial H_y}{\partial x} - \frac{\partial H_x}{\partial y} \quad (3.1-1)$$

$$j\omega\mu H_x = -\frac{\partial E_z}{\partial y} \quad (3.1-2)$$

$$j\omega\mu H_y = \frac{\partial E_z}{\partial x} \quad (3.1-3)$$

if $x = i\Delta x$ and $y = j\Delta y$, making $E_z(x,y) = E_z(i,j) = E_{ij}$, then equations 3.1-1 thru 3.1-3, after substitution, reduce to:

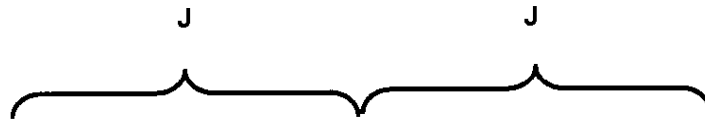
$$E_{i+1j} + E_{ij+1} + [(k^2 - j\omega\mu\sigma)\Delta^2 - 4]E_{ij} + E_{i-1j} + E_{ij-1} = 0 \quad (3.1-4)$$

Using equation 3.1-4, we may calculate the scattered electric field (E_z) at every point in the geometry by discretizing it so that its width (W) and height (H) may be described as $W = I\Delta$ and $H = J\Delta$, where I and J are the number of grid points in the x and y dimensions respectively. Clearly, the geometry may be discretized with whatever resolution is required. Generally, it is regarded as sound practice to discretize the geometry so that Δ or "h," is, at largest, one tenth of the wavelength. One may express the equation for the electric field as a matrix of equations in accordance with equation 3.1-4 as:

$$\bar{A} \cdot \bar{x} = \bar{b} \quad (3.1-5)$$

where the matrix A consists of the diagonal elements and sample i^{th} row shown in equation 3.1-6 consistent with equation 3.1-4.

Diagonal Elements: $A_{ii} = (k_{ii}^2 - j\omega\mu\sigma_{ii})\Delta^2 - 4$ (3.1-6)



$$\bar{A}_i = \begin{bmatrix} 0 & \dots & 0 & 1 & 0 & \dots & 0 & 1 & (k_{ii}^2 - j\omega\mu\sigma_{ii})\Delta^2 - 4 & 1 & 0 & \dots & 0 & 1 & 0 & \dots & 0 \end{bmatrix}$$

and

$$\bar{x} = \begin{bmatrix} E_{11} \\ E_{12} \\ \vdots \\ E_{1j} \\ E_{21} \\ E_{22} \\ \vdots \\ E_{ij} \end{bmatrix} \quad \bar{b} = \begin{bmatrix} E_{11}^{inc} \\ E_{12}^{inc} \\ \vdots \\ E_{1j}^{inc} \\ E_{21}^{inc} \\ E_{22}^{inc} \\ \vdots \\ E_{ij}^{inc} \end{bmatrix} \quad (3.1-7)$$



where E_{ij}^{inc} is the incident field of a plane wave at any point (i,j). Thus, when equation 3.1-5 is solved for the vector x , as it is described in equation 3.1-7, the scattered field can be found at any point in the geometry. When summed with the incident field, this results in the total electric field at every point. The transverse electric (TE), where the magnetic field is oriented normally to the 2-D geometry, formulation may be similarly derived, though with more complication, and is described elsewhere [35].

3.1.2.1.2 Absorbing Boundary Conditions

Without absorbing boundary conditions (ABCs), like those of Mur and Lindman computed near-fields would be inaccurate due to computed reflections off the edge of the geometry [49], [50]. In FDFD, the computational space must be made to look, to the fields, like it goes on infinitely in all directions. In other words, the near-field should look like a sampled window of the fields in free-space instead of a box, where the fields can bounce around.

This research employs the Berenger Perfectly Matched Layer (PML), which was first presented as a two-dimensional space method [51] and later expanded to three-dimensions. The Berenger PML works by splitting each of the three electric field and magnetic field vectors into two components. In the two-dimensional TM formulation, this reduces to splitting only one of the field vectors – E_z – into two components. Doing this, equation 3.1-1 is expanded to equations 3.1-8 and 3.1-9.

$$(j\omega\epsilon + \sigma_x)E_{zx} = \frac{\partial H_y}{\partial x} \quad (3.1-8)$$

$$(j\omega\epsilon + \sigma_y)E_{zy} = -\frac{\partial H_x}{\partial y} \quad (3.1-9)$$

where:

$$E_z = E_{zx} + E_{zy} \quad (3.1-10)$$

Doing this allows one to isolate conductivity in the different propagation directions of any given wave as you can see from equations 3.1-8 and 3.1-9. These conductivities are specified in such a way as to create an environment where there should be no theoretical reflections. But in the finite difference method, which discretizes the space, reflections necessarily occur. To mitigate this, conductivity is increased as depth in the PML increases. In the FDFD program that was used for simulations presented in this chapter, the PML conductivity is as shown in Figure 3-1 [52].

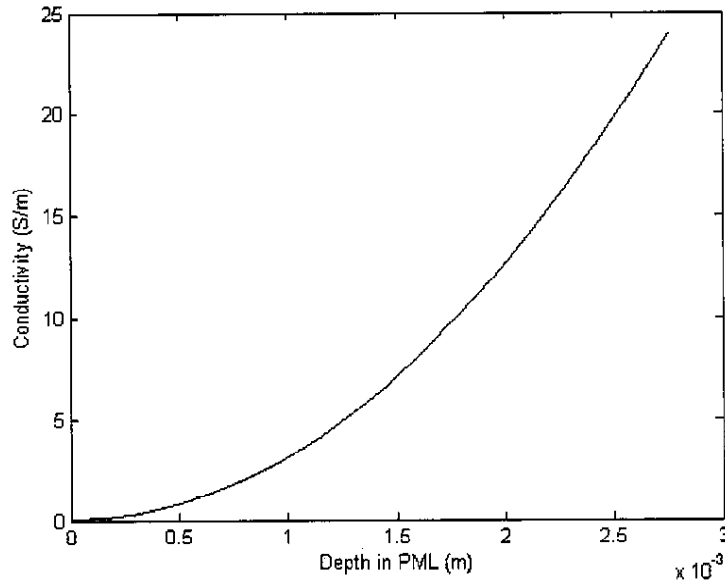
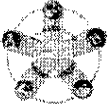


Figure 3-1. Conductivity in the Perfectly Matched Layer (PML)

References [53] thru [58] describe further the implementation of the PML in various applications.

3.1.2.1.3 Far-Field Conversion

In radar applications, the near-field is of little significance. To make these near-field calculations of the total electric field useful to radar applications, one must convert them to their far-field equivalents so that the radiation properties of the scattered field may be examined at multiple observation angles. In order to convert the calculated near-field pattern to the far-field, it becomes necessary to implement the Balanis' induction equivalent theorem, which equates magnetic and electric current densities to the normal components of the magnetic and electric fields according to equations 3.1-11 and 3.1-12 [59].

$$J_i = -\hat{n} \times H_i \quad (3.1-11)$$

$$M_i = \hat{n} \times E_i \quad (3.1-12)$$

This is done on all sides of interest of the geometric space, except each side is treated as an aperture in order to cancel out the electric or magnetic current densities outside the space. Therefore, the magnetic current density – if we are examining the TM case – or the electric current density – if we are examining the TE case – is really twice the quantity shown on the right side of equations 3.1-11 and 3.1-12. These current densities are then fed into equations that ultimately result in calculating the **F** and **A** potentials, where, as demonstrated by Balanis:

$$N = \iint_S 2J_s e^{j\beta r' \cos \psi} ds' \quad (3.1-13)$$

$$L = \iint_S 2M_s e^{j\beta r' \cos \psi} ds' \quad (3.1-14)$$

and



$$A = \frac{\mu e^{-j\beta r}}{4\pi r} N \quad (3.1-15)$$

$$F = \frac{\epsilon e^{-j\beta r}}{4\pi r} L \quad (3.1-16)$$

Now, the electric far-fields, in the TM case, or the magnetic far-fields, in the TE case, are easily calculated from their respective vector potentials using equations 3.1-17 thru 3.1-22 [59].

$$E_r = 0 \quad (3.1-17)$$

$$E_\theta = -\frac{j\beta e^{-j\beta r}}{4\pi r} L_\phi \quad (3.1-18)$$

$$E_\phi = +\frac{j\beta e^{-j\beta r}}{4\pi r} L_\theta \quad (3.1-19)$$

$$H_r = 0 \quad (3.1-20)$$

$$H_\theta = +\frac{j\beta e^{-j\beta r}}{4\pi r} N_\phi \quad (3.1-21)$$

$$H_\phi = -\frac{j\beta e^{-j\beta r}}{4\pi r} N_\theta \quad (3.1-22)$$

Equations 3.1-8 and 3.1-9 are affected somewhat by the fact that, despite the name, the absorbing layer is not perfectly matched and some reflection does occur. However, simulations with larger geometries showed that the field reflected from the PML decayed rapidly so that, at seven grid points into the geometry, the field was 0.16% of its value at the boundary. Thus, the field used for far-field calculations was located seven grid points in to the geometry on each of the four sides.

3.1.2.2 Previous Computer Models

Previous work has been done in the area of two-dimensional modeling of plane waves incident upon body-borne IEDs by Angell. Angell utilized the FDFD modeling method for TM waves incident upon a perfectly flat substrate of skin with and without six uniformly spaced metal cylinders, cross-sectioned as circles, at a frequency of 25 GHz for 0° incidence. Angell reports that, although six cylinders covered by a surface of nails increases the overall return at the location of the radar – the same as the angle of incidence – the return actually decreases when only the six pipes, without nails, are added to the skin substrate. This same FDFD program was modified to allow for the higher frequency of the equipment used in tests that will later be reported in section 3.1.6. The near-field plot at 0° incidence of the skin substrate with pipes, as well as a comparison of the far-field patterns for results with and without pipes, are shown in Figures 3-2 and 3-3 [60], [61].

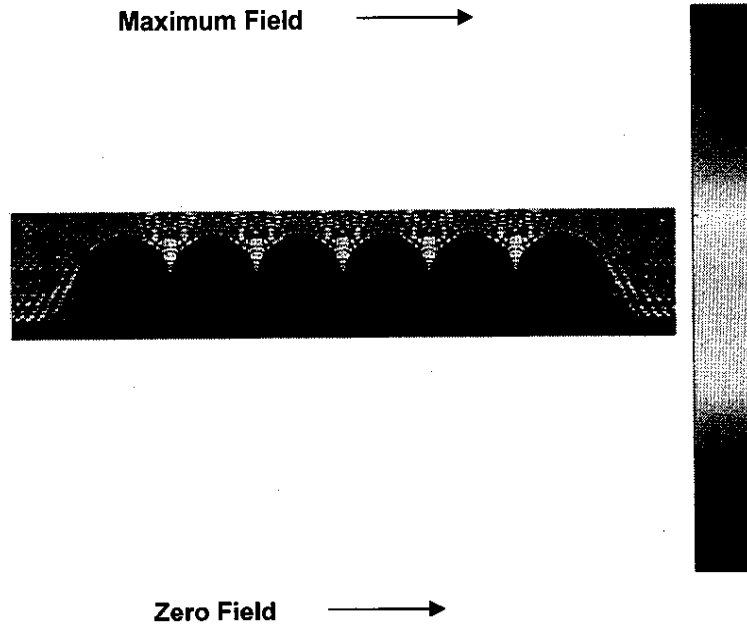


Figure 3-2. Computed Magnitude of Total Electric Field ($|E_T|$) at 77 GHz

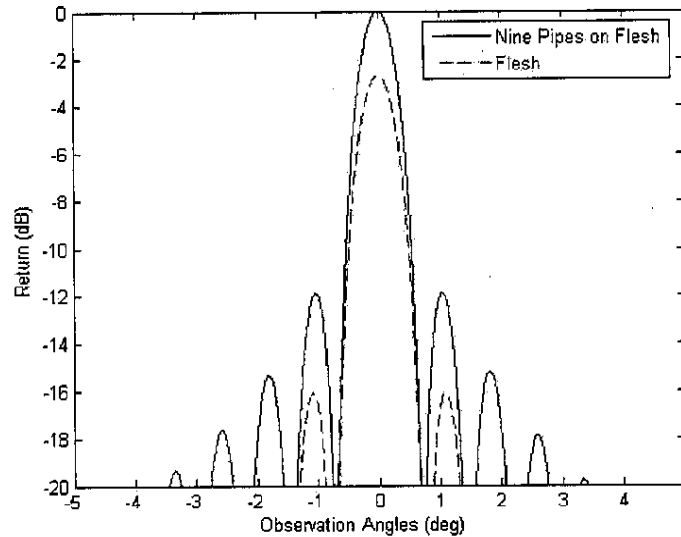
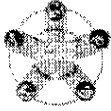


Figure 3-3. Computed Far Field Pattern with and without Pipes

The MATLAB function used for all calculations was originally authored by Ann W. Morgenthaler and Carey M. Rappaport, modified by Amanda Angell to later include TE formulation, and modified further for this project to remove zero-field points [60].

3.1.2.3 Modification of Existing Model

One of the major problems with the previous computational geometry is that it does not reflect the reality of the situation, which is that the human body is anything but a perfectly flat substrate. Therefore, the model was modified even further to reflect a realistic human geometry. This was accomplished using



cross-section photographs of the human body similar to the one shown in Figure 3-4 from the National Library of Medicine's Visible Human Project, which is of a 39 year-old male who died of lethal injection. The figure is important because it takes into account the natural curvature of the human body and adds the arms, from which we also expect reflection.



Figure 3-4. Photograph of Human Chest/Stomach Cross-Section

It takes some processing to convert Figure 3-4 to a geometry that can be used for modeling. Consider the equation for skin depth in meters for a lossy medium [59]:

$$\delta = \frac{1}{\omega \sqrt{\mu \epsilon} \left\{ \frac{1}{2} \left[\sqrt{1 + (\sigma / \omega \epsilon)^2} - 1 \right] \right\}^{1/2}} \quad (3.1-23)$$

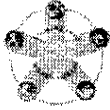
Using 11.9 for the relative permittivity and 55.6 S/m for the conductivity – constitutive parameters for human muscle tissue at 77GHz, extrapolated from previous experiments – this gives a skin depth of 0.37mm. Since the depth of penetration into human skin at 77GHz is infinitesimal the figure is not divided into, for instance, fatty or muscle tissue. Instead, the figure is divided simply into skin and air. The problem with this is that it gives a tremendous amount of computation space depending on the number of points per wavelength used. At 77 GHz, if we sample at 30 points per wavelength in air, the size of our A matrix – see equation 3.1-5 – will be over 4 million elements square. At 20 points per wavelength in air, matrix A will be 1.8 million elements square. Current memory capabilities of PCs necessitate a smaller A matrix in order to perform the matrix division that solves for the scattered electric field.

3.1.2.3.1 Removal of Zero-Field Points

Since waves do not penetrate very far into human skin, there is no field for the majority of the human body portion of the geometry, which is the same case for the interior of metal objects. Since the length of either side of the A matrix is the size of the number of points in the geometry, removing these zero-field points will mean removing each corresponding row and column of the A matrix, making matrix division possible at acceptable sampling rates.

The method of removing each row and column vector from the A matrix at internal metal points was originally proposed by Angell, though it initially applied to only the six metal cylinders as shown in Figure 3-2. The MATLAB program that generates the geometry indexes each material with a different number: 1 for air, 2 for metal, 2/3 for fabric, and 0 for human skin. Angell proposes utilizing this indexing scheme in order to locate internal metal points and subsequently remove them from the A matrix, reducing its dimensions and reducing computational load [60].

In order to do this, Angell proposes generating four additional geometries in addition to the first, where each new individual geometry file is shifted in one of four directions. Multiplying these four matrices by



the original will result in index values of $2^5=32$, occurring only at internal metal points. The exterior metal points need to be retained for the near-field calculations. Thus, if these points can be identified and removed from the already constructed A matrix and B vector, one can calculate the scattered field more quickly and reinsert values of zero at those points after the calculation is complete. The computational geometry generated from Figure 3-4, where the interior points of the human body are given the indexing value for metal, is shown in Figure 3-5. This figure represents the body prior to the addition of pipes [60].

Using the geometry shown in Figure 3-4, a sampling of 1/12 of a wavelength (3.89 mm) per grid point generates a reduced A matrix 387066 elements square. This is the largest matrix division capable of being performed by the PC used for simulation, so all simulations use a grid spacing of 1/12 of a wavelength or 0.324 mm.

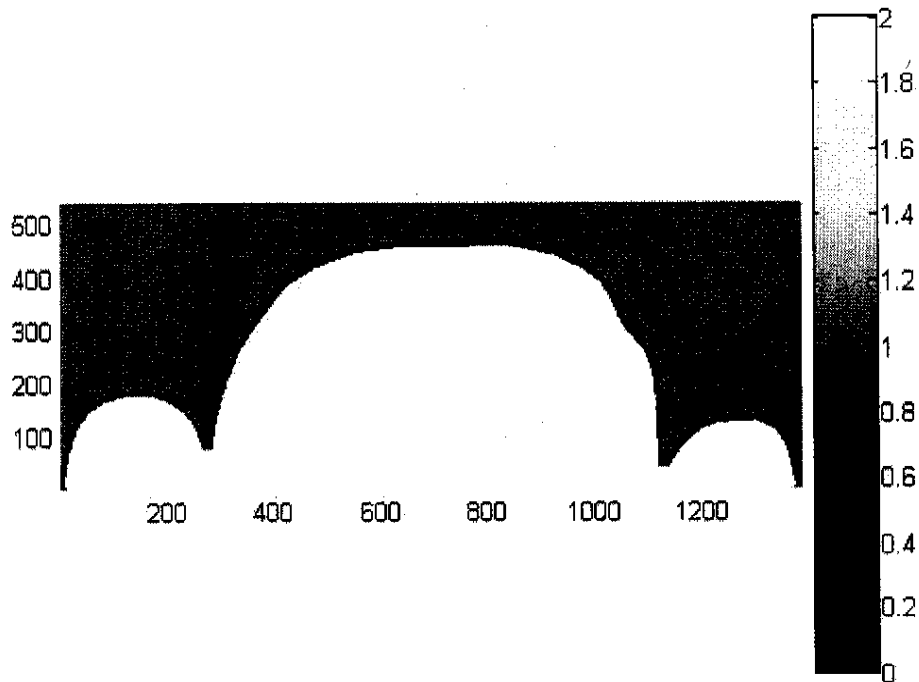


Figure 3-5. Anatomically Correct Computational Geometry

3.1.2.3.2 Thickness of Skin

The thickness of skin shown in Figure 3-5, indexed as value 0, is very small. At a grid spacing of 0.324 mm, the thinnest skin point of the geometry in Figure 3-5 is nine grid points deep, or 0.2922 cm. The sufficiency of this depth for the field inside the skin to decay must be shown in order to show that fields are not being transmitted far enough into the skin to reflect off the zero-field core, which is given the same index as metal. One way to do this is to sample a smaller area of skin, using the same constitutive properties for skin at 77 GHz, as mentioned above, that were used in all simulations. Since it is such a small area, one can sample the computational geometry at a much higher rate. In order to ensure accuracy for this calculation, the skin was sampled at 30 grid points per wavelength in free space. The area simulates a plane wave normally incident on five centimeters of perfectly flat human skin. A plot of the total electric near field for a 0.5 cm section of the skin is shown in Figure 3-6.

Since the transmitted field is uniform across the two inches of skin, one may plot the magnitude of the field one-dimensionally as it enters the skin; this has been done in Figure 3-7. As you can see, the



transmitted field decays quickly. At a depth of 0.2922 cm, the thinnest portion of skin in the simulated geometry of Figure 3-5, the field decays to 0.06% of its value at the skin's surface, or it has decreased by 64.5 dB. This shows that the thinness of the skin in the new anatomically correct computational geometry could not have produced inaccuracies.

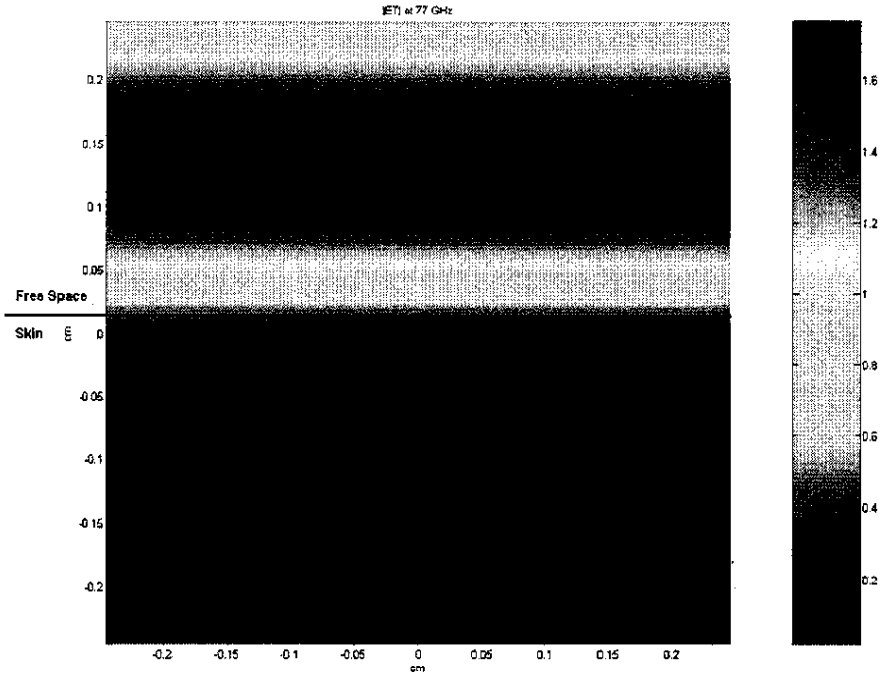


Figure 3-6. Total Electric Field at 77 GHz Incident on Human Skin Sample

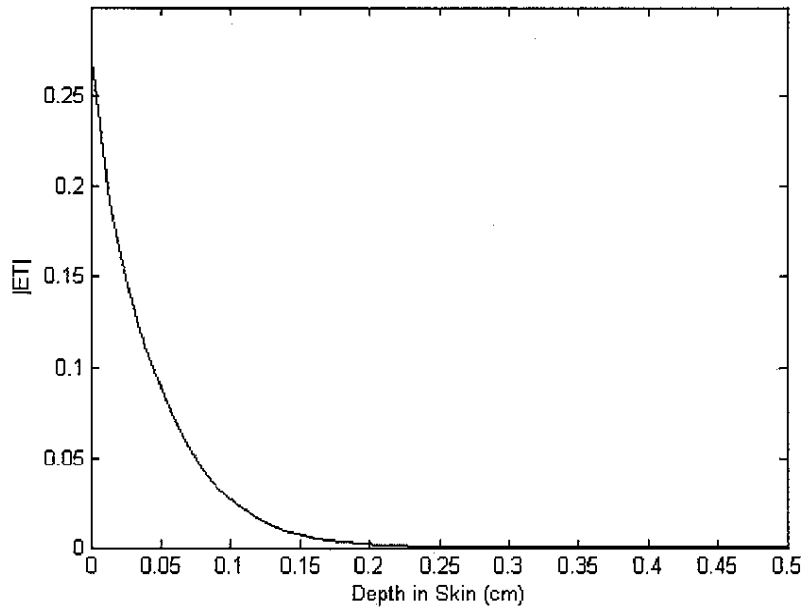
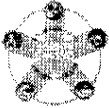


Figure 3-7. Computed Transmitted Electric Field in Human Skin at 77 GH



3.1.2.4 Results

3.1.2.4.1 Transverse Magnetic (TM) Simulations

The in the near scattered electric fields for TM simulations at 77GHz for 0° incidence on the human body with and without pipes are shown in Figures 3-8 and 3-9. Converting these near-field patterns to the far-field gives the results plotted in Figure 3-10.

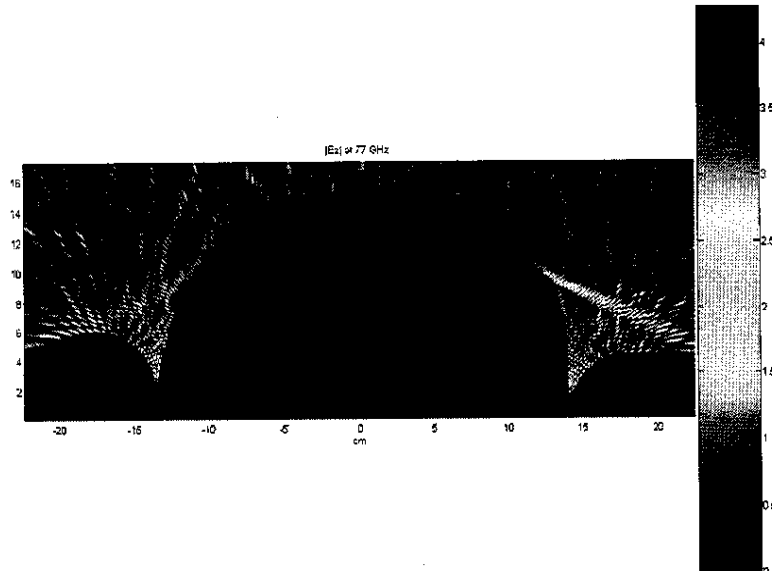


Figure 3-8. Computed Scattered Electric Field ($|E_z|$) at 77 GHz without Pipes

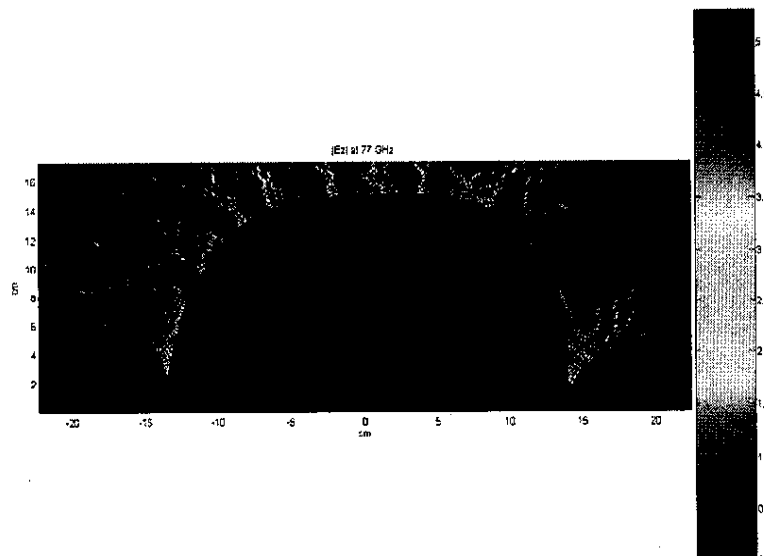


Figure 3-9. Computed Scattered Electric Field ($|E_z|$) at 77 GHz with Pipes

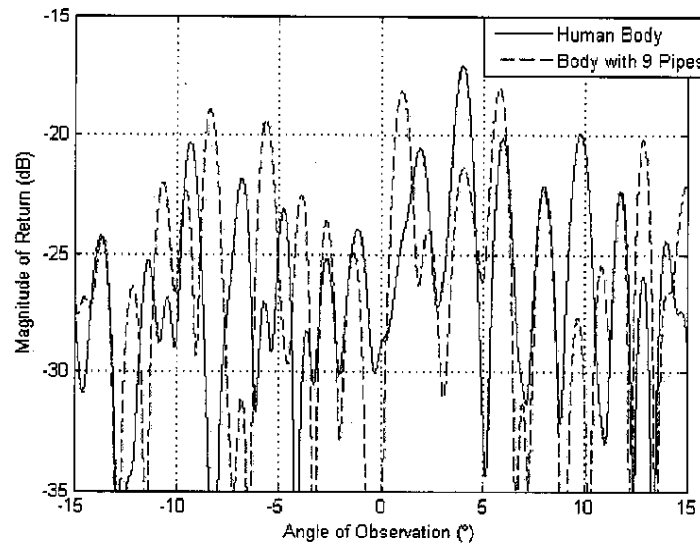
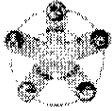


Figure 3-10. Comparative Far-Field Simulations for TM Waves at 0° Incidence

Figure 3-10 shows the simulated magnitude of the backscattered electric field, where the angle of observation equals the angle of incidence. The return is ambiguous, following no uniform pattern. It is apparent that the complexity of the scattering geometry generates a random return not easily subject to interpretation. At some angles, the return from the pipes model is more than the without pipes model, but the increase is not dramatic and seems to vary wildly in accordance with the randomness of the geometry. Magnitude values are in reference to the far-field reflection that would occur from a perfect electric conductor with the same dimensions as the human geometry.

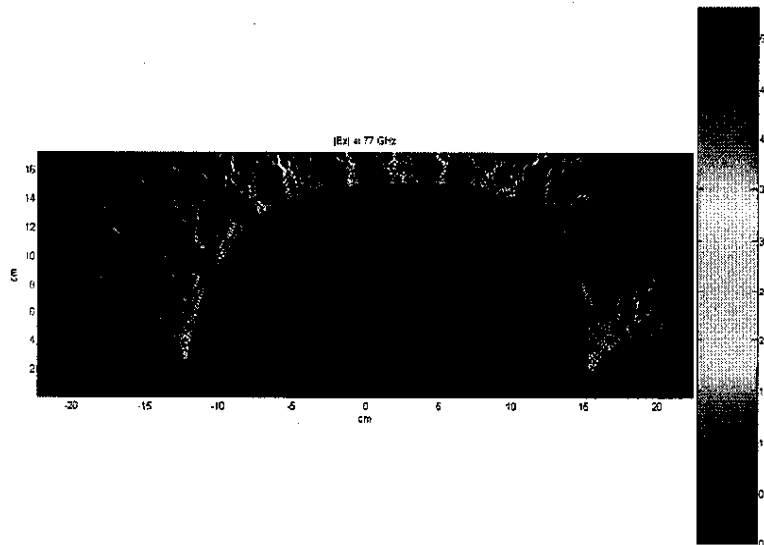


Figure 3-11. Near-Field of Shifted Geometry at 77 GHz

An additional simulation was run where the computational geometry shown in Figure 3-9 was shifted one inch to the right, giving the geometry shown in Figure 3-11. The far-field results of this geometry, compared to those of Figure 3-9, are shown in Figure 3-12.

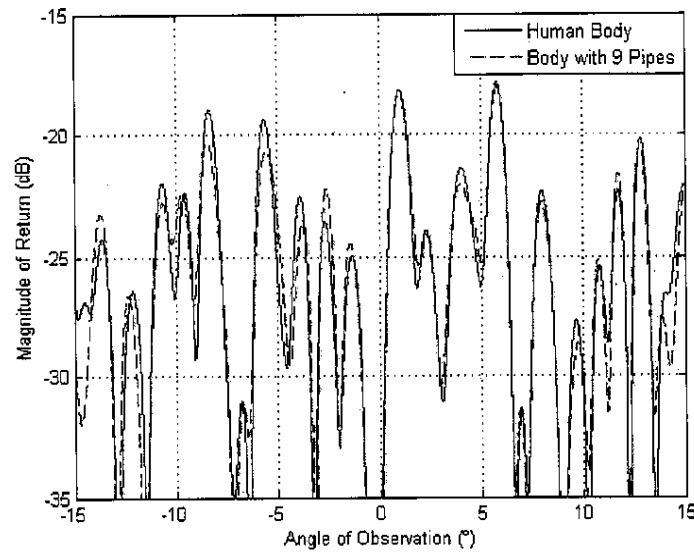


Figure 3-12. Far-Field Comparison of Shifted to Non-shifted Geometry

3.1.2.4.2 Transverse Electric (TE) Simulations

Simulations were also performed for the more complicated TE formulation, where the total magnetic field $|H_T|$ is calculated at all points instead of the electric field.

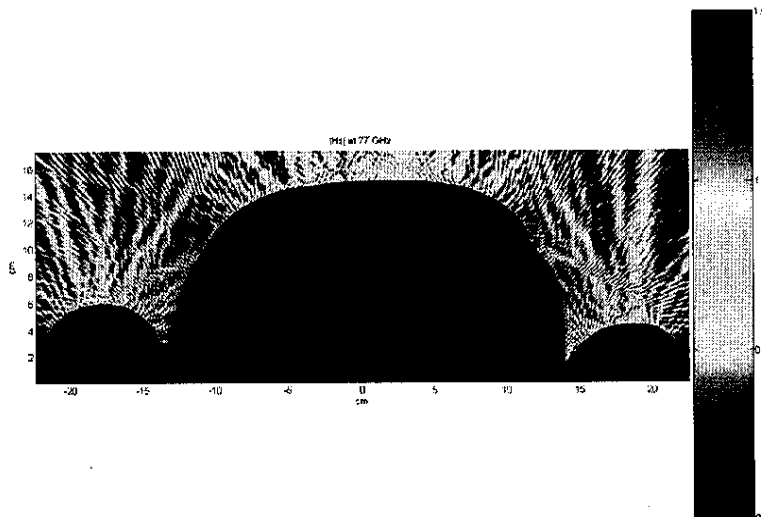


Figure 3-13. Computed Scattered Magnetic Field ($|H_z|$) without Pipes

The TE simulations for 0° incidence on the human body and for the body with pipes in the near field at 77GHz are shown in Figures 3-13 and 3-14. Converting these near-field patterns to the far-field gives the results plotted in Figure 3-15. Again, Figure 3-15 shows that in the TE case, there is no significant increase in return with the addition of pipes. If anything, it would tend to indicate that the actual backscattered field will be randomized due to the complex geometries present on the human body.

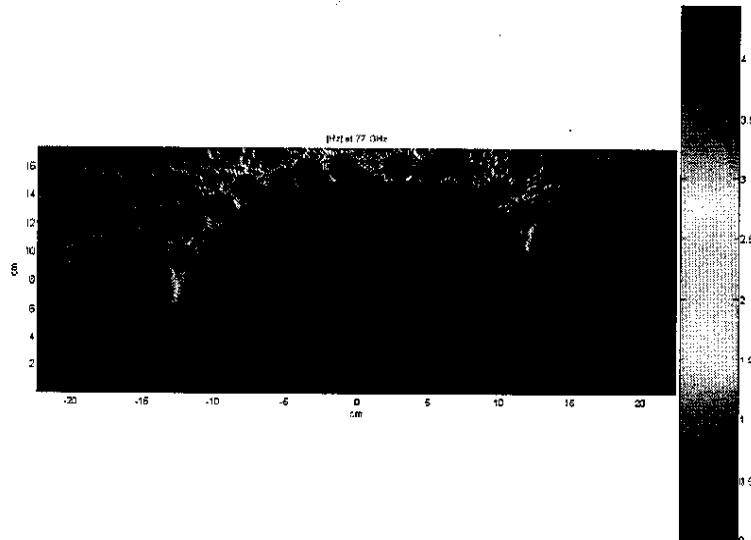
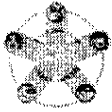


Figure 3-14. Computed Scattered Magnetic Field ($|H_z|$) with Pipes

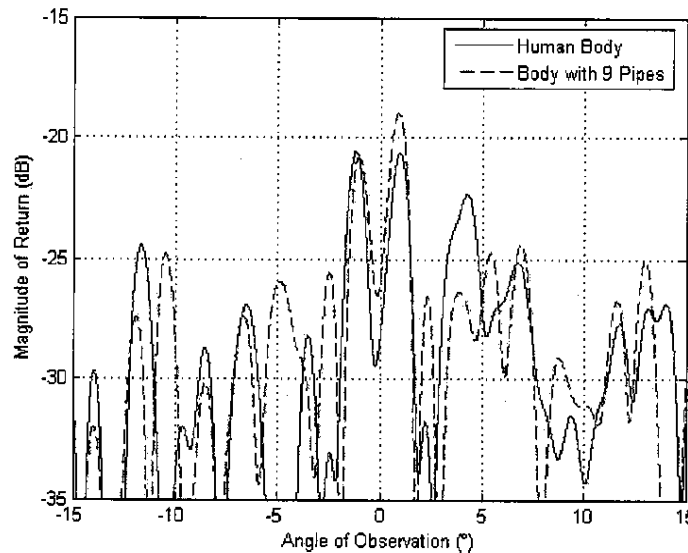


Figure 3-15. Comparative Far-Field Simulations for TE Waves at 0° Incidence

3.1.2.4.3 Cross-Polarization Simulations

Though the testing radar system described in section 3.1.3 is incapable of performing cross-polarization measurements, it is worth examining what happens when we are able to look at backscattered co-polarized and cross-polarized fields. In order to do this, one must add the TE and TM fields for co-polarization and subtract them for cross-polarization. By doing this, one may examine the magnitude of the backscattered co-polarized and cross-polarized fields and compare them for bodies with and without pipes. This analysis is shown in Figures 3-16 and 3-17. These figures show that, while there is some increase in the cross-polarized fields near the backscatter location, it would be, at long ranges, out of scope of the receiver.

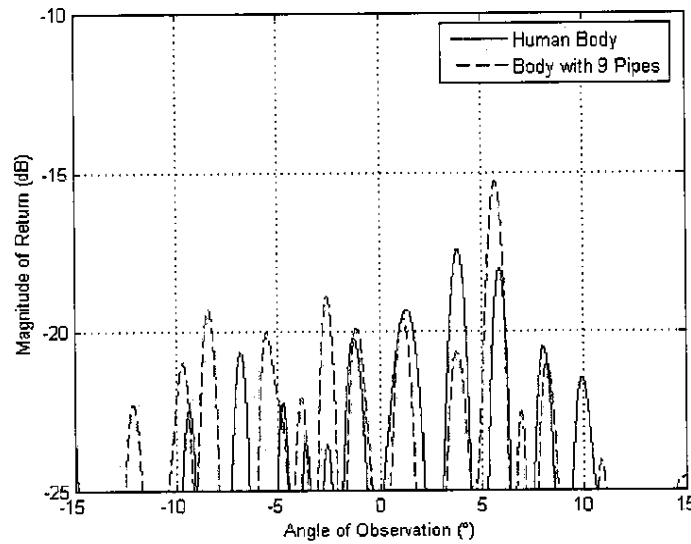


Figure 3-16. Comparative Far-Field Simulations for Co-Polarized Waves

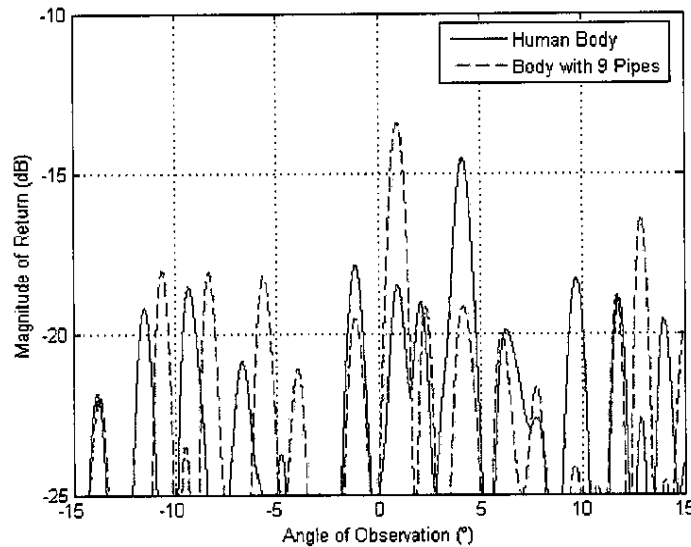
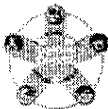


Figure 3-17. Comparative Far-Field Simulations for Cross-Polarized Waves

3.1.2.5 Conclusions Based on Computational Modeling

Based on modeling, experimentation will not be able to distinguish between a body with pipes and one without when a mono-static radar is transmitting in the TM or TE modes. The total backscattered field at normal (0°) incidence is almost a null in some cases. In the co-polarized and cross-polarized field cases, the same effects are observed, namely that the scattered far-fields are a product of the random aggregate of scatterers that are the human body and body with pipes geometries. As rigorous as these modeling techniques are, they cannot take into account every variable that may occur in actual testing conditions. Still, these results provided seemed to predict that the testing hypothesis would prove false.



3.1.3 Testing Equipment

3.1.3.1 Radar

The radar provided for testing was a Raytheon prototype originally developed for an automotive intelligent cruise control (ICC) application. This radar was originally selected by the BomDetec program for its pre-developed processing capabilities as well as its frequency. The radar is, by definition, a commercial-off-the-shelf (COTS) bi-static¹ radar with separate, stacked transmission and receiving antennas, each with dimensions 15λ by 30λ operating at a center frequency of approximately 77GHz (76.5 GHz). The antennas themselves are virtual rectangular apertures of patch arrays fed by a Rotman-Turner lens [65]. A picture of the radar, with the transmitting and receiving antennas highlighted is shown in Figure 3-18.

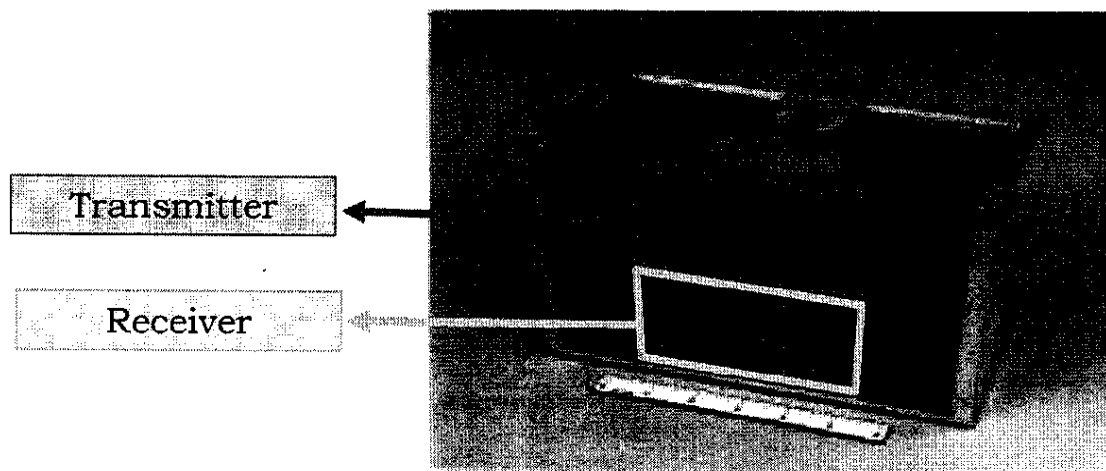


Figure 3-18. Automotive Radar Used for Testing

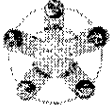
3.1.3.1.1 Polarization

The transmitter and receiver shown in Figure 3-18 are both polarized such that the electric field vector is oriented perpendicular to the floor as the radar rests in the figure. As polarization is "defined by the orientation of the electric field," this polarization can be referred to as vertical (V) polarization [62]. The radar can also be rotated for the purposes of testing another polarization, meaning the radar shown in Figure 3-18 would be rotated ninety degrees in either direction. In this case, the electric field would be oriented parallel to the ground, resulting in horizontal (H) polarization. Since the two antennas cannot be separated from one another, we can only send and receive the same polarization, meaning we can only test vertical transmission with vertical reception (VV) or horizontal transmission with horizontal reception (HH).

3.1.3.1.2 Half Power Beam-Width

With an operating frequency centered at 77GHz, the radar lends itself to long-range detection. Half-power beam width for rectangular apertures is directly proportional to wavelength and thus inversely

¹ The term "bi-static" is somewhat misleading here. A mono-static radar is one that transmits and receives using the same antenna. However, this radar presents a pseudo-mono-static situation here in that the transmitter and receiver are removed by a mere fifteen wavelengths and one can only observe backscatter at what is, for all practical purposes, the location of transmission.



proportional to frequency [63] Since the radar sensor is intended to identify potential threats at distances up to 50m, a frequency in the MMW² region is required in order to achieve a feasible beam width to would illuminate a single human torso. The approximate half power (3 dB) beam width in either dimension is:

$$\theta_{3dB}(\text{deg.}) = \frac{59\lambda}{a} \quad (3.1-24)$$

Equation 3.1-24 was derived due to the fact that, in order to achieve the radiation pattern reported in the Russell paper, the two antennas of the Raytheon-provided radar must have a current distribution of $A(x) = 1-(1-\rho)(2x/a)^2$ and $A(y) = 1-(1-\rho)(2y/b)^2$, where $\rho=0.3$, a is the size of the aperture in the x dimension, b is the size of the aperture in the y dimension, and A is the current. The coefficient 59 was interpolated from Hovanessian's data using a second order polynomial [64], [65], [66]. At dimensions of 15λ and 30λ in height and width respectively, this means the radar has a half power beam width of 3.93° in elevation and 1.97° in azimuth.

3.1.3.1.3 FMCW Waveform

The test radar employs a frequency-modulated coplanar-wave (FMCW), using pulse compression techniques that are able to "simultaneously achieve the energy of a long pulse and the resolution of a short pulse" [62]. The pulse compression used by this radar is linear frequency modulation (FM), also known as chirp, which is a popular class of compression in radar. The transmitted linear FM waveform is of constant amplitude during a period T during which the frequency increases linearly from f_1 (76.35 GHz) to f_2 (76.65 GHz). While most FMCW radars have both an up chirp and down chirp in the waveform, where the frequency both increases and decreases linearly within the transmission period, the Raytheon-supplied radar uses only the up chirp. At a pulse interval of 1.024 ms, this radar operates at a pulse repetition frequency (PRF) of 978 pulses per second, which categorizes it as a low PRF radar [64]. The received signal, upon pulse-compression filtering, is the autocorrelation function of the input to the filter, and is proportional to $(\sin(\pi Bt))/(\pi Bt)$. The received signal, due to the sinc envelope, has high time-sidelobes which are reduced by applying an amplitude weighting on the received signal. The Raytheon-supplied automotive radar employs a Hamming weighting function of $0.08 + 0.92 \cos^2(\pi f/B)$ [62], [65].

3.1.3.1.4 Range Resolution

Range resolution is the property of the radar system that dictates how finely one can discern the distance of targets. If the distance between two targets reflecting a radar's transmitted pulse is less than the range resolution of that radar system, the two targets will really look like one target to the radar. The range resolution of a radar utilizing the FM chirp waveform is inversely proportional to its bandwidth, the difference between f_1 and f_2 . The pulse compression filtering technique, combined with a transmitted FM chirp waveform, means "the range resolution of a pulse can be independent of its duration." Given that the supplied radar has a bandwidth of 306 MHz – the intermediate Frequency (IF) – and range resolution is equal to the speed of light divided by twice the bandwidth, the radar system used for testing was capable of a range resolution of 0.5 m [65], [67]. This range resolution is possible since the entire bandwidth is contained in one continuous chirp. Tighter resolution is possible in other radar systems, but larger bandwidths, in addition to increasing a system's complexity, make "greater demands on the signal processing," and increase the chances of electromagnetic interference [62].

² It should be noted that though this radar is nominally in the MMW band at 77GHz, with a wavelength of 3.89mm, the testing radar is technically operating at the lower end of the W band according to IEEE standards of 1984 [62].



3.1.3.2 Anechoic Chamber

Testing was performed in an anechoic chamber that was sufficient for our frequency, but limited testing range to approximately ten meters.

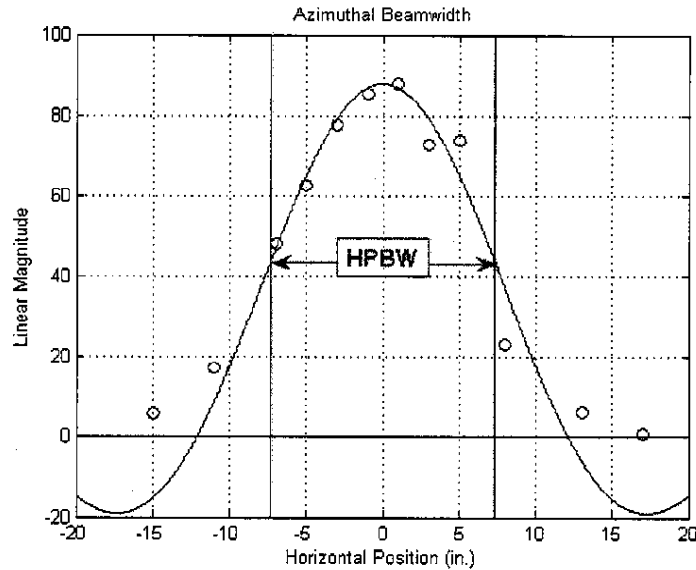


Figure 3-19. Data Determining Azimuthal Testing Beam-Width

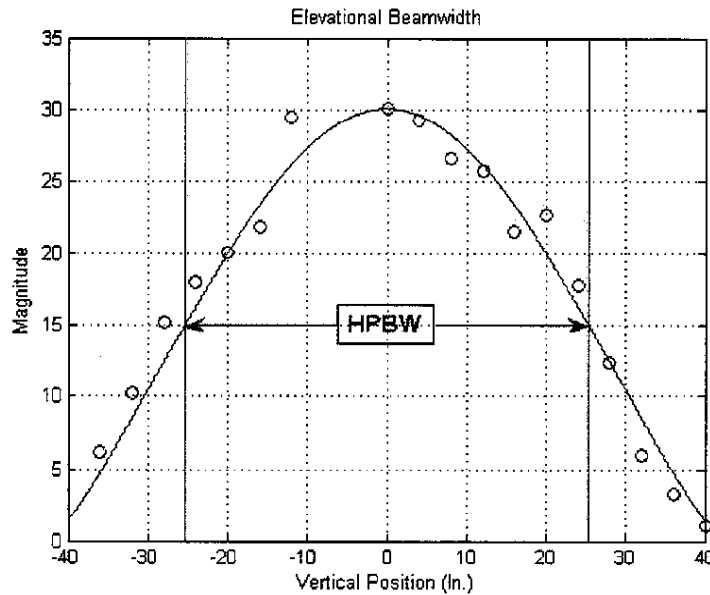
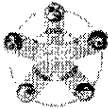


Figure 3-20. Data Determining Elevational Testing Beamwidth

At this distance, given azimuthal and elevational half power beamwidths of 1.97° and 3.93° respectively, the target area was theoretically 0.34 m (13.5") by 0.69 m (27.0"). However, using a corner reflector whose position was varied in the horizontal and vertical directions and fitting a sinc function to the linear data, the half power beamwidth at the location of the target was determined to be 0.37 m (14.59") by 1.28



m (50.55") – see Figures 3-19 and 3-20. Though the program goal is to achieve distances up to 50m, this arrangement is sufficient for testing since, at these half-power beamwidths, the radar illuminates a single human being in this anechoic chamber from just below the waist, up to and including the head.

3.1.3.2.1 Long-Range Testing

Outdoor, long-range testing to reach 50 m was initially a part of the test plan, but FCC regulations precluded moving the radar system outdoors.

3.1.3.3 IED Simulates

The operative testing hypothesis is that metal objects, such as those worn by many suicide bombers, will reflect more than the average human body. Therefore IED simulates were chosen to model the amount, orientation, and geometry of known body-borne IEDs.

The configuration of these devices is typically that of metal pipes worn around the torso in such a way that the pipes are oriented lengthwise along the body, with their end caps pointing towards the head and down towards the feet. These pipes are then filled with explosive materials such as TNT and sometimes also packed with additional shrapnel: screws, nails, ball bearings.

The attachment of these pipe bombs to the body is less consistent. Some may be worn in the pants or the pipes may be taped against the body. For the sake of testing, it was deemed sufficient that the pipes be oriented lengthwise anywhere along the torso. An associate of the project supplied a canvas vest with pipe-sized pockets for this purpose. Figures 3-21 thru 3-23 show the vest, the vest filled with metal plumbing pipes, and a human subject wearing the pipe-filled vest.

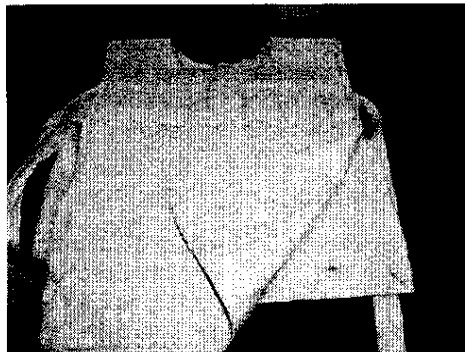


Figure 3-21. Canvas Vest Used for Testing

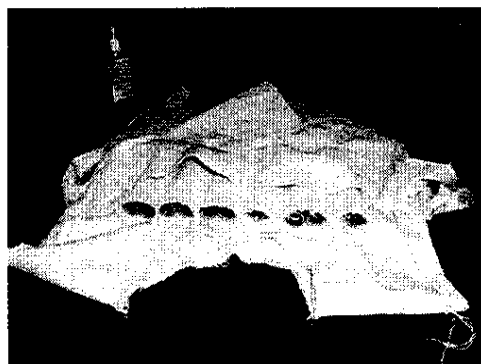


Figure 3-22. Canvas Vest Filled with Ten Pipe-Bomb Simulates



Figure 3-23. Human Subject Wearing Pipe-Filled Vest

3.1.4 Test Procedure

3.1.4.1 Iterative Testing

Testing was iterative in that the first tests determined all subsequent tests on a continuous basis. When in this chapter a brief reference is made to previous results inasmuch as they determine aspects of the operative testing procedure, the reader is encouraged to consult the corresponding result in section 3.1.6. In all, 808 separate experiments were performed with the radar.

3.1.4.2 Stationary Objects

The original hypothesis was that metal would not only reflect electromagnetic waves at a greater intensity than the rest of the human body – much the same way mirrored objects, which reflect light at a high intensity, would glitter at a greater intensity in a flash photograph, but that pipes oriented in the same direction as the electric field would reflect at a greater intensity than pipes not oriented in the same direction. This conforms to theory given that in order for the tangential electric field to be zero on the surface of a perfect electric conductor, the reflected electric field must be 180 degrees different in phase and equal in amplitude to the incident electric field. With this in mind, some effort was made to test individual pipes at various orientations.

Other stationary objects were also tested; objects that were thought to also simulate potential body-borne IEDs. One of those was the metal filled PVC pipe. While suicide bombers sometimes use metal pipes, relying on the pipe as container and shrapnel, they will also employ a PVC pipe filled with various types of shrapnel: nails, screws, or ball-bearings.

Additionally, the vest itself, shown in Figure 3-21, was also tested with and without pipes. The first reason was in order to determine whether or not the vest itself would be detected as a target. Given its construction of entirely fabric, the testing hypothesis was that the vest itself would not reflect. The second reason was to determine how much the pipes themselves, apart from a human body, would reflect.



3.1.4.3 Human Subjects

The main thrust of this project was to perform human testing in order to determine whether or not subjects with IED simulates, considered as “threats,” could be distinguished from those without, considered as “innocents.” At 77 GHz, humans are efficient reflectors of electromagnetic energy. It was vital that the majority of testing be done on humans in order to see whether or not such a strong reflector as a human looked different, electromagnetically speaking, from a strong reflector adorned with a finite amount of an even better reflector: metal pipes. However, with human subjects comes all the fickleness of human behavior. Unlike stationary objects like car bumpers – a target this radar was originally intended to detect – humans breathe, their hearts beat, they have a tendency to rock on their heels and move their joints, so it was also important to keep in mind that testing the inherent variance of experiments was also valuable to the proof-of-concept for radar detection. In order to provide a baseline record of experimental error, human subjects were asked to reposition themselves in between measurements.

3.1.4.3.1 Adding Simulates

Since it was the goal of this experiment to discriminate innocent subjects from threats, the majority of the human subject tests were performed while adding and subtracting the IED simulates described and pictured in section 3.1.3.3. While the primary simulate we wished to measure was the metal pipe, many measurements were also taken where the subject wore only the empty vest. This was because earlier measurements of stationary objects confirmed the fact that the vest itself did indeed reflect.

Initial testing with simulates began by adding small numbers of pipes. However, it soon became apparent that small amounts of metal were not driving the return up by a noticeable amount. Accordingly, many measurements were taken with the subject wearing the vest filled with nine pipes, since this was the most a subject could wear practically on one side of the vest.

3.1.4.3.2 Angular Variation

In a few experiments, subjects were asked to rotate in either five- or ten-degree increments. These experiments were done with the idea that a subject wearing metal pipes might provide a unique angular profile that could be distinguished from an ordinary human subject. It has been shown in past experiments at 2 GHz using tapered slot transceivers that a human subject’s chest, back, and sides give distinct responses [8]. If these distinct responses can be altered by the addition of pipes, one may detect their presence.

3.1.4.4 Data Processing

Much of the data processing for the radar system available took place prior to delivery of data to Northeastern. The Raytheon system takes a fast-Fourier-transform (FFT) of incoming voltage data. Given the linearly modulated frequency of the waveform, this transform, along with the Hamming weighting, can provide fairly accurate range information within half a meter as described in 3.1.3.1.4. Some data processing was performed at Northeastern University after the initial data were received from the radar system.

The radar system, as described in section 3.1.3.1.3, uses an FMCW waveform, commonly known as a “chirp.” One chirp is received and transmitted at a time. In order to obtain a measurement that could be considered a suitable average return, most measurements were based upon 2,000 chirps per measurement. A sample of one returned chirp as recorded by the given radar system is shown in Figure 3-24.

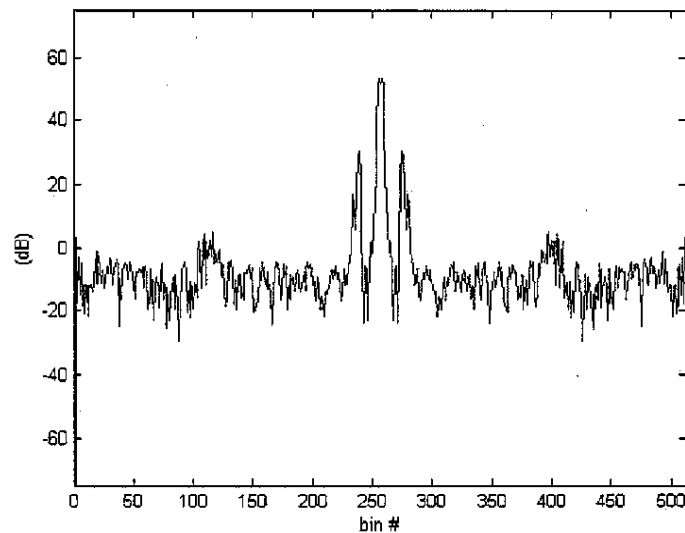


Figure 3-24. Fully Sampled Returned Chirp

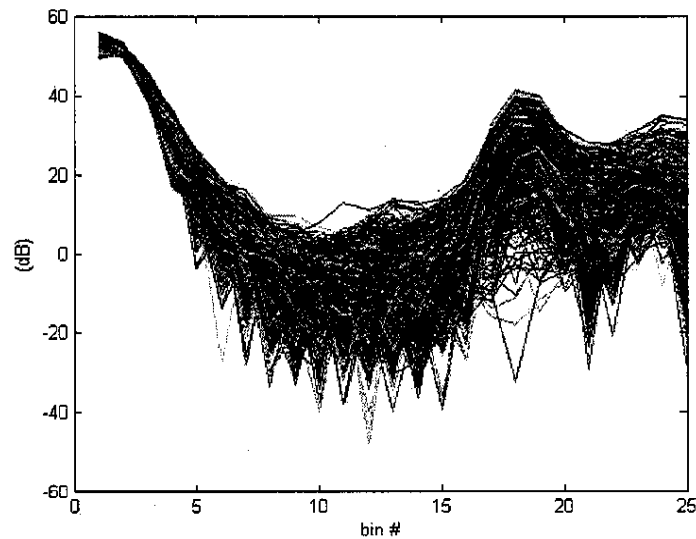


Figure 3-25. 2,000 Chirp Returns from Human Subject

The magnitude of return in decibels was, for the purposes of these experiments quite arbitrary given that the power to which the reference dB level was in proportion is Raytheon proprietary information. For the purposes of this research, it was sufficient to normalize the raw data with respect to the power level occurring from the coupling between transmitter and receiver. One may notice in Figure 3-25 variation at this transceiver point. An internal actuator caused a periodic jump in measurement at all bins. The second peak is the location of the target. At the nineteenth bin, using a bin value of 0.5 m, the target is located at nine meters, which was confirmed by measuring the chamber along the length of the floor. Most measurements were taken when the target was located another meter back, at the twenty-first bin.

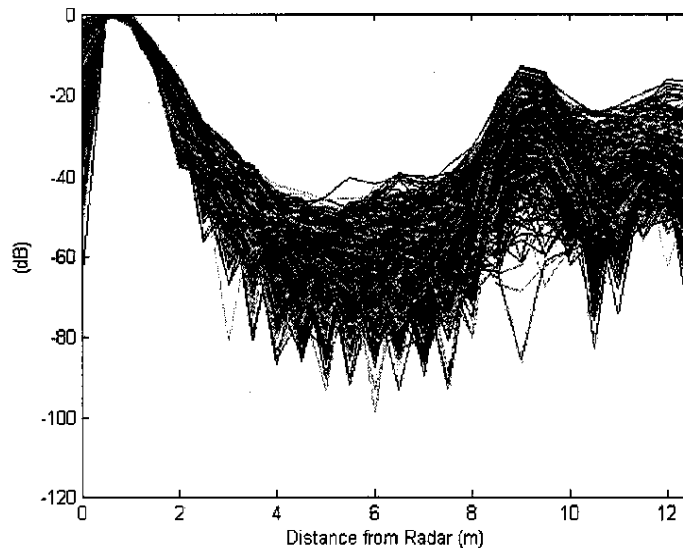
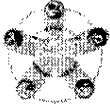


Figure 3-26. Normalized 2,000 Chirp Returns from Target

Additional data processing was performed in order to remove the actuator jump, normalize all measurements in accordance with setting the transmitter coupling at 0dB, and apply distance notation to the range bins, resulting in the plot shown in Figure 3-26.

3.1.5 Radar Detection Methods

3.1.5.1 Conventional Methods of Radar Detection

Radar detection methods are concerned with locating a target. The optimal detection method for a radar system is one that locates, with minimal false alarm and maximum probability of detection, the desired target while rejecting clutter through processing. It may be as simple as a binary detection scheme in which the mere presence of any target is sufficient information without any other reference to the target's features. This may be the case in a no-fly zone or some other area of space that the user does not expect to be normally occupied. In other cases, one may wish to distinguish more complex targets from one another. This is the case for this research where we wish to distinguish a subject wearing body-borne IEDs from a subject without them in a busy crowd. Therefore, the goal of this research was to develop a detection scheme that delivered more information than merely the presence of a target [62], [68].

3.1.5.1.1 Reflectivity of Target as Detection Characteristic

The characteristics that determine a target's reflectivity are its constitutive properties of permittivity and conductivity as well as its shape-dependent scattering amplitude. Historically, radar has been used to scan spaces for moving targets and depends upon statistical analysis for detection. In our experience, only the simplest stationary case was examined, testing also proved that the amount of signal reflected back toward the radar, and therefore the target's radar cross-section, fluctuated dramatically as a function of time. This was observed to occur not merely scan to scan, but even from pulse to pulse, sometimes referred to as "fast" target scintillation. Thus, traditional statistical methods of detection may apply to this research [64].



Detection based on statistical analysis of reflectivity must contend with two factors: background noise and the reflective properties of the target. If background noise is present, one must rely on the statistics of multiple scans in order to pick targets out of existing noise. Experimental results presented in this thesis were obtained in the clutter-free environment of an anechoic chamber which was described more thoroughly in section 3.1.3, thus background noise is negligible and will not be considered [69].

3.1.5.1.2 Statistical Decision Theory

The core of radar detection is modeling echoed signals from anticipated targets as ergodic random processes. A process' ergodicity implies that its mean and variance do not vary with respect to time; therefore, detection signals should follow statistical trends. The central limit theorem states that, as the number of trials increase for any given random variable, its probability density function tends towards the Gaussian or Normal density function, although DiFranco states that the random return from targets consisting of "an aggregate of many random scatterers" tends towards a Rayleigh density [69]. In either case, if differing targets can be modeled as ergodic random processes with time-invariant means and variances, there is the possibility of distinguishing between them, particularly if the means differ. This is something that was anticipated: the hypothesis was that human subjects wearing metal objects would reflect more signal than human subjects alone [69].

This detection based upon separation of normal density functions is the most basic method of detection. Detection takes place when a decision is made based upon a preset threshold as illustrated in Figure 3-27, borrowed from Immoreev. In the figure, the intensity of the echoed signal at the radar is plotted as the dependent variable "U" with respect to time. As you can see, the random return resolves itself, over time, into a normal probability curve. The threshold $U_{\text{thresh}}=U_0$ is set at a user-defined level. For the purposes of detection, all echoed signals exceeding that threshold denote the presence of a target [68].

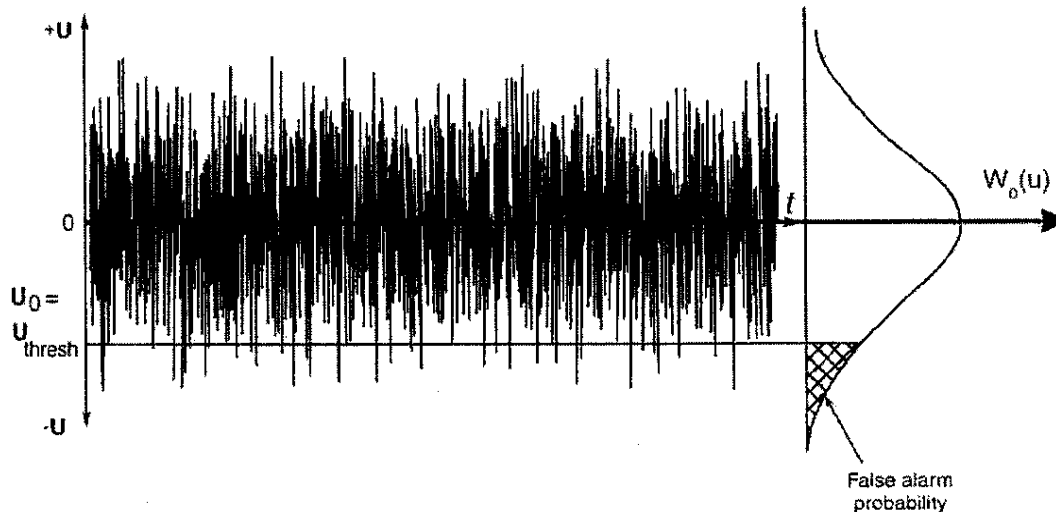


Figure 3-27. Illustration of Threshold Setting for Radar Return

Figure 3-27 shows the probability density function of a random radar return resolving to a Gaussian density function, a tendency that can be used to distinguish one return from another. This is most pronounced when trying only to distinguish a target from the surrounding environment. This method is illustrated in Figure 3-28, where the distributed return from the target, W_1 is shown as returning a higher value than the noise W_0 . The threshold must be set so as to minimize the probability of false alarm, F, and to maximize the probability of detection, D.



The preceding theory is more applicable to presence detection, where the only purpose of the radar system is to detect object presence as distinguished from the natural surrounding environment. But it was thought that the return from a human subject wearing body-borne IED simulates can be similarly distinguished from a human subject without them.

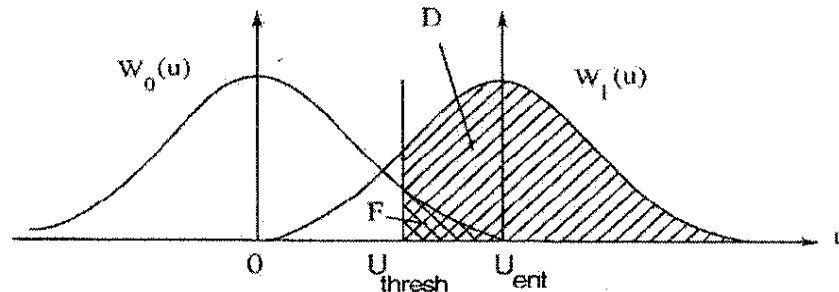


Figure 3-28. Statistical Decision, where Noise is W_0 and the Target is W_1

3.1.5.2 Detection by Means of an Angular Profile

Detection of targets by one-dimensional radial profiles that relies on a target's shape has been proposed in the past. High range resolution radars are capable of creating one-dimensional images based upon the "individual scattering centers" of complex targets. However, these profiles have typically been radial profiles of moving targets at different aspect angles [62]. In these experiments, only the simplest case was examined: a stationary individual. For this case, shape detection could only be made based on the angular variation experiments. The only aspect angle was varied for a stationary target. It is theoretically possible to obtain an image from these data since the target – in some cases a human body and in others a human body with vertically-oriented pipes – would have had many reflectors responding uniquely to different aspect angles. Since the range resolution of 0.5 m is larger than the width of the human body itself, even more in the case of the 0.75" diameter metal pipes, one would not have expected much in the way of imaging capabilities. The reflected field appears as a sum of individual reflectors, the target – body and pipes – providing one return. Nevertheless, there is the possibility that the return would be unique for each aspect angle, providing a 360° profile.

Beyond the difficulties in achieving such a profile, there has been concern among members of the radar community as to the viability of profile detection in any form. In order to detect based on any one or two-dimensional target profiles, one must draw from and compare received signals to a library of reference profiles. In the case of human subjects, this task would be practically impossible, given that innocent human subjects could, in theory, be wearing a number of reflective materials on a wide variation of body shapes. The acquisition of data in these libraries is not feasible due to cost and sheer volume. Still, it is a detection method that can possibly be applied to these experiments [62], [70].

3.1.5.3 Polarimetry

When electromagnetic fields are incident upon a complex target, the reflected field will be changed in polarization from the incident field. Polarimetry deals with the examination of this change in order to extract information about the target by means of a polarization matrix. Boerner implies that this method is particularly helpful when operating in the optical region where "polarization effects play a greater role" [71]. This is most likely because a target's shape in this region affects radar cross-section more than its size. Due to the testing radar's extremely small wavelength, 3.89mm, the system operated in the optical region, where targets are greater than or equal to thirty times the wavelength [62].



Target recognition by means of polarimetry relies upon the polarization or scattering matrix which utilizes co-polarized and cross-polarized backscattered signals as its elements. It may be written as:

$$S = \begin{bmatrix} S_{HH} & S_{VH} \\ S_{HV} & S_{VV} \end{bmatrix} \quad (3.1-25)$$

The components of this matrix consist of the backscattered signals transmitted at both V and H polarizations and received at both H and V polarizations. For example S_{HV} denotes a backscattered signal transmitted at horizontal polarization and received at vertical polarization. This matrix can be linked the Jones vectors, to produce a Kennaugh matrix, or in the representation known as the polarization fork in order to create target signatures based upon polarization.

While this is an interesting method, it is not considered a reliable form of detection. Additionally no cross-polarized backscatter information is possible with the radar available for testing given that the radar can only transmit and receive in one polarization at a time. Furthermore, the scattering matrix is most useful when both phase and amplitude are available from the backscattered signal. Only magnitude was available with the radar setup used for testing [62], [72].

3.1.6 Experimental Results

3.1.6.1 Magnitude, a Parabolic Interpolation

In any given run of an experiment only one result was obtained: the magnitude of the return at the target location. Returns from the adjacent range bins, coming from 0.5 meters both in front of and behind the target's maximum return, could be analyzed. Additionally, there has been some interest in a target's effect on the return from the back wall. One may notice this return at 12 meters in Figure 3-26. Indeed, experiments were taking place in an anechoic chamber, where reflections of any kind from non-targets, and certainly from a back wall blanketed in absorber, are supposed to be nonexistent. However, at 77GHz, reflection was in fact observed off the back wall. But the operative hypothesis is that an increased return will be recorded from a target containing metal objects. Thus we are primarily concerned with the single value at the range bin corresponding to the target.

Each experimental run contained returns from 2,000 transmitted chirps, to acquire a meaningful average. By converting the received data, as shown in Figure 3-26, to a linear scale and taking the mean value at each of the thirty two range bins, a mean plot can be obtained as shown in Figure 3-29. However, the maximum shown at the peak range bin representing the target is not the absolute maximum. Using the adjacent points, one can use a parabolic interpretation of the three points to find a maximum, where the equation of the parabola, if y_0 , y_- , y_+ represent the points of the peak and the fore and aft points, is:

$$f(x) = \left(\frac{y_+ + y_-}{2} - y_0 \right) x^2 + \left(\frac{y_+ - y_-}{2} \right) x + y_0 \quad (3.1-26)$$

The logarithm of the equation for this parabola is also plotted in Figure 3-29. It is the apex of this parabola that is used in all results reported in this thesis.

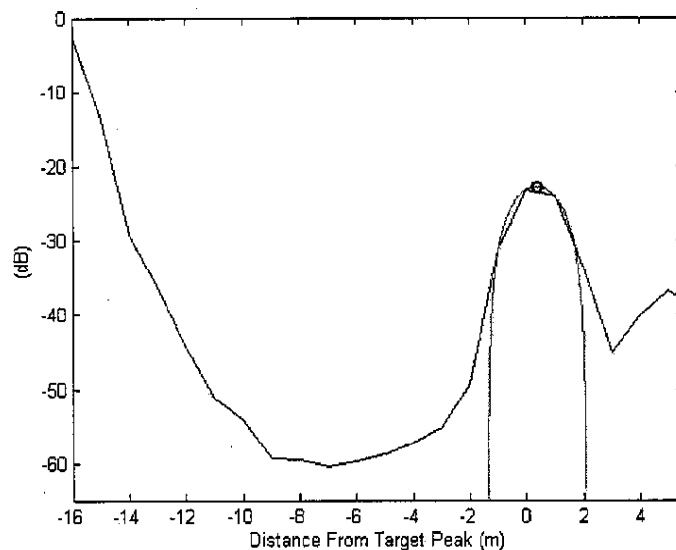


Figure 3-29. Average Return with Parabolic Fit and Maximum

3.1.6.1.1 Comparison of Subjects With/out Simulates

Figures 3-30 and 3-31 show the comparative returns of experimental runs of human subjects with and without various amounts of simulates for both polarizations. In order to plot the results on a bar graph for examination, the results, which were all in the negative decibel range, had to be made positive. For figures 3-30 and 3-31, 30dB was added across the board to all measurements. This does not, of course, affect their relative value in decibels. Runs of four or five pipes were only performed once because a satisfactory increase was not being obtained with the addition of small amounts of pipes; therefore, testing proceeded to the addition of dramatic amounts of metal: usually nine pipes in the front of the vest.

The results do not validate the initial hypothesis that metal objects will increase the reflection of electromagnetic waves at 77 GHz from that of the same human body. In these results, we observed as much as 6dB variation in return from the same individual and as much as 9dB variation between different human subjects. This is for the simplest case: a human subject standing, more or less, perfectly still. The fact that these measurements are averaged over 2,000 returned signals would tend to cancel out randomized movements such as breathing and minor swaying. What the data say is that, on average, the return from a subject at 77 GHz, in both polarizations, decreases when a significant amount of metal pipes are added between the signal wave front and the body.

The sheer variability of measurement to measurement observed in Figures 3-30 and 3-31 is problematic for detection algorithms since they depend largely on mapping experimental data as random variables in order to make a detection decision, a random variable being A variable whose values are random but whose statistical distribution is known or can be determined. Given that the 2,000 chirp data presented do not have consistent means, something characteristic of a statistical distribution, random variable mapping cannot be used.

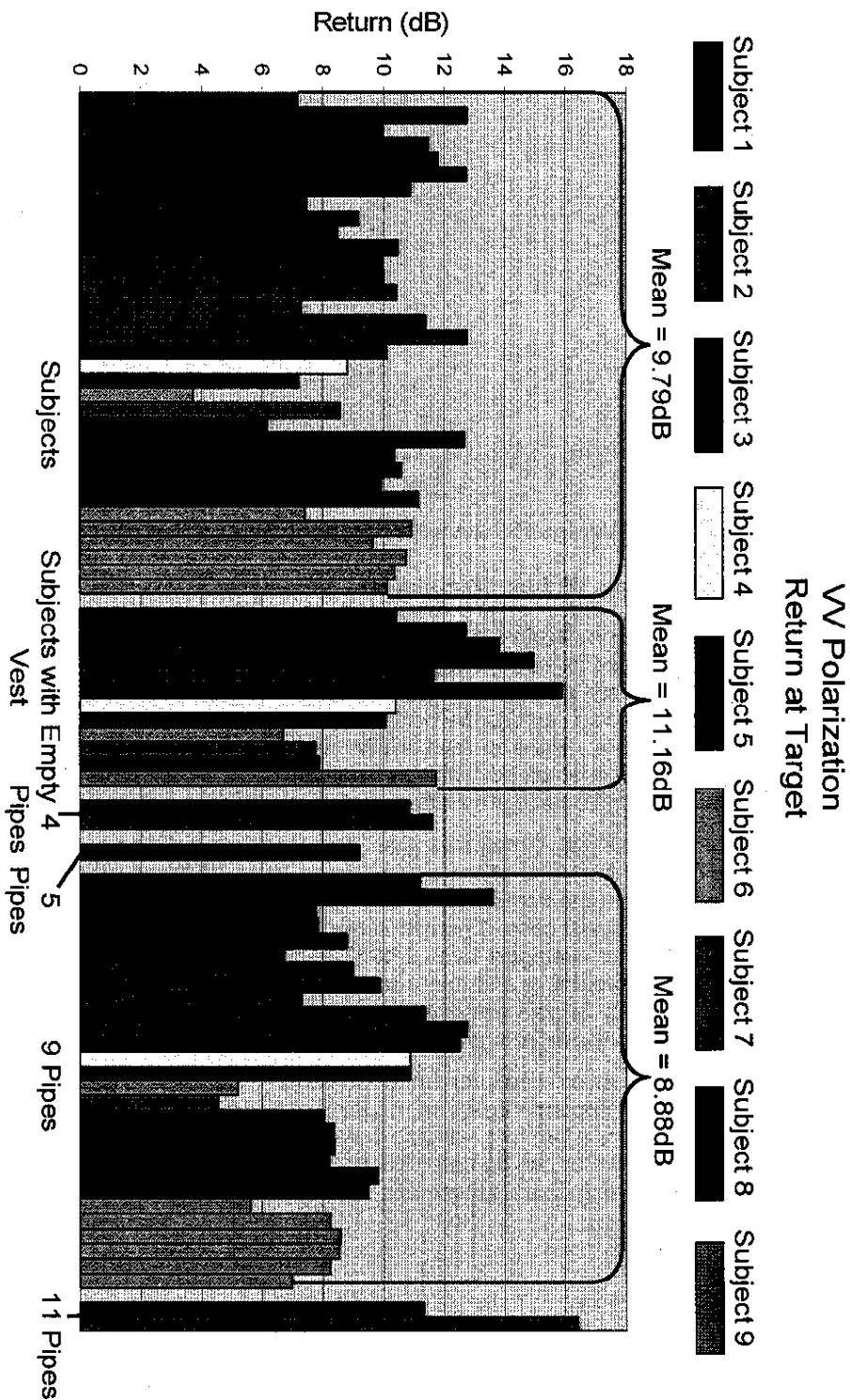
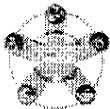


Figure 3-30. Target Return for Subject with IED Simulates, VV Polarization

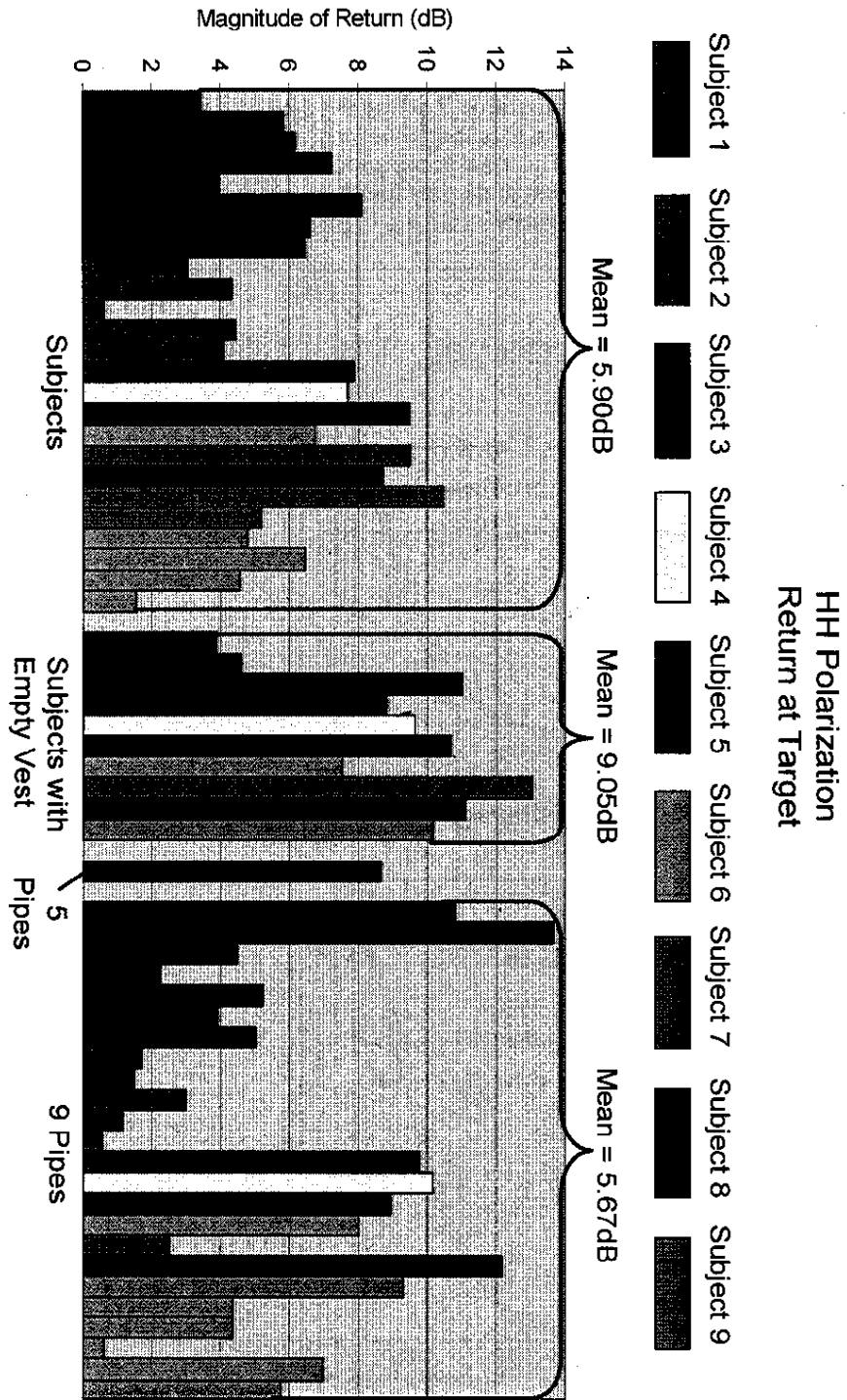
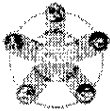


Figure 3-31. Target Return for Subject with IED Simulates, HH Polarization



3.1.6.1.2 Histograms

Traditionally, target detection has relied upon statistical decisions culled from a theorized probability density function [68]. Such functions can be constructed from data collected during testing in the form of histograms. For the purpose of these histograms, one received chirp was considered one count. Figures 3-32 and 3-33 show the histogram results of testing involving subjects and body-borne IED simulates in VV and HH polarization respectively. The peak occurrences are different because more experiments were done in certain cases. Thus, the virtual density functions peak at different levels. However, mean levels have been highlighted in order to demonstrate the comparison between the various tests.

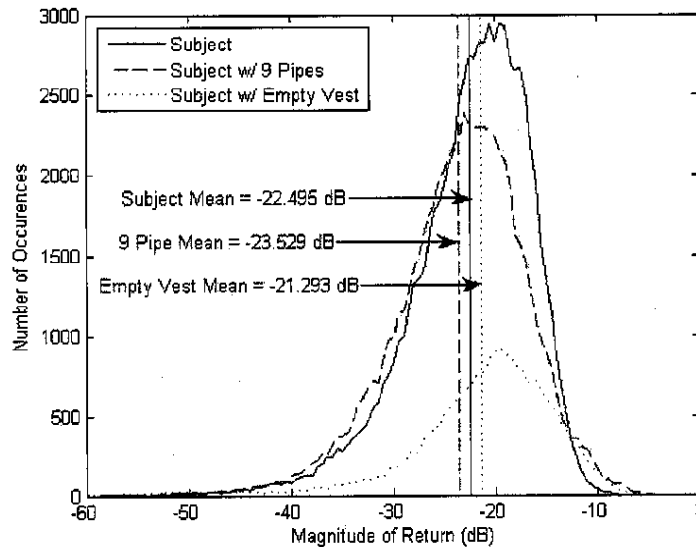


Figure 3-32. VV Histograms for IED Simulates on Subjects

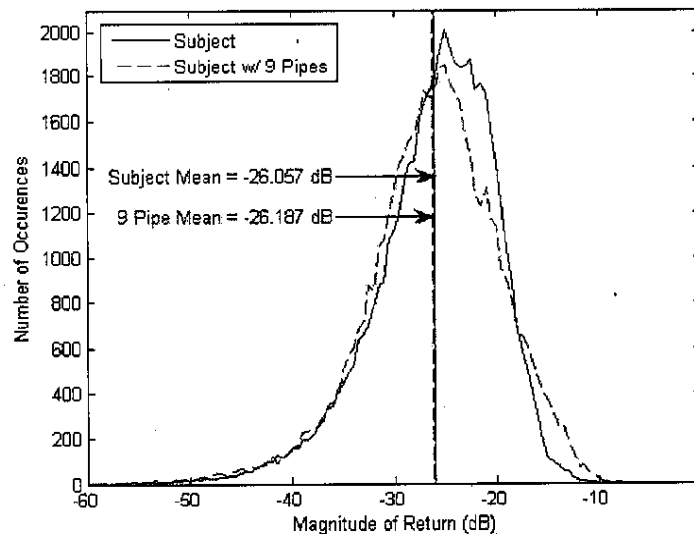
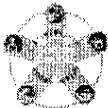


Figure 3-33. HH Histograms for IED Simulates on Subjects



These results are taken from the parabolically interpolated maximum return from the target. For VV, three experiments are summarized: human subject with clothes alone, human subject donning the empty vest shown in Figure 3-21, and human subjects donning the empty vest filled with nine pipes as shown in Figure 3-22. The HH results are similar except that not enough tests were done with the empty vest to warrant its inclusion as a histogram. As one can see in Figures 3-32 and 3-33, the statistical results of human subjects with and without IED simulates are virtually indistinguishable from one another. In fact, the results once again defy the hypothesis that scattered fields in the direction of the incident angle of the radar increase with addition of metal objects on the body: the mean of the nine pipe vest is markedly below that of human subjects wearing only their clothes. All of the counts shown in these two histograms are for stationary human subjects facing the radar, where incident angle equals zero degrees. This implies there is no possible way of detecting the difference between a human subject and a human with pipes using this radar at 77GHz when examining only the reflection characteristics of the entire human with and without simulates. The preceding language is chosen carefully given that results were limited to the testing radar's range resolution capabilities. This is, after all, a measurement of the total field, where "individual scatterers add vectorially" from the target's echo to form a total amplitude that is received at the location of the radar [62]. The total amplitude we are measuring is the result of adding any and all scattered fields within 0.5m of the human target, the range resolution of the test radar.

3.1.6.2 Angular Profiles

A target's radar cross-section varies with the shape of the projected area. Thus, changes in angles of incidence for our testing scenario should change the target's cross-section and the resultant scattered field appropriately. The question is whether or not this allows us to discern a threat from a non-threat: a person with metal pipes placed against the chest or back from a person with nothing on their body.

The initial hypothesis was that the more cylindrical shape of the pipes would result in less variation across the incident angle spectrum when a human subject wore the vest with pipes than there would be for a human body alone. This is in spite of the fact that any examination of a human cross-section will show the human body to be anything but flat. Pipes arrayed across either side of the body might provide a distinct angle-dependent reflection though, as discussed in section 3.1.2, the complexities of the geometry require computer modeling to develop any sort of prediction.

Tests were done using ten degree variation in incident angle for three different subjects with and without the vest in only VV polarization for the 180° encompassing the front of the body where the pipes were located on the subjects. Once it was determined that ten degree variation could not provide adequate resolution to determine angular characteristics of the body with and without simulates, more tests were done with five degree variation in incident angle, though with only one subject, at both VV and HH polarizations for all 360°. All angular test results are presented in Figures 3-34 through 3-38. 0° orientation denotes a subject whose chest is facing the radar and ±180° orientation denotes a subject whose back is facing the radar³.

³ For Subject 9, the graph for whom is shown in Figure 3-36, the data point at 10° in the nine pipe case was lost and is therefore not presented.

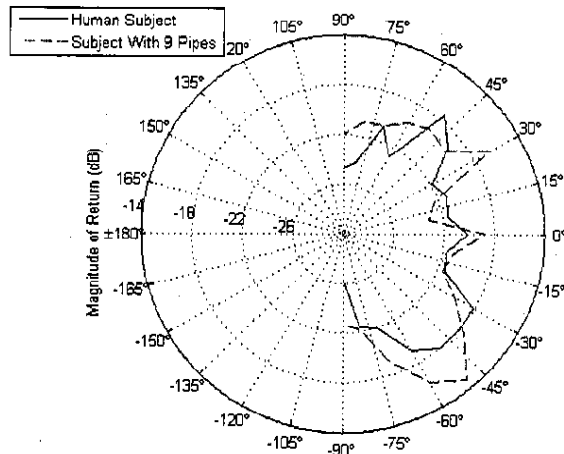
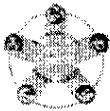


Figure 3-34. Angular Profile of Subject 1, 10° Intervals, VV Polarization

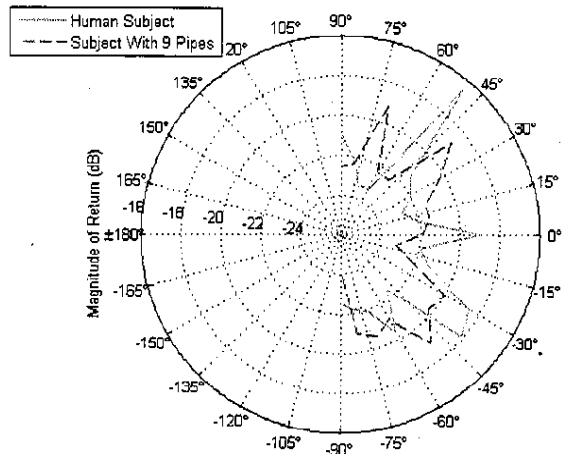


Figure 3-35. Angular Profile of Subject 2, 10° Intervals, VV Polarization

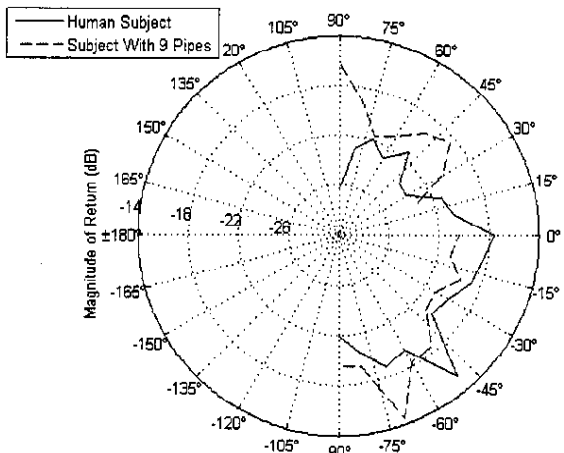


Figure 3-36. Angular Profile of Subject 9, 10° Intervals, VV Polarization

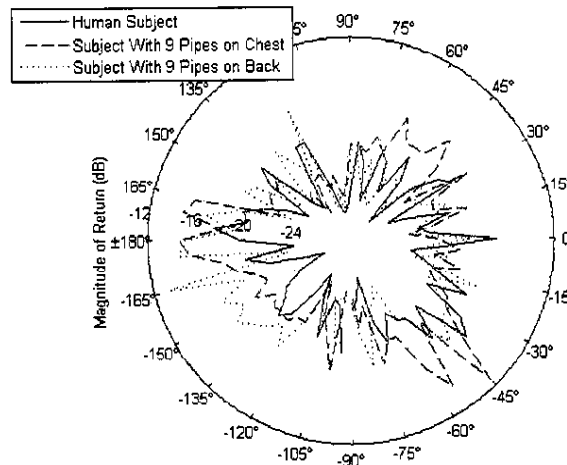


Figure 3-37. Angular Profile of Subject 1, 5° Intervals, VV Polarization

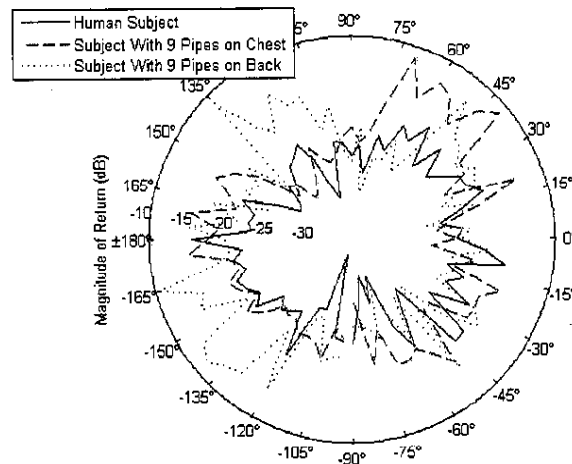


Figure 3-38. Angular Profile of Subject 1, 5° Intervals, HH Polarization

3.1.6.3 Data Analysis with PPT Algorithms

PPT performed additional data analysis with proprietary algorithms. Being proprietary, it is not known exactly how one arrives at any given quantity using any of the algorithms, but it is presumed that the algorithms use the magnitude of return at the range bin location of the target either as an average of or one of the 2,000 total returned signals per experiment. Some of the PPT algorithms rely on simultaneous VV and HH polarizations; therefore, PPT also developed other algorithms not dependent on simultaneous polarizations and, for the algorithms that did require it, PPT made comparisons between VV and HH results occurring under the same conditions, albeit at different times. Thresholds were set for these cases using known innocent cases. The results of these algorithms are shown in tables 3.1 and 3.2. The last three of both the "Innocent" and "Threat" cases were blind tests. The other twenty one cases were known by PPT beforehand.



Table 3.1 – Results of PPT Algorithms

Case	Results* by Algorithm #															
	1	2	3	4	5	6	7	8	9a	9b	10a	10b	11a	11b	15	16
Innocent†	-	-	-	-	-	-	-	-			-	-	-	-	-	-
Innocent†	-	-	-	-	-	-	-	-			-	-	-	-	-	-
Innocent†	-	-	-	-	-	-	-	-			-	-	-	-	-	-
Innocent	-	-	-	-	-	-	-	-			-	-	-	-	-	-
Innocent	-	-	-	-	-	-	-	-			-	-	-	-	-	-
Innocent	-	-		-	T	-		-			-	-	-	-	-	-
Innocent	-	-		-		-		-			-	-	-	-	-	-
Case	Results* by Algorithm #															
	1	2	3	4	5	6	7	8	9a	9b	10a	10b	11a	11b	15	16
Innocent	-	-		-		-		-			-	-	-	-	-	-
Innocent	-	-		-		-		-			-	-	-	-	-	-
Innocent	-	-		-		-		-			-	-	-	-	-	-
Innocent	-	-	-	-	-	-	-	T		-	-	-	-	-	-	-
Innocent																
Innocent	T	T			T		T									
Innocent		T													T	
Threat†	-	-	-	-	-	-	-	-			-	-	-	-	-	-
Threat†	-	-	-	-	-	-	-	-	T	T	-	-	-	-	-	-
Threat†	-	-	-	-	-	-	-	-		T	-	-	-	-	-	-
Threat	-	-	T	-		-	T	-	T		-	-	-	-	-	-
Threat 45°	-	-	T	-		-	T	-	T	T	-	-	-	-	-	-
Threat	-	-	T	-	T	-	T	-	T		-	-	-	-	-	-
Threat 45°	-	-	T	-	T	-	T	-		T	-	-	-	-	-	-
Threat 90°	-	-	T	-		-	T	-			-	-	-	-	-	-
Threat	-	-	T	-	T	-	T	-		T	-	-	-	-	-	-
Threat	-	-	-	-	-	-	-	-		T	-	-	-	-	-	-
Threat	T				T											
Threat						T	T	T	T	T	T	T	T			
Threat				T		T	T	T	T	T	T	T		T		T

* | = Innocent, T = Threat, † Synthesis of five experiments

Table 3.2 – Summary of Probabilities for PPT Algorithms

Probability	Percentages by Algorithm #							
	1	2	3	4	5	6	7	8
Detection	33.3	0.0	66.7	33.3	44.4	67.7	88.9	66.7
False Alarm	33.3	66.7	0.0	0.0	25.0	0.0	12.5	0.0
Missed Detection	66.7	100	33.3	66.7	55.6	33.3	11.1	33.3

Probability	Percentages by Algorithm #							
	9a	9b	10a	10b	11a	11b	15	16
Detection	46.2	61.5	66.7	66.7	33.3	33.3	0.0	33.3
False Alarm	7.1	0.0	0.0	0.0	0.0	0.0	33.3	0.0
Missed Detection	53.8	38.5	33.3	33.3	66.7	66.7	100	66.7

The results of these algorithms are ineffective for detection purposes. Algorithms 9a and 9b, the only algorithms to examine all twenty five of the experiments PPT selected for analysis, give a detection rate



on the scale of a coin flip, where the probability of detection would be 50%. Algorithm 7, which provides the only feasible results, examines only eight “innocent” cases (three blind) and nine “threat” cases (three blind) where at least 100 experiments with human subjects and sixty experiments with human subjects wearing pipes fit the criteria for use in algorithm seven. At 8% and 15%, these are very poor statistical samples and thus a very poor representation of overall experimentation.

As stated in section 3.1.6.1.1, the use of an algorithm relies upon mapping a random variable to a quantitative space. Examining Figures 3-30 and 3-31, one can see variability in return from experiment to experiment. Each result in this figure is an average of 2,000 returns. The variance can be anywhere from 18 dB to 34 dB for a human subject and anywhere from 21 dB to 36 dB for a subject with nine pipes. As variance and mean are therefore not time invariant – they change dramatically between experiments – mapping the return as a random variable in an algorithm is an untenable method.

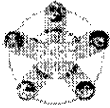
3.1.7 Recommendations

3.1.7.1 “Speckle” Effect

The likeliest suspect in the randomness of the data presented in section 3.1.6 is what Sheen calls speckle, which he defines as the phenomenon of “constructive and destructive interference from multiple scattering locations or depths within a single resolution cell.” Resolution cells for the radar testing system are 0.5 m as previously discussed in section 3.1.3.1.4. Therefore, all constructive and destructive interferences within 0.5 m range of the transceiver are resolved into a single magnitude. When the target is something like a human body which could be considered a complex, rough surface, the return is bound to change drastically between experiments as the scattered fields construct and destruct differently between measurements within the 0.5 m range cell.

This is observed most explicitly in the case of the last five measurements of subject 1, subject 2, and subject 9 oriented at 0° and standing still without pipes in both HH and VV polarizations as presented in Figures 3-30 and 3-31. These measurements were taken on the same day at approximately two minute intervals. In this case, the radar was not adjusted nor did the subject change clothes. The return was the parabolic interpolation of a 2,000 trace average, as described in section 3.1.6.1, which should also cancel out variations in body movement. The subjects were not wearing anything other than cotton shirts. Even in this simplest of cases, we observed as much as 5 dB variation in HH polarization and 4dB variation in VV polarization from successive measurements, that is, from measurements that occurred only two minutes apart from each other. This might be acceptable if not for the fact that the average of all cases for subjects wearing pipes is nowhere near 4 dB above the average for subjects without pipes – see Figures 3-32 and 3-33. As it is, this speckle effect renders useless the magnitude of the backscattered field, our only measurable, as a random variable [73].

Sheen does observe that wider bandwidth reduces the speckle effect since it can resolve targets to within finer range bins. His paper on the speckle effect provides experimental evidence that imaging improves when moving from a 3 GHz bandwidth to a 12 GHz bandwidth. Using the radar system supplied, we did not have the capability to image as presented in Sheen’s paper, but what his results do confirm is that the magnitude of the backscattered field is a truer representation of its target when the bandwidth is increased and the speckle effect reduced. Sheen concludes that “narrowband or single frequency systems are most susceptible to speckle.” The radar system used for testing could certainly be described as narrowband given that its bandwidth – 306 MHz – is a mere 0.4% of its center frequency of 76.503 GHz. This prototype radar, which was well suited toward its original application of intelligent cruise control, does not have a bandwidth well-suited for detecting minute scatterer variations in a target. Being that the variations we wish to detect are 0.5 – 1.0” diameter pipes on a human body, this radar system is incapable of performing suicide bomber detection at this bandwidth [73].



The size of the beam also enhances the speckle effect. Because of a lack of range resolution, all fields are constructing and destructing within a range bin of 0.5 m. These fields are also coming from all the scatterers within a 0.37 m by 1.28 m area – see section 3.1.3.2. Sheen observes that the speckle effect can also be reduced by “tightly focusing the illumination over a small area” [73].

The speckle effect, this random constructive and destructive interference produced by multiple scatterers is the reason for the non-ergodic return. Therefore, it is the recommendation that further work in the area of long-range suicide bomber detection using MMW radar should be developed and tested with wider bandwidths and smaller beams.

3.1.7.2 Recommended Improvements to Current System

3.1.7.2.1 Bandwidth

The current bandwidth, as discussed in the previous section, results in only 0.5 m range bins. In order to improve this, the bandwidth should be expanded to the point that the range bins are of fine enough resolution to detect accurate reflections off the human body. If one considers that the pipes can be anywhere from 0.5” to 1.0” plumbing-type pipes, it would be desirable to use a radar with a bandwidth that results in a resolution of approximately 1.5 cm. According to section 3.1.3.1.4, this would require a bandwidth on the scale of 10 GHz. Using a bandwidth on this scale that results in small enough range bins to capture the reflections off small diameter pipes, is the only way to prevent the constructive and destructive interferences from the complex scatterers of the human body that prevent one from capturing an accurate return if interference (“speckle”) is the problem.

3.1.7.2.2 Gregorian Confocal Dual Reflector Antenna

As stated earlier, a smaller beam width lessens the speckle effect since the transmitted power is focused over a tighter area. A large beam, which is affected by the many constructive and destructive scattered fields from complex surfaces, gives one less information than a smaller beam. For instance, if a beam is focused to a width of three quarters of an inch, a 3/4” diameter metal pipe can be discerned more easily from skin. One problem when improving beam width is that it requires increasing the size of the antenna, see section 3.1.3.1.2. To focus the beam to a width of three inches in order to capture single metal objects, the testing distance of 10 m would necessitate an aperture antenna approximately 0.53 m (1’ 9”) square operating at 77 GHz with a parabolic current distribution according to equation 3.1-24. At 50 m, the desired stand-off detection distance, one would require an aperture 2.6 m (8’ 8”) square. These antennas, particularly the second, would be impractical for any mobile application and extremely expensive to build. One proposed method to reduce beam width is the Gregorian Confocal Dual Reflector Antenna (GCDRA), a diagram of which is shown in Figure 3-39.

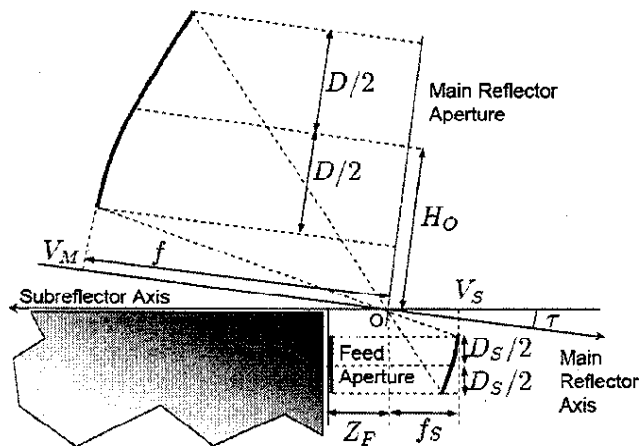
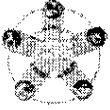


Figure 3-39. Gregorian Confocal Dual Reflector Antenna



The GCDRA works by virtually enlarging the aperture to obtain a smaller beam width in order to illuminate smaller areas at long ranges. The GCDRA consists of two reflectors, both of which are shaped as sections of parabolas whose vertices lie on the same axis and which share the same focal point. Referring to Figure 3-39, this means that both the sub reflector and the main reflector parabolas have their vertex on the central axis that lies a distance of H_{SO} above the center of the antenna, called the "Feed Aperture" and both of their focal points at "O." The parabolic sections are taken from the total parabola to the extents of illumination. The amount of magnification is the ratio between the main and sub reflector's focal points, or:

$$M = \frac{f}{f_s} \quad (3.1-27)$$

Additionally, Martinez has developed an algorithm to allow for scanning by the feed aperture. When the aperture scans to either side, the path length originating at either extremity of the aperture will be different, resulting in a moving focal point. This is accomplished by an optimized sub reflector whose geometry is not exactly parabolic. In this way, focus and gain problems can be eliminated in scanning [74].

The GCDRA is extremely useful for the BomDetec program's application, which requires long-range detection. Initially, the GCDRA was going to be designed and built for long-range testing, but, as mentioned in section 3.1.3.2.1, long-range testing never occurred. Using the example earlier of a three inch beam width, the GCDRA would require a magnification, "M," of 4.5 at 10 m or 22.5 at 50 m where the current testing aperture has a large dimension of 11.7 cm. These magnification requirements can be reduced for a larger aperture. In any case, the GCDRA would be useful in reducing the beam to a usable size in order to reduce the speckle effect.

3.1.7.2.3 Imaging

While it may be possible, using a wider bandwidth and the GCDRA to produce a smaller beam, to reduce the speckle effect to the point that one may see a significantly increased return when small metal objects are placed against the human body, it is believed that using those two improvements to develop a two-dimensional imaging scheme will be most useful. Current research has produced promising results using two-dimensional imaging, albeit at close ranges. It should be the goal of BomDetec, in future work phases, to attempt to adapt these technologies to longer ranges. Using the GCDRA, with an optimized sub reflector, a radar system with a square transmitter and receiver, electronic scanning, and a bandwidth in the 10 GHz range, one may develop a radar system that can record returns from multiple points of a human subject at long ranges and reassemble them into a useful image.

3.1.8 Conclusions

3.1.8.1 Feasibility of Provided Radar to Application

One cannot distinguish between an individual wearing or not wearing a non-uniform array of metal objects using MMW radar of single transmit/receive polarization at 77GHz with a bandwidth of 306 MHz. The original goal was to determine whether or not MMW radar, as a technology, was capable of detecting suicide bombers. The data presented have not proven this impossible. What the data show is that one cannot make this distinction using a radar system with the specifications of the one provided by Raytheon. The main limitations of this system are bandwidth, single polarization, and large beam especially inasmuch as they contribute to the speckle effect. It is also possible that at 77 GHz there is too little difference between the scattering from metal and the scattering from a human body. Further research should be done in accordance with the recommendations made in the previous section.

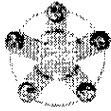


3.1.9 Bibliography

- [1] M. M. Hafez, Manufacturing Human Bombs: the Making of Palestinian Suicide Bombers, Washington, DC: United States Institute of Peace, 2006.
- [2] C. Reuter, My Life is a Weapon: A Modern History of Suicide Bombing, New Jersey: Princeton University Press, 2004.
- [3] CanWest News Service, "Attacks in Iraq deadlier," Edmonton Journal, 3 Apr., p. A4, 2007.
- [4] K. Cullen and C. M. Sennott, "Police suspect 4 Britons carried out suicide blasts," The Boston Globe, 13 Jul., p. A1, 2005.
- [5] E. Oziewicz, "Strategies honed in Iraq give Taliban a killer edge," The Globe and Mail, 5 Jul., 2007.
- [6] H. Östmark, S. Wallin, A. Pettersson, and H. Oser, "Real-time detection of IED explosives with laser ionization mass spectrometry," Stand-off Detection of Suicide Bombers and Mobile Subjects, Ed. H. Schubert and A. Rimski-Korsakov, Dordrecht, The Netherlands: Springer, 2006, pp. 35-50.
- [7] D. Novak, R. Waterhouse, and A. Farnham, "Millimeter-wave weapons detection system," Proc. 34th Applied Imagery and Pattern Recognition Workshop, 2005.
- [8] A. R. Hunt, R. D. Hogg, and W. Foreman, "Concealed weapons detection using electromagnetic resonances," Proc. SPIE Conference on Enforcement and Security Technologies, Boston, pp. 62-67, 1998.
- [9] A. S. Ibrahim, K. J. Liu, D. Novak, and R. B. Waterhouse, "A subspace signal processing technique for concealed weapons detection," IEEE ICASSP, pp. 401-404, 2007.
- [10] A. Kuznetsov and A. Evsenin, "MS-SRIP – Microwave system for secret standoff inspection of people," Stand-off Detection of Suicide Bombers and Mobile Subjects, Ed. H. Schubert and A. Rimski-Korsakov, Dordrecht, The Netherlands: Springer, 2006, pp. 5-9.
- [11] M. A. Slamani, M. Alford, D. Ferris, and V. Vannicola, "Comparison of a wide variety of concealed weapon detectors," Proc. SPIE, vol. 2942, pp. 82-93, 1997.
- [12] D. M. Sheen, D. L. McMakin, and T. E. Hall, "Three-dimensional millimeter-wave imaging for concealed weapon detection," IEEE Transactions on Microwave Theory and Techniques, vol. 49, no. 9, pp. 1581-1592, 2001.
- [13] D. M. Sheen, D. L. McMakin, H. D. Collins, T. E. Hall, and R. H. Severtsen, "Concealed explosive detection on personnel using a wideband holographic millimeter-wave imaging system," Presented at Pacific Northwest National Laboratory, Richland, WA.
- [14] J. C. Dickinson, T. M. Goyette, A. J. Gatesman, C. S. Joseph, Z. G. Root, R. H. Giles, J. Waldman, and W. E. Nixon, "Terahertz imaging of subjects with concealed weapons," Proc. SPIE Vol. 6212, 2006.
- [15] R. Doyle and J. McNaboe, "Stand-off detection of concealed improvised explosive devices (IEDs)," Stand-off Detection of Suicide Bombers and Mobile Subjects, Ed. H. Schubert and A. Rimski-Korsakov, Dordrecht, The Netherlands: Springer, 2006, pp. 77-87.
- [16] E. N. Grossman and A.J. Miller, "Active millimeter-wave imaging for concealed weapons detection," Proc. SPIE Vol. 5077, 2003.
- [17] J. Powell, H. Kim, and C. G. Sodini, "A 77-GHz receiver front end for passive imaging," IEEE Radio Frequency Integrated Circuits Symposium, pp. 145-148, 2007.
- [18] A. Agurto, Y. Li, G. Y. Tian, N. Bowring, and S. Lockwood, "A review of concealed weapon detection and research in perspective," Proc. IEEE International Conference on Networking, Sensing and Control, London, pp. 443-448.



- [19] S. Stanko, F. Klöppel, J. Huck, D. Nötel, M. Hågelen, G. Briese, A. Gregor, S. Erukulla, H. Fuchs, H. Essen, and A. Pagels, "Remote concealed weapon detection in the millimeter wave region: active and passive," Proc. SPIE Vol. 6396, 2006.
- [20] J. J. Lynch, J. N. Schulmann, and H. P. Moyer, "Low noise direct detection sensors for millimeter wave imaging," IEEE, pp. 215-218, 2006.
- [21] T. Rayner, M. Weida, M. Pushkarsky, and T. Day, "Remote explosive and chemical agent detection using broadly tunable mid-infrared external cavity quantum cascade lasers," Proc. SPIE Vol. 6540, 2007.
- [22] B. Zollars, B. Sallee, M. Durrett, C. Cruce, and W. Hallidy, "Concealed weapons detection using low-frequency magnetic imaging," Proc. SPIE Vol. 2935, 1997.
- [23] D. K. Kotter, L. G. Roybal, and R. E. Polk, "Detection and classification of concealed weapons using a magnetometer-based portal," Proc. SPIE Vol. 4708, pp. 145-155, 2002.
- [24] J. S. Heyman, A. Achanta, M. Hinders, K. Rudd, and P. J. Costianes, "Non-linear acoustic concealed weapons detection (CWD)," Proc. SPIE Vol. 5807, pp. 162-169, 2005.
- [25] P. K. Varshney, H. Chen, and R. M. Rao, "On signal/image processing for concealed weapon detection from stand-off range," Proc. SPIE Vol. 5781, pp. 93-97, 2005.
- [26] R. Blum, Z. Xue, "Multisensor concealed weapon detection by using a multiresolution mosaic approach," IEEE, pp. 4597-4601, 2004.
- [27] S. Lee, R. Rao, and M. Slamani, "Noise reduction and object enhancement in passive millimeter wave concealed weapon detection," IEEE ICIP, pp. 509-512, 2002.
- [28] P. Helistö, A. Luukanen, L. Grönberg, J. S. Penttilä, H. Sepä, H. Sipola, C. R. Dietlein, and E. N. Grossman, "Antenna-coupled microbolometers for passive THz direct detection imaging arrays," Proc. 1st European Microwave Integrated Circuits Conference, pp. 35-38, 2006.
- [29] M. Slamani, P. K. Varshney, R. M. Rao, and M. G. Alford, "Image processing tools for the enhancement of concealed weapon detection," IEEE, pp. 518-522, 1999.
- [30] B. R. Abidi, Y. Zheng, A. V. Gribok, and M. A. Abidi, "Improving weapon detection in single energy x-ray images through pseudocoloring," IEEE Transactions on Systems, Man, and Cybernetics, vol. 36, no. 6, 2006.
- [31] H. M. Chen and P. K. Varshney, "Automatic two-stage IR and MMW image registration algorithm for concealed weapons detection," IEEE Proc.-Vis. Image Signal Process., vol. 148, no. 4, pp. 209-216, 2001.
- [32] R. W. McMillan, N. C. Currie, D. D. Ferris, Jr., and M. C. Wicks, "Concealed weapon detection using microwave and millimeter wave sensors," IEEE, 1998
- [33] B. J. McCartin and J.F. Dicello, "Three dimensional finite difference frequency domain scattering computation using the control region approximation," IEEE Transactions on Magnetics, vol. 25, no. 4, pp. 3092-3094, 1989.
- [34] C. M. Rappaport and B. J. McCartin, "FDFD analysis of electromagnetic scattering in anisotropic media using unconstrained triangular meshes," IEEE Transactions on Antennas and Propagation, vol. 39, no. 3, pp. 345-349, 1991.
- [35] C. M. Rappaport, Q. Dong, E. Bishop, and A. Morgenthaler, "Finite difference frequency domain (FDFD) of two dimensional TE wave propagation and scattering," URSI EMTS, pp. 1134-1136, 2004.
- [36] C. M. Rappaport and A. Morgenthaler, "Scattering from dielectric objects buried beneath random rough ground: Validating the semi-analytic mode matching algorithm with two-dimensional FDFD," Proc. IGARSS Vol. 4, pp. 1634-1636, 2000.
- [37] C. M. Rappaport and E. B. Smith, "Anisotropic FDFD computed on conformal meshes," IEEE Transactions on Magnetics, vol. 27, no. 5, pp. 3848-3851, 1991.

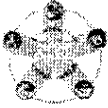


- [38] C. S. Lavranos and G. A. Kyriacou, "Eigenvalue Analysis of Curved Open Waveguides Using a Finite Difference Frequency Domain Method Employing Orthogonal Curvilinear Coordinates," Progress In Electromagnetics Research Symposium, Hangzhou, China, 2006.
- [39] F. Xu, Y. Zhang, W. Hong, K. Wu, and T. J. Cui, "Finite-difference frequency-domain algorithm for modeling guided-wave properties of substrate integrated waveguide," IEEE Transactions on Microwave Theory and Techniques, vol. 51, no. 11, pp. 2221-2227, 2003.
- [40] Y. Zhao, K. Wu, and K. Cheng, "A compact 2-D full-wave finite-difference frequency-domain method for general guided wave structures," IEEE Transactions on Microwave Theory and Techniques, vol. 50, no. 7, pp. 1844-1848, 2002.
- [41] S. Wu and E. N. Glytsis, "Finite-number-of-periods holographic gratings with finite-width incident beams: analysis using the finite-difference frequency-domain method," Journal of the Optical Society of America, vol. 19, no. 10, pp. 2018-2029, 2002.
- [42] M. Lui and Z. Chen, "A direct computation of propagation constant using compact 2-D full-wave eigen-based finite-difference frequency-domain technique," Proc. International Conference on Computational Electromagnetics and Its Applications, pp. 78-81, 1999.
- [43] S. Wu and E. N. Glytsis, "Volume holographic grating couplers: rigorous analysis by use of the finite-Difference frequency-domain method," Applied Optics, vol. 43, no. 5, pp. 1009-1023, 2004.
- [44] L. Kulas and M. Morozowski, "Reduced-order models in FDTD," IEEE Microwave and Wireless Components Letters, vol. 11, no. 10, pp. 422-424, 2001.
- [45] N. J. Champagne, J. G. Berryman, and H. M. Buettner, "FDFD: A 3D Finite-Difference Frequency-Domain Code for Electromagnetic Induction Tomography," Journal of Computational Physics, vol. 170, no. 2, pp. 830-848, 2001.
- [46] S. Guo, F. Wu, S. Albin, and R. Rogowski, "Photonic band gap analysis using finite-difference frequency-domain method," Optics Express, vol. 12, no. 8, pp. 1741-1746, 2004.
- [47] J. S. Reynolds, C. A. Thompson, K. J. Webb, F. P. LaPlant, and D. Ben-Amotz, "Frequency domain modeling of reradiation in highly scattering media," Journal of Applied Optics, vol. 36, no. 10, pp. 2252-2259, 1997.
- [48] C. Yu and H. Chang, "Compact finite-difference frequency-domain method for the analysis of two-dimensional photonic crystals," Optics Express, vol. 12, no. 7, pp. 1397-1408, 2004.
- [49] G. Mur, "Absorbing boundary conditions for the finite-difference approximation of the time-domain electromagnetic-field equations." IEEE Transactions on Electromagnetic Compability, vol. 23, no. 4, pp. 377-382, 1981.
- [50] E. L. Lindman, "'Free space' boundary conditions for the time dependent wave equation." J. Comput. Phys., vol. 18, pp. 67-78, 1975.
- [51] J. P. Berenger, "A Perfectly Matched Layer for the Absorption of Electromagnetic Waves," Journal of Computational Physics, vol. 114, no. 2, pp. 185-200, 1994.
- [52] J. P. Berenger, "Three-dimensional perfectly matched layer for the absorption of electromagnetic waves," Journal of Computational Physics, vol. 127, no. 127, pp. 363-379, 1996.
- [53] E. A. Marengo, C. M. Rappaport, and E. L. Miller, "Optimum PML ABC conductivity profile in FDFD," IEEE Transactions on Magnetics, vol. 35, no. 3, pp. 1506-1509, 1999.
- [54] C.M. Rappaport and S. Winton, "Using the PML ABC for Air/Soil Wave Interaction Modeling in the Time and Frequency Domains," Journal of Subsurface Sensing Technologies and Applications, pp. 289-303, 2004.
- [55] S. J. Al-Bader and H. A. Jamid, "Perfectly matched layer absorbing boundary conditions for the method of lines modeling scheme," IEEE Microwave and Guided Wave Letters, vol. 8, no. 11, 1998.



- [56] Y. S. Rickard and N. K. Niklova, "Enhancing the PML absorbing boundary conditions for the wave equation," IEEE Transactions on Antennas and Propagation, vol. 53, no. 3, pp. 1242-1246, 2005.
- [57] D. S. Katz, E. T. Thiele, A. Taflove, "Validation and extension to three dimensions of the Berenger PML absorbing boundary condition for FD-TD meshes," IEEE Microwave and Guided Wave Letters, vol. 4, no. 8, pp. 268-270, 1994.
- [58] T. Tischler and W. Heinrich, "The perfectly matched layer as lateral boundary infinite-difference transmission-line analysis," IEEE Transactions on Microwave Theory and Techniques, vol. 48, no. 12, pp. 2249-2253, 2000.
- [59] C. A. Balanis, Advanced Engineering Electromagnetics, New York, John Wiley & Sons, Inc., 1989.
- [60] A. Angell and C. M. Rappaport, "Computational modeling analysis of radar scattering by metallic body-worn explosive devices covered with wrinkled clothing," IEEE MTT-S International Microwave Symposium Digest, Honolulu, HI, 2007.
- [61] A. Angell, "Computational Modeling Analysis of Radar Scattering by Clothing Covered Arrays of Metallic Body-Worn Explosive Devices."
- [62] M. I. Skolnik, Introduction to Radar Systems, 3rd ed., New York: McGraw-Hill Companies, Inc., 2001.
- [63] C. A. Balanis, Antenna Theory Analysis and Design, 3rd ed. ed., Hoboken, New Jersey: John Wiley & Sons, Inc., 2005.
- [64] S. A. Hovanesian, Radar Detection and Tracking Systems, n.p.: Artech House, Inc., 1980.
- [65] M. E. Russell, A. Crain, A. Curran, R. A. Campbell, C. A. Drubin, and W. F. Miccioli, "Millimeter-wave radar sensor for automotive intelligent cruise control (ICC)," IEEE Transactions on Microwave Theory and Techniques, vol. 45, no. 12, pp. 2444-2452, 1997.
- [66] J. A. Martinez-Lorenzo and C. M. Rappaport, "Gregorian Confocal Dual Reflector Antenna for Active Millimeter-Wave Radar," Presented at BomDetec Radar Meeting. Boston, MA, 2006.
- [67] J. C. Toomay and P. J. Hannen, Radar Principles for the Non-Specialist, 3rd ed. ed., Raleigh, North Carolina: SciTech Publishing Inc., 2004.
- [68] I. I. Immoreev, "Feature detection in UWB radar signals," Ultra-Wideband Radar Technology, Ed. J. D. Taylor, Boca Raton, Florida: CRC Press LLC, 2001, pp. 21-46.
- [69] J.V. DiFranco and W.L. Rubin, Radar Detection, Englewood Cliffs, New Jersey: Prentice-Hall Inc., 1968.
- [70] C. R. Smith and P. M. Goggans, "Radar Target Identification," IEEE Antennas and Propagation Magazine, vol. 35, no. 2, pp. 27-38, 1993.
- [71] W. M. Boerner, H. Mott, and E. Lüneburg, "Polarimetry in remote sensing: basic and applied concepts," IEEE, pp. 1401-1403, 1997.
- [72] A. Germond, E. Pottier, and J. Saillard, "Bistatic radar polarimetry theory," Ultra-Wideband Radar Technology, Ed. J. D. Taylor, Boca Raton, Florida: CRC Press LLC, 2001, pp. 379-413.
- [73] D. M. Sheen, D. L. McMakin, and T. E. Hall, "Speckle in active millimeter-wave and terahertz imaging and spectroscopy," Proc. SPIE Vol. 6548, Ed. R. Appleby and D. A. Wikner, 2007.
- [74] J. A. Martinez-Lorenzo, C. M. Rappaport, R. Sullivan, and A. G. Pino, "A Bi-static Gregorian Confocal Dual Reflector Antenna for Bomb Detection Radar system," Presented at IEEE AP-S International Symposium, Honolulu, HI, 2007.

This page intentionally left blank.



3.2 Terahertz Sensor (RPI, Masashi Yamaguchi)

In the Terahertz sensor statement of work for phase I, we have promised to achieve the following goals.

- Development of library of terahertz spectrum of explosive materials (through 3 phases).
- Stand-off detection of explosive materials.
- Stand-off and real-time THz spectroscopic operation.

3.2.1 Summary

The Terahertz wave sensor in the BomDetec program is a real-time spectroscopic sensor of explosives and ERCs. Typical acquisition time for the THz spectrum is less than 1 second. This sensor is based on femtosecond laser technology, and is able to detect a target at stand-off distance. Currently, the sensor detects targets with material density as low as 25 mg/cm² at 3 m distance. As a part of BomDetec multi-modal sensor, The Terahertz sensor will be activated after the initial screening by intelligent video and radar sensors.

Terahertz electromagnetic wave has low energy and is a non-ionizing radiation. It is considered to safe to irradiate human body at the power level of the Terahertz sensor. A Terahertz wave is reflected by metallic objects but can penetrate through many types of dielectrics such as plastics, paper, and clothing. These features are particularly suitable for the detection of IEDs under clothing. However, Terahertz is strongly absorbed by water. The effects of this absorption on stand-off detection of explosives are specifically discussed later, and we will show that stand-off detection under water absorption conditions is feasible.

The Terahertz wave sensor is:

- Real time spectroscopic sensor of explosive materials
- (Data acquisition time <1 sec)
- Laser-based stand-off Terahertz spectroscopic system
- (Currently target distance up to 3 m)
- Able to detect chemicals with density of 25 mg/cm²
- Activated after the initial screening by video, and radar sensors.

Characteristics of Terahertz waves:

- Safe radiation (non-ionizing).
- Reflected by metal, and penetrates through dielectrics, such as many types of clothing, paper, and plastic materials.
- Absorbed by water

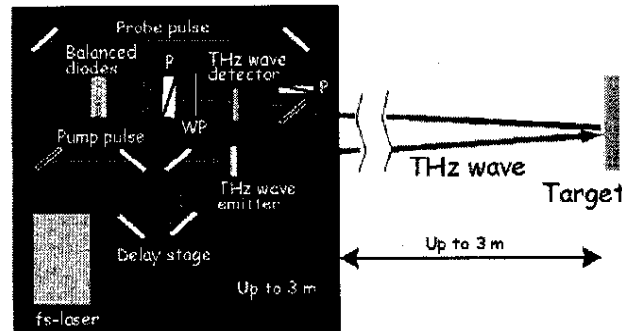
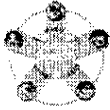


Figure 3-40a. Schematics of THz spectroscopy sensor

- Photonic-based THz wave generation and detection
- Pump-probe detection scheme
- Coherent detection: Both THz wave amplitude and phase are detected



3.2.2 Theory of operation

3.2.2.1 Generation and Detection of Pulsed Terahertz beam

Femtosecond laser pulses are used for the generation and detection of Terahertz wave. Laser pulses are split into pump and probe pulses. Pump pulse is used to excite Terahertz wave. Generated Terahertz wave propagates toward target, and reflected terahertz wave will be detected by the combination of Electro-optic crystal and balanced diodes. The relative timing between pump and probe pulses is changed by using optical delay line. In this detection scheme, both amplitude and phase of terahertz pulses are simultaneously observed. Currently, spectroscopic data from a target at the distance up to 3 m have been measured in real time (<1 sec).

3.2.2.2 Terahertz wave absorption by explosive materials

THz wave is absorbed by polar vibrational/rotational modes of explosive molecules in Terahertz frequency range. These modes have molecular specific frequencies and the absorption spectra can be used as molecular fingerprints. Since vibrational/rotational mode patterns are typically spread over larger area compared to (Mid) Infrared vibrational mode pattern. THz absorption peak frequencies are typically molecular specific while (Mid) Infrared absorptions are usually chemical bond specific and x-ray is atom specific.

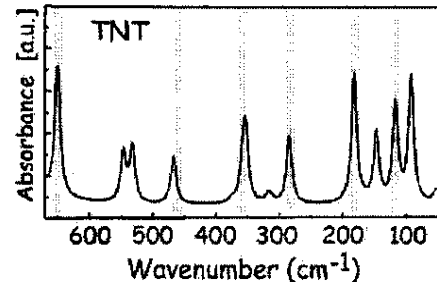


Figure 3-40b. THz wave absorption spectrum of TNT

3.2.2.3 Coherent detection and signal processing

THz wave is detected as a time domain signal using coherent detection scheme, and both of amplitude and phase are detected simultaneously. We can deduce molecular absorbance from either transmission or reflection measurement directly, while Fourier Transform Infrared Spectrometer typically requires Kramers-Kronig calculations to deduce absorbance from reflectivity data since the intensity of the infrared light is detected. Detected time domain wave form is will be Fourier Transformed and compared with reference data gives frequency dependent absorption, and phase spectra. If explosive material exists, the molecular specific absorption peak appears in the spectrum.

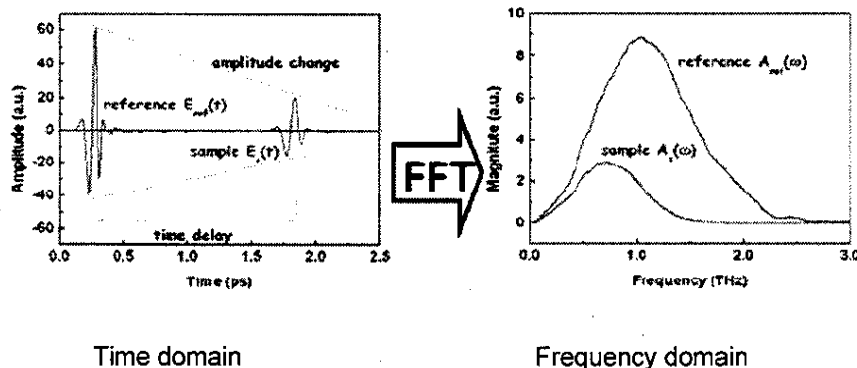


Figure 3-40c. THz wave form in time domain and its Fourier Transformed amplitude spectrum

- Changes of both amplitude and phase of THz pulses will be detected (Coherent detection)
- Frequency dependent reflectivity gives absorption spectrum



3.2.3 Capability and purpose

The most prominent feature of THz spectroscopic sensor is the capability of molecular identification. Particularly, a large number of explosives and ERCs have molecular specific features in the terahertz frequency range of electromagnetic spectrum, and these features can be used as an identifier of chemical species at stand-off distance. The figures below show some examples of THz spectrum of explosives.

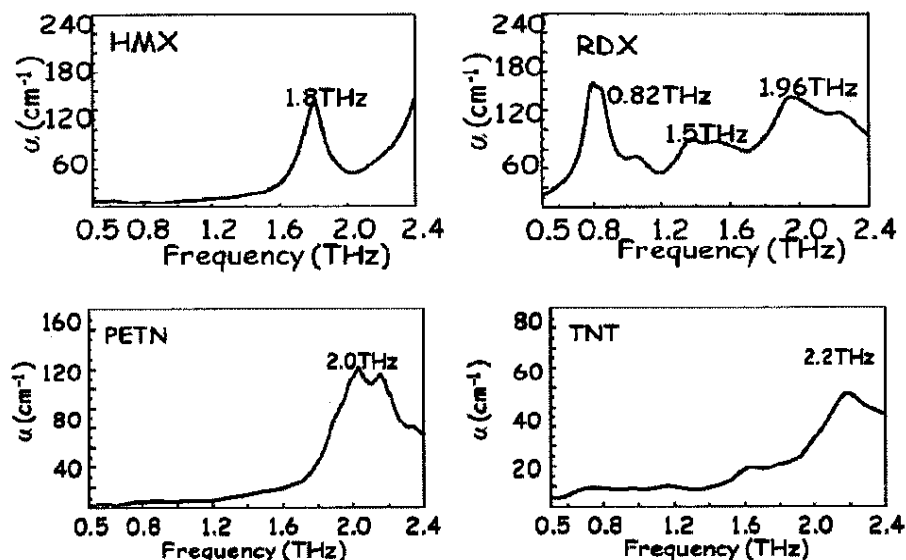


Figure 3-40d. Examples of THz spectrum of explosive materials.

Sensor capability: *Molecular Identification*

Purpose: *Identify explosives and ERCs at stand-off detection*

3.2.4 Activity highlights in Phase I

The following is a summary of the achievements of THz sensor development during phase I.

3.2.5 Building THz spectrum library

3.2.5.1 Explosives and ERCs

For the identification of chemical species, a comparison between the measured spectrum and library spectrum is necessary. Many explosives and ERCs have molecular specific features in THz spectrum.

Below are an example of THz spectrum of explosives and ERCs. We have tested 15 explosive materials, 12 of which have specific signatures in the 0.5-5THz range. We have also tested 12 ERCs, 10 of which have signatures in that frequency range. The names of the explosives and ERCs with and without specific signatures are shown in below.



Materials tested:

- Explosives : THz signatures found in TNT, RDX, HMX, PETN, Tetryl, TATP, HMTD, Nitroguanidine, Black powder, KClO_4 , 3,5-dinitro-aniline, 2-nitro diphenyl amine, but no signatures in Red dot, Ammonium Nitrate, KClO_3 .
- ERCs: THz signatures found in 2,3-dimethyl-2,3-dinitro Butane, 2,4-DNT, 2,6-DNT, 2-amino-4,6-DNT, 4-amino-2,6-DNT,, 4-NT, 1,3-DNB, 1,4-DNB, 1,3,5-TNB, 2,3-dimethyl-2,3-dinitro butane, but no signatures in 2-NT, 3-NT

Some of compounds tested did not show THz signatures in the frequency range of 0.5 THz -5THz. It does not necessarily mean that these molecules do not have THz signatures at all. It is possible that these molecules have THz signatures in higher frequency range than the frequency range of the test, it may be possible to detect such molecules in future when the bandwidth of THz emitter is improved. For example, micro-plasma based air THz emitter can generate terahertz wave up to 15 THz, which is three times wider spectrum range than the range used in the current test. Plasma based THz emitter is an emerging class of THz emitter, and it did not exist in the beginning of Phase I proposal. It is not unusual for THz technology to exhibit such drastic improvement since it is still a young and rapidly developing technology.

Figure 3-40e shows the examples of THz spectrum for explosives and ERCs. These spectra show distinct THz signatures, which can be used to identify these molecules. Also, the figure shows the examples of THz spectrum which shows distinguished spectrum for isomers. For example, 2,6-DNT and 2,4-DNT have identical chemical content, but have difference in the relative position of nitro and methyl groups attached to the benzene ring. THz spectra of these spectra are clearly distinguishable. This is because that vibrational motion in THz frequency range is related to spatially larger scale motion, such as intermolecular vibration, and low frequency phonons and sensitive to the change of surroundings of molecules when the configuration of nitro and methyl group is changed whereas vibrational modes observed in Mid-IR region is localized in bond or chemical group and generally not all peaks are sensitive to such changes and require the comparison of multiple peaks to distinguish isomers. These facts make THz spectroscopy a more suitable tool for the identification of explosives and ERCs.

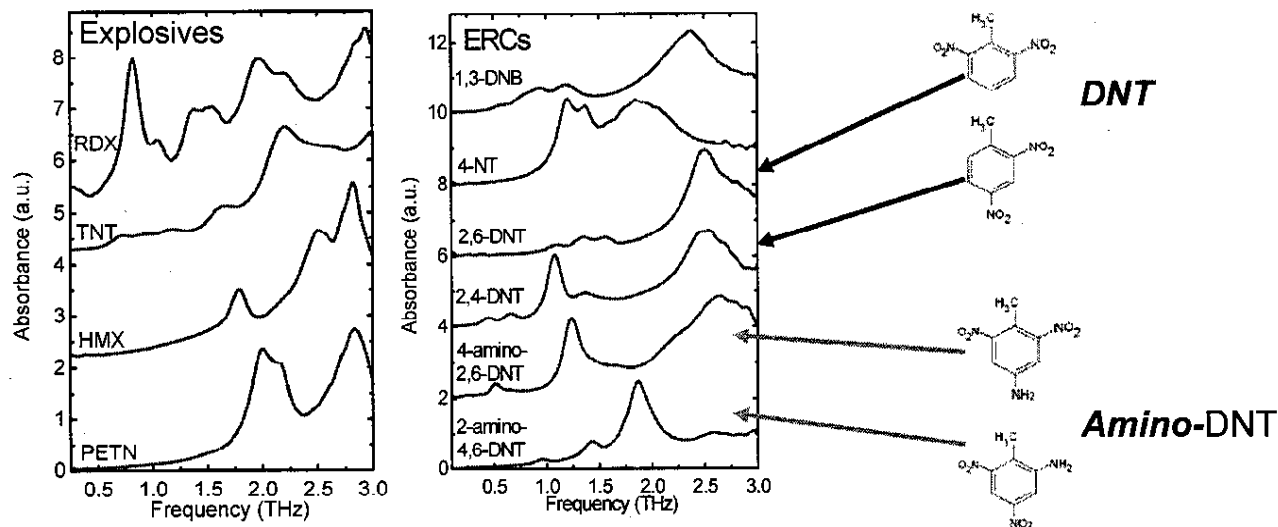
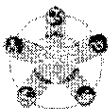


Figure 3-40e. THz signatures of explosives and ERCs. Isomers are clearly distinguishable in THz spectroscopy while Mid-IR absorption spectra of isomers tend to be similar. This is because vibrational peaks in Mid-IR range are localized in bond, and chemical groups, while THz signatures are mainly related to spatially larger scale motions such as intermolecular vibrations and low frequency phonons.

3.2.5.2 Non explosives

Many of polymeric materials, such as clothing do not have sharp features in the THz frequency range. This is because these materials typically have amorphous structures and do not show sharp phonon absorptions. This characteristic of terahertz transmission makes it extremely advantageous for us to use THz spectroscopy for the identification of explosives/ERCs underneath human clothing. Figures 3-41 and 3-42 show examples of such materials.

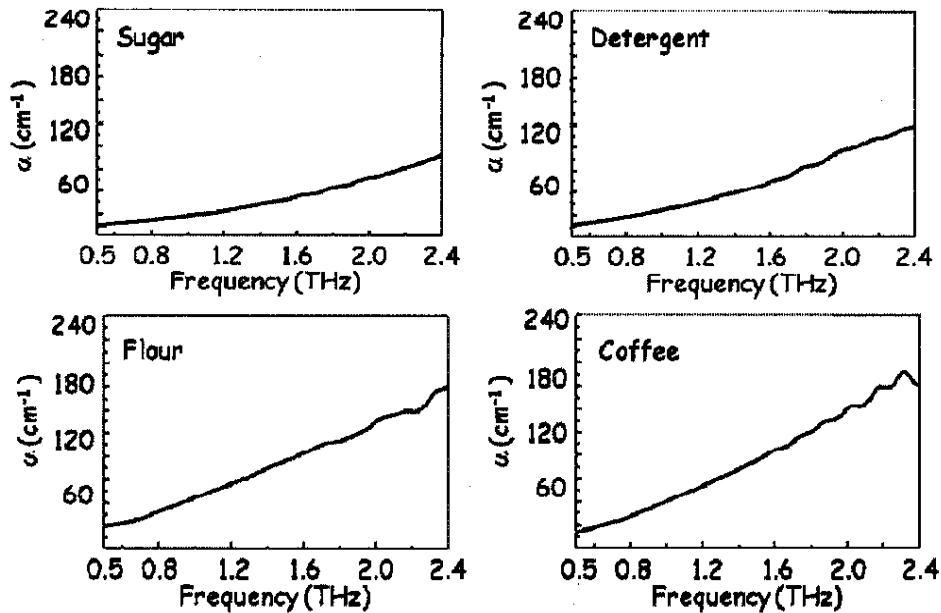
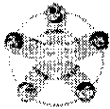


Fig 3-41. THz spectrum of non-explosive materials without signatures

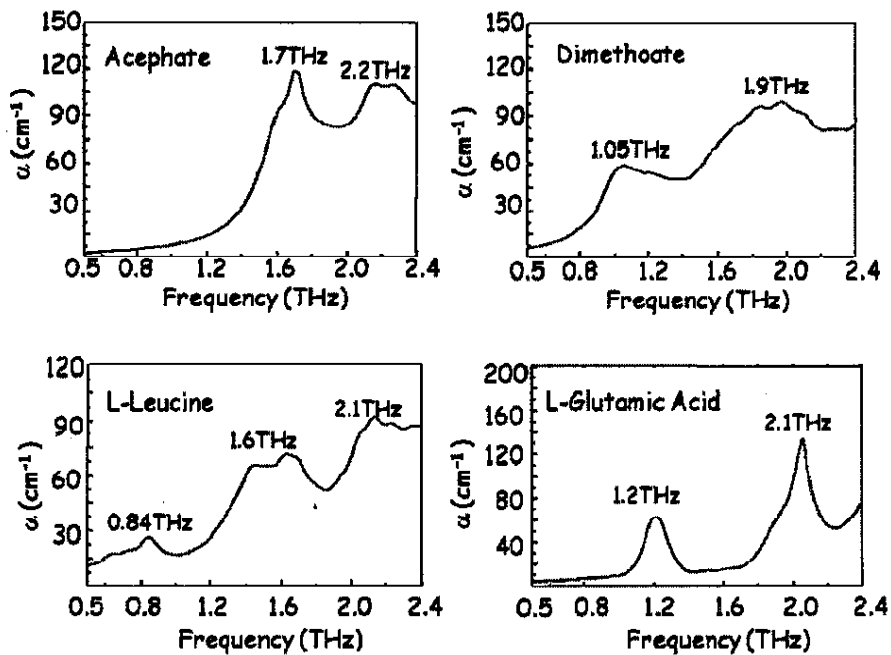


Fig 3-42. THz spectrum of non-explosive materials: Pesticides and biomaterials

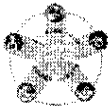


Figure 3-42 shows the examples of pesticides and biomaterials. They show clearly distinguishable THz signatures. These results demonstrate the possible usefulness of THz spectroscopy in chemical and biological not limited to explosive materials.

3.2.5.3 THz spectroscopy of RDX under cover

For suicide bomber detection, it is necessary to detect explosive materials in more realistic conditions. Initial tests of such conditions were performed using typical explosive material RDX under paper, polyethylene, and polyester covers to simulate clothing; figure 3.43 shows results. THz signature peak of RDX (0.82 THz) is clearly observable under different types of covers. Although RDX under Polymer, plastic covers tend to have broader spectral feature, *RDX signature peak at 0.82 THz is observable under different covers*. This series of experiments were performed in short distance and reflection geometry.

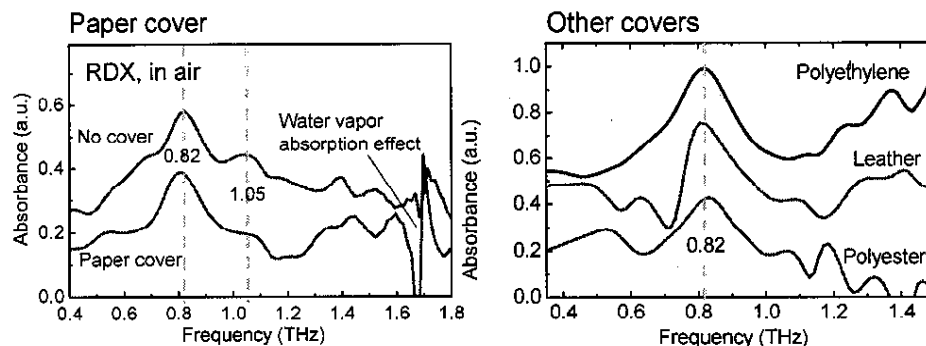


Figure 3-43. THz spectrum of RDX under cover. THz signature around 0.82 THz is observable under different kind covers.

Cover thickness

Paper: ~ 0.05 mm; Polyethylene: ~ 0.1 mm; Leather: ~ 0.3 mm;
Polyester cloth: ~ 0.4 mm.

3.2.5.4 Transmission of THz waves through real clothing

THz wave transmission through real clothing was tested. As similar to many of other polymer materials, clothing is largely transparent to THz waves. The main effect of clothing on the transmission of THz wave is (a) the shift of the pulse arrival time and (b) attenuation of THz wave amplitude.

Shift of arrival time:

The shift of the arrival time is due to the dielectric constant of clothing materials, and the effect of this is to add extra phase on Fourier components of pulse profile. However, this will be not affect the chemical identification since THz spectrum is related to the amplitude of THz wave, and is not related to the phase of the Fourier components.

The attenuation THz wave amplitude:

Attenuation of THz wave amplitude will decrease S/N in THz spectrum. This effect could be compensated by using higher power laser pump source as we will propose for Phase II. Also, many of clothing materials are amorphous materials, and these materials are known to have featureless broad spectrum (Figure in A-2) due to the disordered atomic structures of these materials. Superimposed these broad features on the THz signatures of explosive materials would not obscure the chemical identification and this is a favorable feature of THz spectroscopy for suicide bomber detection.

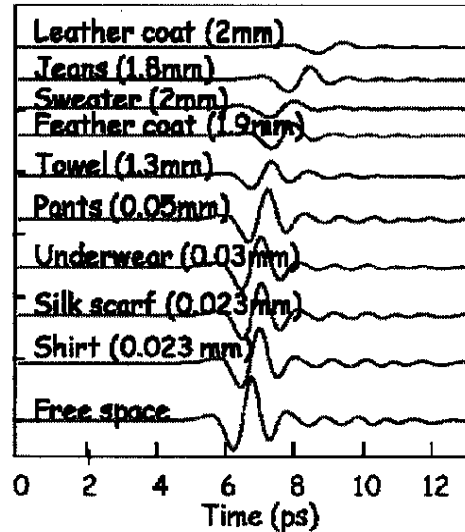


Figure 3-44. THz transmission of real clothing materials

Jeans: Route 66
Sweater: Mercury
Feather coat: Bossini
Pants: Great Land
Towel: 414
Underwear: Puma
Shirt: Basic Edition

3.2.5.5 Water absorption and THz spectrum

In this section, we try to minimize the effect of water absorption using reference signal of atmosphere. THz wave is strongly absorbed by water vapors in the atmosphere. These absorption lines cause sharp absorption features in THz spectrum, and they may interfere the extraction of THz signature from observed explosive spectrum. However, the absorption spectrum of water vapor is well known, and also it is straightforward to obtain reference water absorption spectrum at the location of the THz sensor.

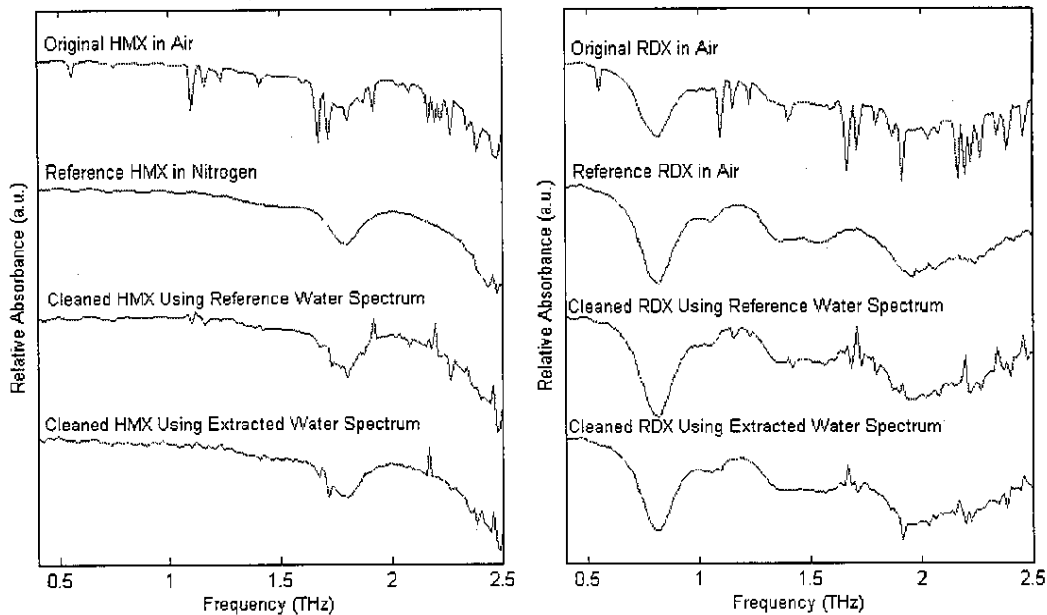
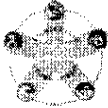


Figure 3-45. Elimination of water absorption peaks to increase the accuracy of chemical identification.

Figure 3-45 shows examples of eliminating water absorption peaks from HMX and RDX observed in the atmospheric condition. Top traces are water absorption line is superimposed on the explosive absorption spectrum. The second traces are THz spectra in nitrogen purged conditions. (no water absorption) Few different algorithms for elimination of water absorption peaks have been tested (3rd and 4th traces from the top). So far, an independent component analysis is the most efficient for this purpose. This part of the work will be further explored in future, and will be beneficial to extend the stand-off distance for the THz chemical identification.

3.2.5.6 Real-time and stand-off THz spectroscopic operation

Currently, Phase I configuration of THz spectroscopic sensor can be operated in real-time (<1 sec) for a target at stand-off distance (3m). Measurement is spectroscopic measurement, and we have observed a clear THz signature from the test sample (α -Lactose) in this real-time-stand-off THz spectrometer. A sample was placed in front of a metallic mirror to simulate a metallic object that a suicide bomber may have. The video taken of this test demonstrates the operation of stand-off THz spectroscopy. The left side of the panel shows the time domain signal, and the right side of the panel shows its Fourier spectrum. There is a distinctive dip in the spectrum due to the THz absorption by the sample (α -Lactose). The screen is refreshed every two scans, (real scan is twice faster) and the scanning time is currently limited by the data transfer time (electronics) and S/N is limited by the power of the laser source. We would expect faster operation and higher S/N after the software and laser source is upgraded in Phase II.



3.2.5.7 Sensitivity of stand-off THz spectroscopic sensor

Sensitivity of the THz sensor has been tested by measuring a target sample with different mass densities at stand-off distance of 3m and real time (<1 sec) scanning. α -Lactose was used as target material and was detected at the minimum mass density of 25 mg/cm^2 . The samples were homogeneously dispersed in a 3-inch diameter paraffin disk with different densities. Figure 3-46 shows a dip in the middle of Fourier spectrum of the time domain THz spectroscopy signal as indicated by an arrow. This dip is a THz signature of α -Lactose (at 0.5 THz). This absorption peak was observed in a real time single scan at stand-off distance of 3m, the spectrum in the figure is averaged 10 times for clarity. This sensitivity is limited by S/N and the mechanical stability of optical delay stage used in the current configuration of THz sensor subsystem. The sensitivity is expected to increase at least an order when the S/N ratio and the mechanical stability are improved by the use of higher optical pumping power and higher stability stages as we proposed as task in phase II.

THz signature of α -Lactose at 3 m

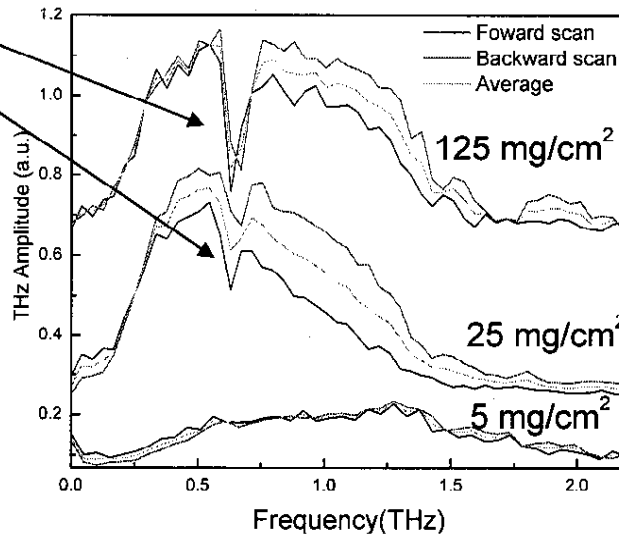
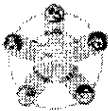


Figure 3-46. Sensitivity of THz spectroscopic sensor. α -Lactose sample with density of 25 mg/cm^2 has been observed at 3 m distance real time operation (<1sec). The spectrum in the figure is averaged 10 times for clarity.

3.2.5.8 Derived confidence level

Chemical identification using the real-time stand-off THz spectrometer has been demonstrated and the confidence level of the identification has been derived. A chemical target was placed at a distance of 3 m and measured in real time operation. The measured spectrum was compared with the reference spectrum taken with short target distance. Cross correlations of between measured spectrum and reference spectrum of various chemicals were compared.

In the figure below, α -Lactose was used as a sample for the real time stand-off detection. Figure 3-47(a) is for the THz spectral measurement of α -Lactose at 3m with a single scan (acquisition time <1 sec), and Figure 3-47(b) shows the result of average scan for the same target (at 3m) with average scan (10 times, acquisition time <10 sec). The measured THz spectra are compared with the spectra of 5 different chemical species. For both measured spectra, the cross correlation values show the highest match with α -Lactose reference. The cross correlation value indicates the confidence level of identification. The cross



correlation value increases from 0.38 to 0.78, when the signal is averaged for 10 times. This result of the average scan simulates future performance when the signal to noise ratio is increased.

It is preferable for the correlation values with materials other than α -Lactose be as small as possible. There are several possible algorithms to use for identification of chemical species in the future including cross correlation and partial least square methods. To identify a more suitable algorithm is a future task in Phases II and III.

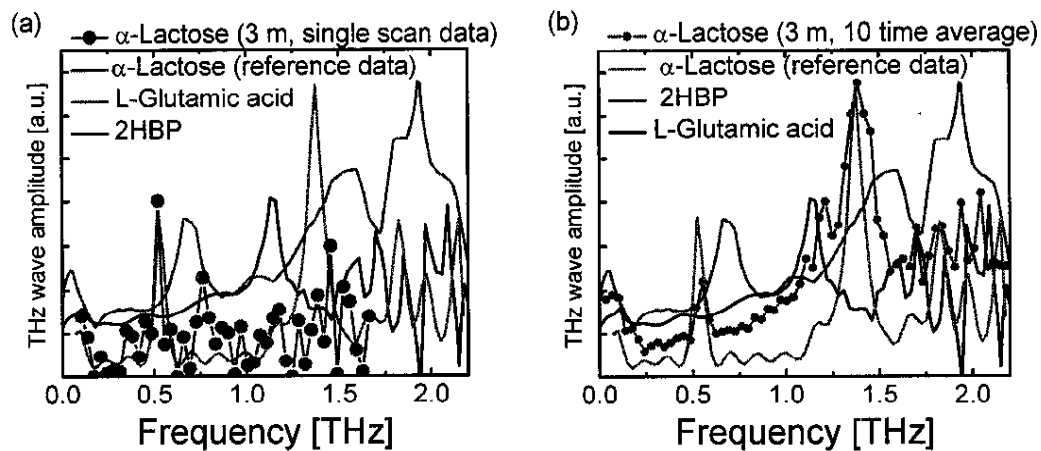


Figure 3-47. Comparison of THz spectra of α -Lactose measured in real-time-stand-off THz spectrometer, and 3 kinds of library signals. (a) Single scan data (acquisition time <1 sec) (b) 10 times average (acquisition time < 10 sec)

Cross correlation of measured α -Lactose spectra and reference spectrum

	Lactose	2HBP	L-Glutamic Acid	RDX	Theophyline
Average lactose (10 times)	0.7810	0.4716	0.1499	0.4389	0.4890
Single Scan	0.3365	0.1542	0.0285	0.1869	0.0765

3.2.5.9 THz wave propagation in the atmosphere

THz wave propagation at a stand-off distance has been tested to observe the effects of water vapor in the atmosphere. THz wave propagates through the atmosphere and is reflected from a mirror target. The measurement is done with averaging a waveform for a few minutes. Target distances of 3, 5 and 11 m have been successfully observed (THz wave path lengths are 6, 10 and 22 m). Fourier spectrum shows sharp absorption peaks due to water vapor absorption; see Figure 3-48 for results. Although these measurements are not done in a real time operation, it shows possible real time performance when the signal-to-noise ratio is improved in the future.

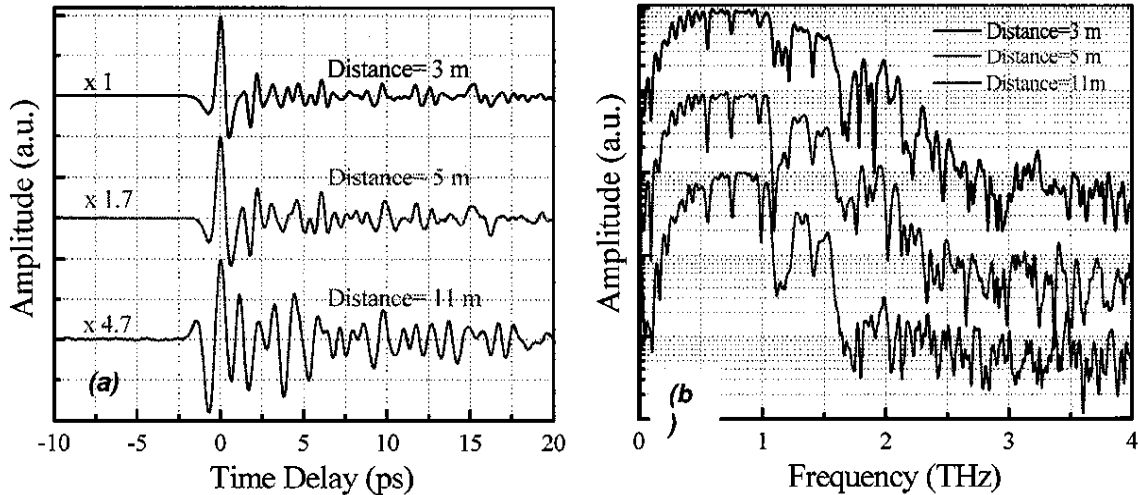
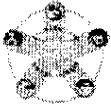


Figure 3-48. THz wave propagation in atmosphere. THz wave is reflected from mirror target at distance of 3m, 5, and 11 m away. (Path length 6, 10, and 22 m) (a) Time domain signal and (b) Fourier spectrum

3.2.5.10 Future performance

Although the Phase I study showed the powerful ability of chemical “identification” and also the feasibility in the propose sensor suite configuration, current performance of the THz sensor can be improved greatly. This is because THz sensor specification envelope is coming from S/N and mechanical stability. These two factors are mainly limited by the performance of instrumental components used in the current THz sensor system and can be improved by introducing newly developed technologies. Many of these technologies did not exist at the time of our Phase I proposal. Possible further improvements and future performance are listed below; a large factor of performance improvement is not unusual for the development of THz instruments, since THz technology is still a young technology and rapidly developing.

- Improvement of S/N ratio >10-100 times: use of newly available high repetition rate and higher power fiber laser, (IMRA FCPA μ Jewel D-1000) (current pump energy 1.3 nJ at 75MHz \rightarrow 1 μ J 1MHz) (IMRA)
- Improvement of S/N ratio >8-10 times: use of developed antenna detector with Si lens, higher S/N >8-10 times. (RPI)
- Improvement of mechanical stability: use of integrated optics mounts and body by high impact resistance stereo lithography materials.(Design Prototyping technologies)
- Improvement of mechanical stability and repeatability (18 μ m \rightarrow 1.8 μ m): use of newly available fast and stable commercial mechanical stage with piezo ultrasonic motor (Nanomotion LTD, FB100).
- Integration of chemical identification algorithm, and fast data transfer scheme: improved acquisition time, and improved derived confidence level.(RPI)



3.2.5.11 Operating Envelope

Significant reduction of sensor size, weight, and power consumption has been achieved during Phase I. This is mainly achieved by changing the sensor design from Ti-Sapphire amplifier base system (high power low repetition rate) to Er:doped fiber oscillator system (low power high repetition rate). A fiber laser-based system has advantages in weight, size, power consumption, and mechanical stability. Environmental characteristics are mainly limited by the laser itself, and can be improved by local shielding of laser oscillator.

3.2.5.12 THz sensor control software

Data structures:

- Spectrum: X-Y Text data. (1K points)
- Time domain data: X-Y text data (1K points)
- Threshold level(s): Real number (%)
- Chemical Name(s): String

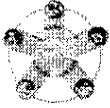
Events & status:

- Input
 - Inquiry of sensor status, (ok, busy, search, error)
 - Sensor on, off
 - Initialize sensor
 - Request data
 - Analysis method
 - Threshold level
 - Target coordinate
- Output
 - Sensor status
 - Spectral data
 - Time domain waveform data
 - Threat level
 - Name(s) of chemicals

3.2.6 Summary of phase I accomplishment of Terahertz sensor

1. Real-time: < 1 sec THz spectroscopic operation at stand-off distance (3 m) was achieved (Acquisition time is limited by software and data transfer).
2. Sensitivity for spectroscopic measurement: 25 mg/cm² at 3 m distance.
3. Explosive detection: 22 out of 27 ERCs with THz resonance.
4. Met weight, size and power requirements established by AS&E.

This page intentionally left blank.



3.3 Backscatter X-ray Sensor (AS&E, (b) (6))

3.3.1 Executive Summary

Backscatter x-ray imaging systems are robust and user friendly. They are currently deployed in both domestic and international markets and are operated in the field by specialized users such as police bomb squads. The backscatter sensor's ability to identify organic material anomalies (explosive elements on a suicide bomber) by presenting an easily interpreted "photographic like" x-ray image to the operator and its ability to operate outdoors under a variety of weather conditions makes it an ideal and integral part of the BomDetec system.

The backscatter sensor's proven performance in the field makes it so the operator can formulate a more informed decision when confronted with a Suicide Bomber.

3.3.2 What are Backscatter x-rays

Z® Backscatter excels in the detection of organic or "low Z" materials and the photographic quality images revealed provide context and clarity.

- Organic materials (containing low atomic number elements) scatter better than materials containing high atomic number elements (e. g. metals)
- AS&E collects the scatter and knows where it came from
 - Patented "Flying Spot" x-ray beam
 - The x-ray Fan Beam is Converted to a Rastering Pencil Beam by a "Chopper Wheel"
 - "Flying Spot" Interrogates a Only a Very Small Portion of the target at a Time (typical Spot Size is 1 - 2mm)
- The resulting image preferentially highlights low atomic number materials and produces a "photo-like" representation. This image is easier to read and interpret than a radiographic image.
- All Matter Is Made Up Of One Or More Of The Elements
- Elements are Organized by Atomic Number, Z, for the Number of Protons
 - The Small Number Above The Element Abbreviation
- Generally, Backscatter x-ray "sees" Material in the Low Z Range, Unlike Standard Transmission x-ray (see figure 3-49 below).

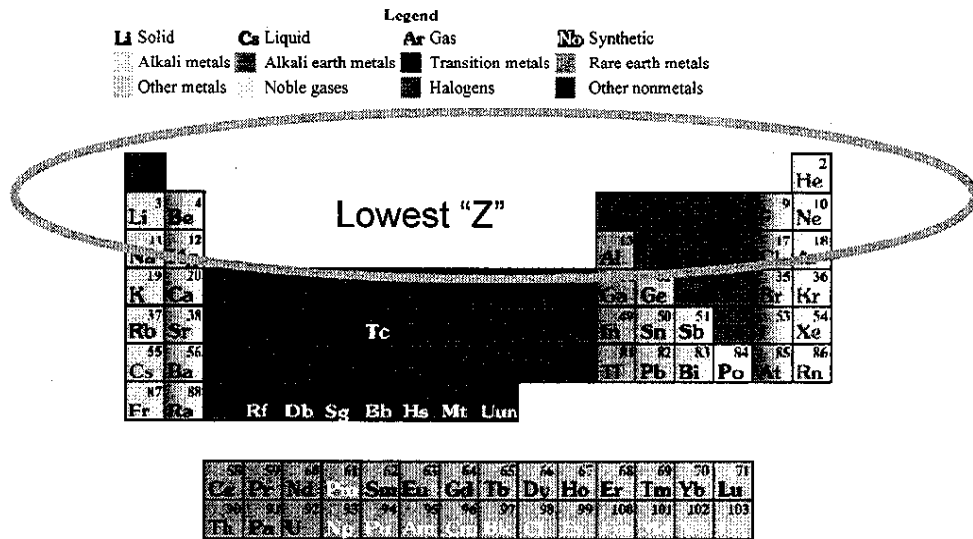
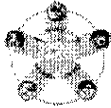


Figure 3-49

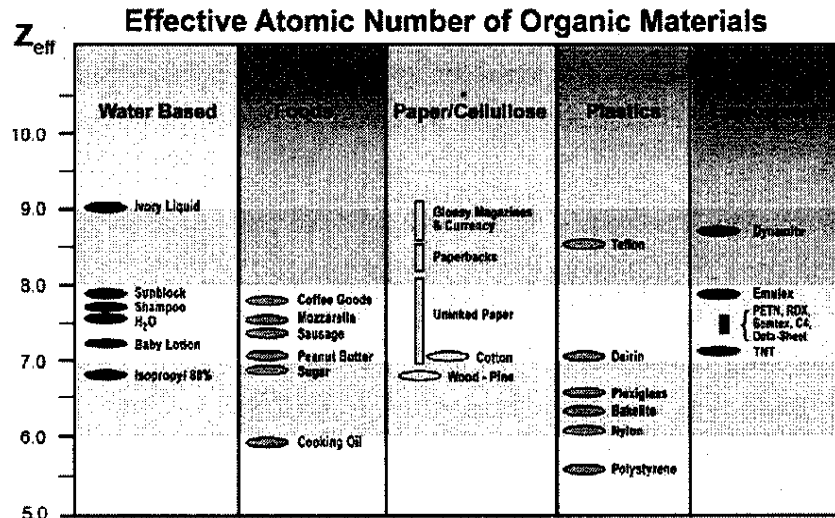


Figure 3-50. Overview Of Effective "Z" Numbers For Organic Materials

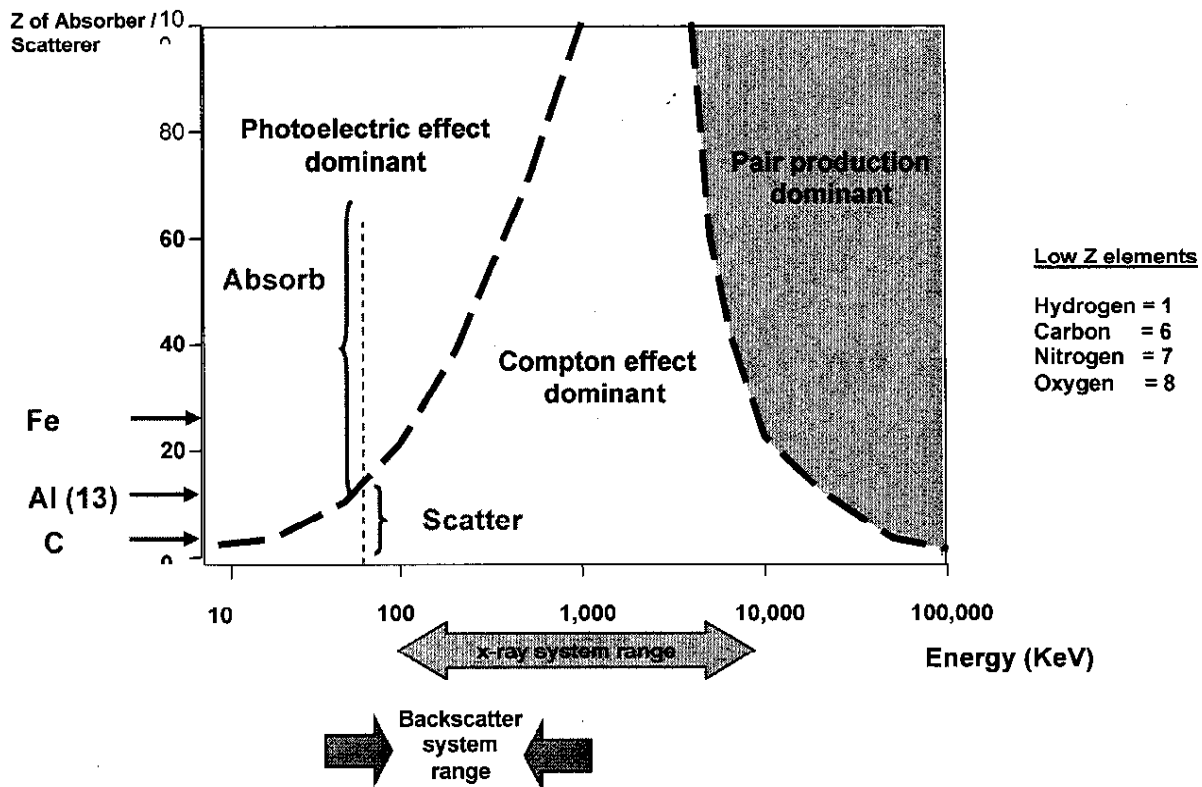
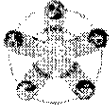


Figure 3-51. Compton Backscatter Dominant for Low Z Materials over Most of the Spectrum

- How x-rays work
 - x-ray Energy Will Do One Of Three Things When Interacting With Material
 - Become Absorbed (Absorption)
 - Pass Through (Transmission)
 - Scatter (Compton Scattering)
- These Basic Principles form the Basis of x-ray Imaging
 - Transmission x-ray Imaging
 - Absorption / Transmission
 - Z Backscatter x-ray Imaging
 - Compton Scattering

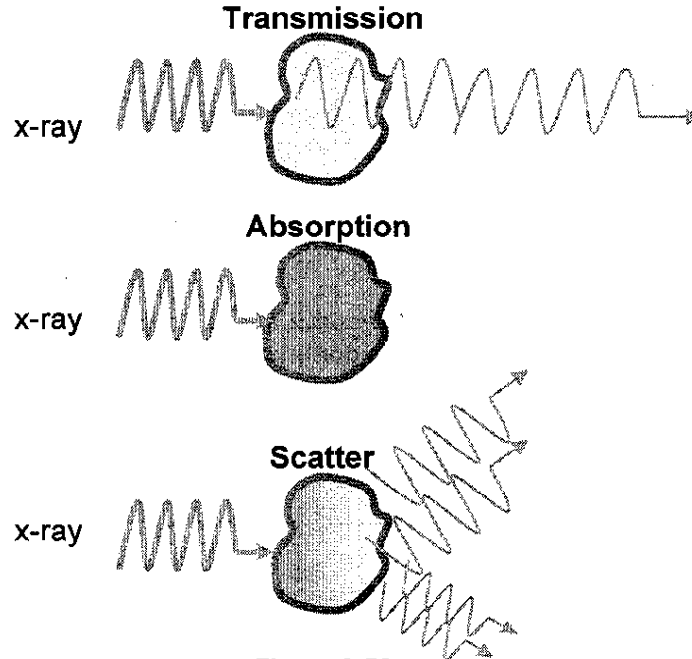


Figure 3-52

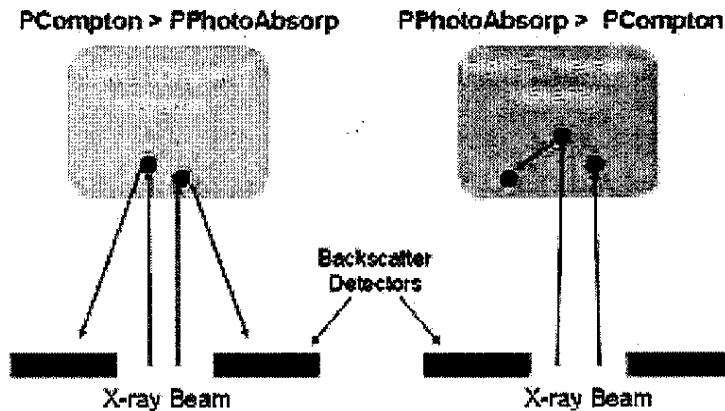


Figure 3-53

3.3.3 Backscatter x-ray Imaging

Backscatter x-ray imaging is a unique x-ray imaging technique whereby the x-rays scattered (or reflected) from an object in the backward direction are detected, rather than detecting the x-rays transmitted through the object. In the more common x-ray transmission method, an x-ray source is placed on one side of the object being inspected and an x-ray transmission detector is placed on the opposite, far side of the object. These x-ray transmission images show regions of high x-ray attenuation, which typically correspond to metallic materials (high atomic number or high-Z materials) or to thick objects with a high density.



One advantage of backscatter imaging is that the backscatter x-ray detectors can be placed on the same side of the object being inspected as the x-ray source, allowing for "one-sided inspection" to be carried out, as opposed to transmission radiography which requires an x-ray detector on the far side of the object. This allows backscatter images of the contents of vehicles or cargo containers to be taken by mounting the detectors and x-ray source on a mobile platform that drives past the objects of interest. Such systems are particularly useful in environments where access to the far side of the object is limited, making transmission x-rays impractical or impossible.

A second advantage of backscatter radiography is that the images highlight organic materials, which scatter x-ray photons much more intensely than metallic or non-organic objects. This means that organic threats or contraband materials such as explosives and drugs can be more easily detected in the backscatter images than in the corresponding transmission images.

Backscatter images are also photographic in nature. They are typically easier to interpret.

3.3.4 How an x-ray Beam becomes an Image

A sealed chamber is lined with scintillating material and equipped with a number of Photo-Multiplier Tubes (PMTs). Incident x-rays illuminate the ^{(b) (4)} in the scintillating material, creating light. The PMTs sense the light and output a DC signal.

- The PMT HVPS supplies high voltage DC power to the PMTs in each backscatter detector. The output of the PMT HVPS is split and fed into the Potentiometer Box behind each detector array.
- The PMT HVPS converts 24 V DC input via a step up switching voltage regulator that generates approximately ^{(b) (4)}
- The output of the PMT HVPS is split across the inputs to two "tuning" boxes equipped with multiple potentiometers. The potentiometers can be adjusted to vary the output voltage sent to individual PMTs in the detector assemblies. Adjusting the voltage allows a technician to electrically "tune" the images coming from the detectors.

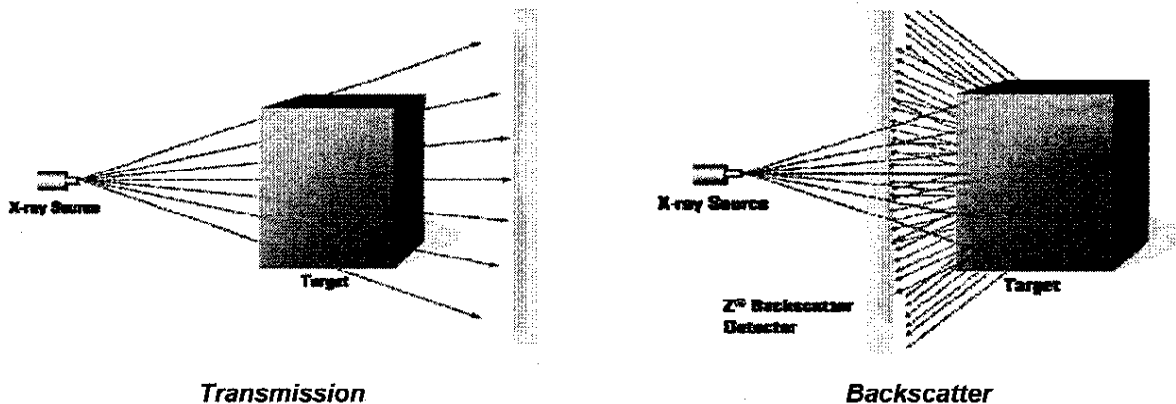


Figure 3-54

- A Pencil beam of X-rays is created and scanned in a line scan traversing a target
 - Scan is performed by selecting rays from a fixed fan beam by means of a rotating collimator
- Detectors (on the same side of the object as the X-ray source) collect Compton scattered X-rays



- Scattered X-rays are collected as the beam scans, pixel-by-pixel
- At each instant, the scattered beam intensity is measured and displayed. Each time a rotating collimator traverses target object, 1 line of scatter data is produced
- As the target object moves, new lines are displayed, building up a 2-D image

The beam formation geometry shown below describes how the system scans from one end of the fan to the other. The beam spot is shaped by the overlapping collimator and slots in the chopper wheel (referred to as 'jaws'). Therefore, it has a rectangular shape when the wheel slot is horizontal, at the center of the scan, and a trapezoidal shape at all other wheel angles. The trapezoid is most extreme at either end of the scan.

- Organic Low atomic number elements materials (e. g. plastics) are better than materials containing metals
- The resulting image preferentially highlights high atomic number materials and produces a "photolike" representation

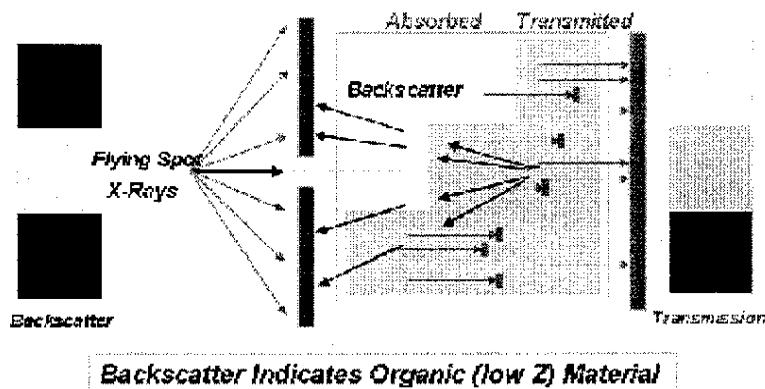


Figure 3-55



3.3.4.1 Five things affect the Lightness/Darkness of the Backscatter Image

- Atomic weight of material being scanned (Z)
 - Higher atomic weights create a darker image (gold 79)
 - Lower atomic weights create lighter image (aluminum 13)
- Thickness of material being scanned
 - The more material x-rays can scatter off of, the lighter the image (10 cm)
 - The less material x-rays can scatter off of, the darker the image (1 cm)
- Density of material being scanned
 - The more compressed the material is, the brighter the image (chocolate)
 - The less compressed the material, the darker the image (cotton candy)
- Proximity to the Backscatter Detector
 - The closer to the detector, the brighter the image
 - The further away from the detector, the darker the image
- Shielding between the organic target and the backscatter detector
 - A sheet a paper between the organic and detector will give a bright image
 - A lead block between the organic and detector will absorb all refracted x-rays give a dark image

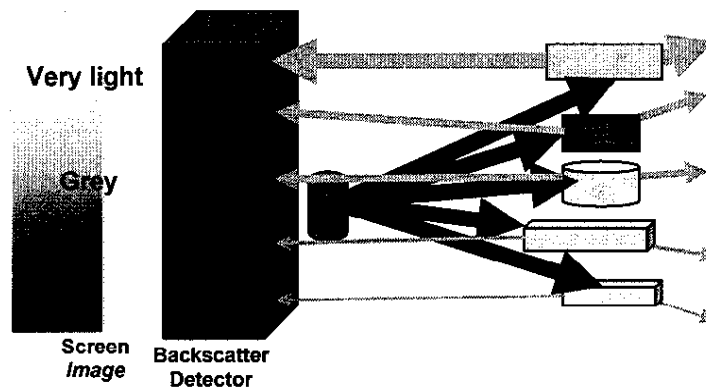
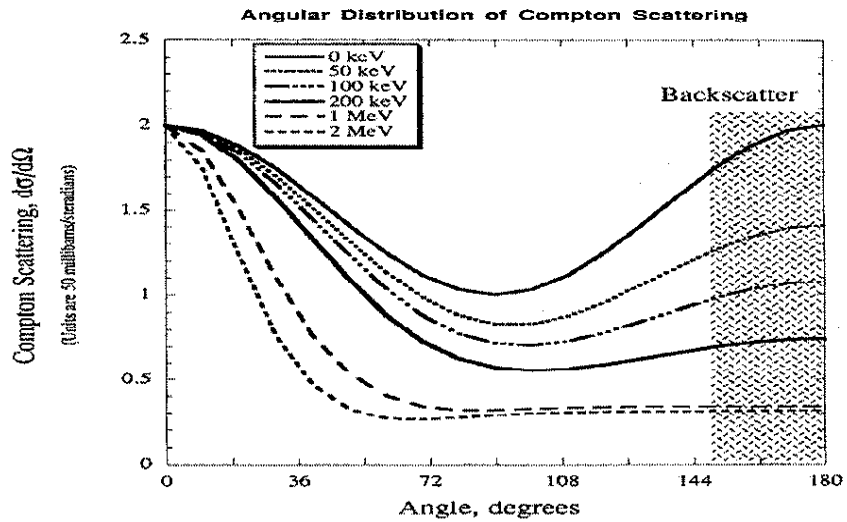


Figure 3-56



3.3.4.2 Standard Transmission Image (Golden Tube)

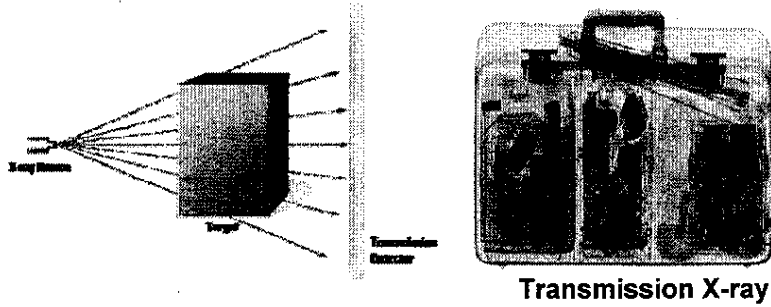


Figure 3-58

3.3.4.3 Backscatter Image

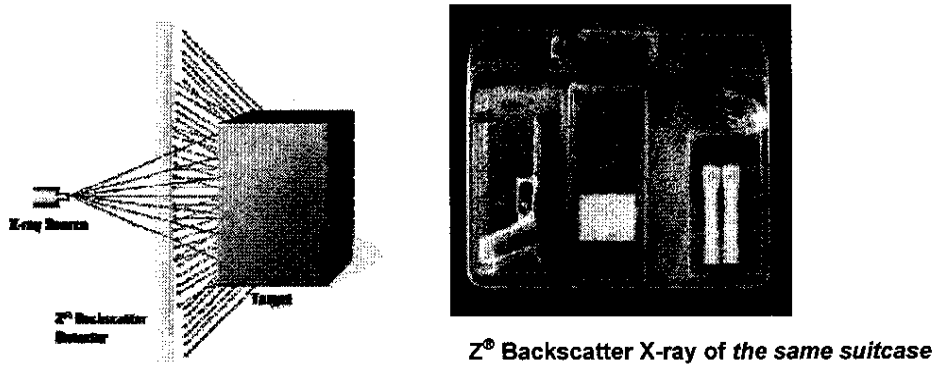
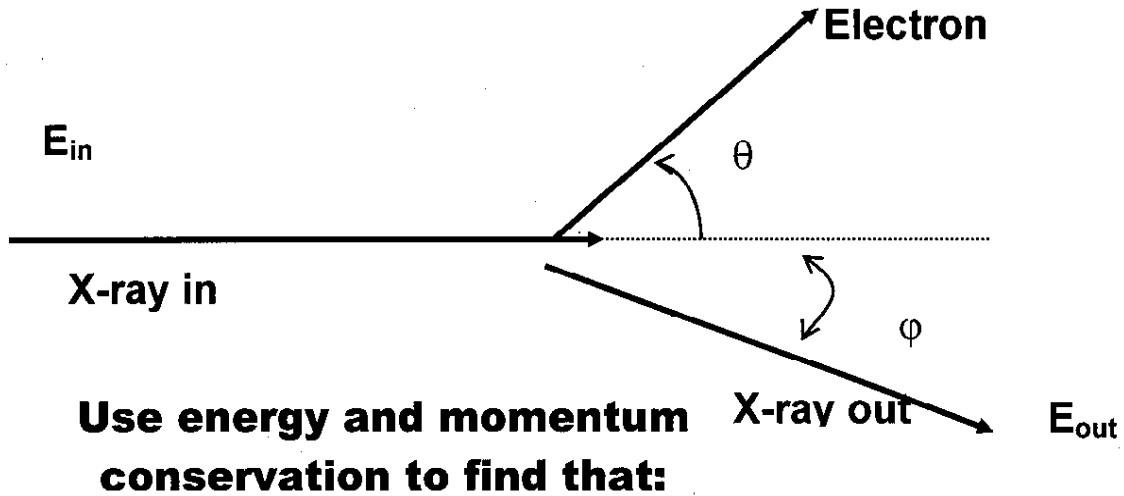


Figure 3-59

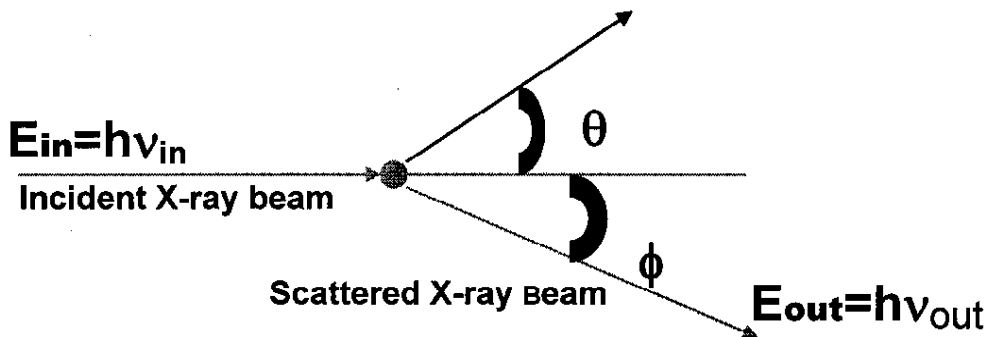


3.3.4.4 Definition of Compton Scattering



$$E_{out} / E_{in} = 1 / (1 + \alpha (1 - \cos\phi))$$

where $\alpha = E_{in} / m_e c^2$



Energy Conservation: $h\nu_{in} + m_e c^2 = h\nu_{out} + E_{electron}$

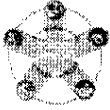
Momentum conservation:

$$h\nu_{in}/c = (h\nu_{out}/c) \cos \phi + p_{electron} \cos \theta$$

$$0 = (h\nu_{out}/c) \sin \phi - p_{electron} \sin \theta$$

$$E_{out} = E_{in} / (1 + \alpha (1 - \cos\phi))$$

where $\alpha = E_{in} / m_e c^2$



Note that: $mec2$ is a constant = 0.511 MeV

Interesting Point: when ϕ is 180 degrees,

$$E_{out} = E_{in} / (1 + 2\alpha) = \alpha mec2 / (1+2\alpha)$$

So for $\alpha \gg 1$, $E_{out} < mec2/2$

No matter how large E_{in} is, E_{out} can never be larger than $mec2/2$, or 255 keV, in the backward direction

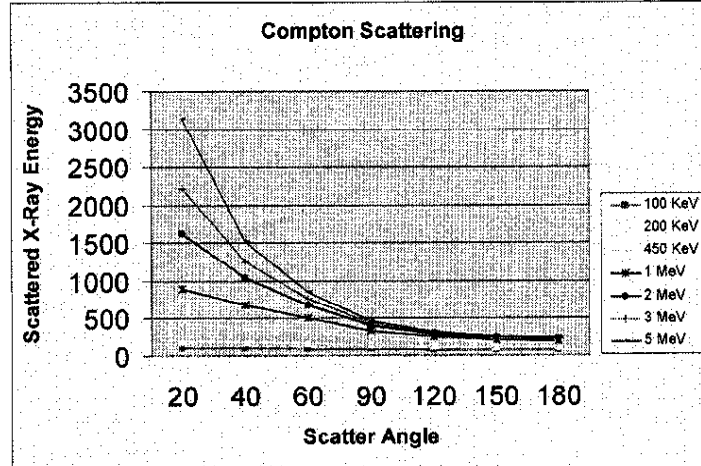


Figure 3-60. Scattered x-ray Energy vs. Angle for Different Incident Energy x-rays

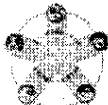
The effect of penetration of a backscatter system can be quantified by simulating the level of backscatter signal from a simple plastic X-ray scatter target placed behind a sheet of steel. The Signal to Noise ratio (SNR) of the backscatter signal from the plastic target is defined as follows:

$$SNR = \frac{N_{Plastic\ target} - N_{No\ plastic\ target}}{\sqrt{N_{No\ plastic\ target}}} \quad (3.3-1)$$

where $N_{Plastic\ target}$ and $N_{No\ plastic\ target}$ are the number of detected backscattered x-ray photons with and without the plastic target present, respectively. The term in the denominator comes about because the probability of detection of the backscattered x-rays follows Poisson statistics, and the expected fluctuation (or noise) in the detected signal is equal to the square-root of the number of detected x-ray photons. The value of the signal to noise ratio therefore determines how visible the plastic target will be in the backscatter image, given the expected fluctuation in the backscatter signal coming from the steel and from air-scatter.

The SNR is calculated for a set of different steel thicknesses for each of five primary beam energies. The first three lines in the table show how the SNR falls exponentially with increasing steel thickness. The practical limit of penetration will depend on the details of the object being inspected. For example, in the test in one can see 4-6mm of steel penetration. The final five lines of the table show, for a range of energies, steel thicknesses that produce an SNR of 5.0, which roughly corresponds to the experiment in. a 140 kV system will penetrate about 40% more steel than a 120 kV system with the same flux. If a 120 kV backscatter system images a given object behind a given thickness of steel, then a similar 140 kV system will produce the same image quality through a 40% greater thickness of steel.

- SNR is defined in equation 3.3-1. The SNR is calculated for 5×10^6 X-rays in the incident beam, with the x-ray energy distribution of the beam sampled from Bremstrahlung spectrum with the relevant endpoint energy, using 2.5mm of Aluminum filtration.



Performance of the backscatter radiography system will vary from one image to the next due to the large number of parameters that can be customized for each scan, including choice of scan time, and scan area. The quality of the image also ultimately depends on the thickness and composition of any intervening material between the backscatter system and the object of interest.

THE ELECTROMAGNETIC SPECTRUM

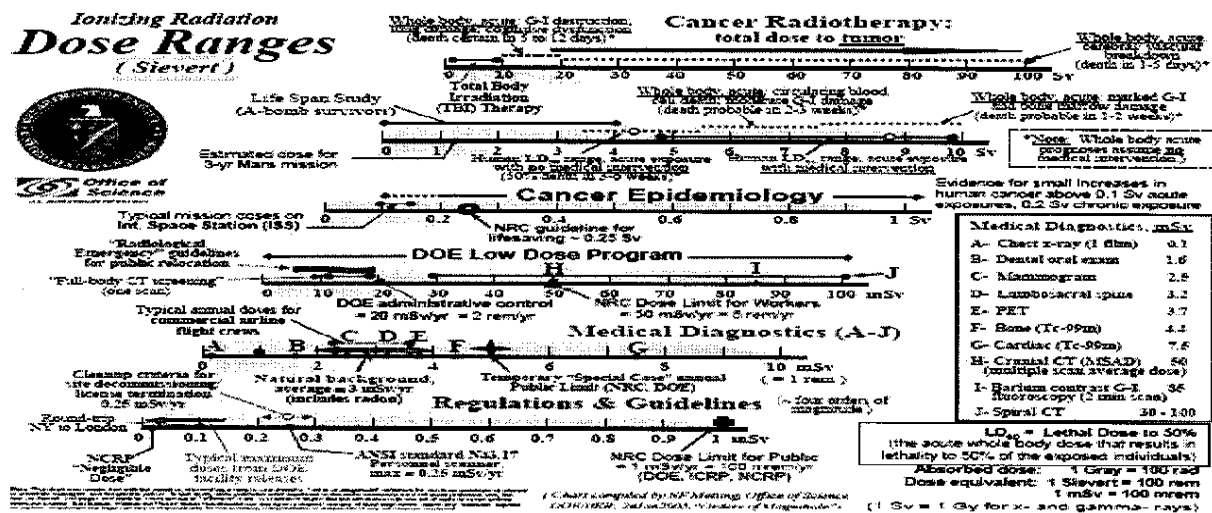
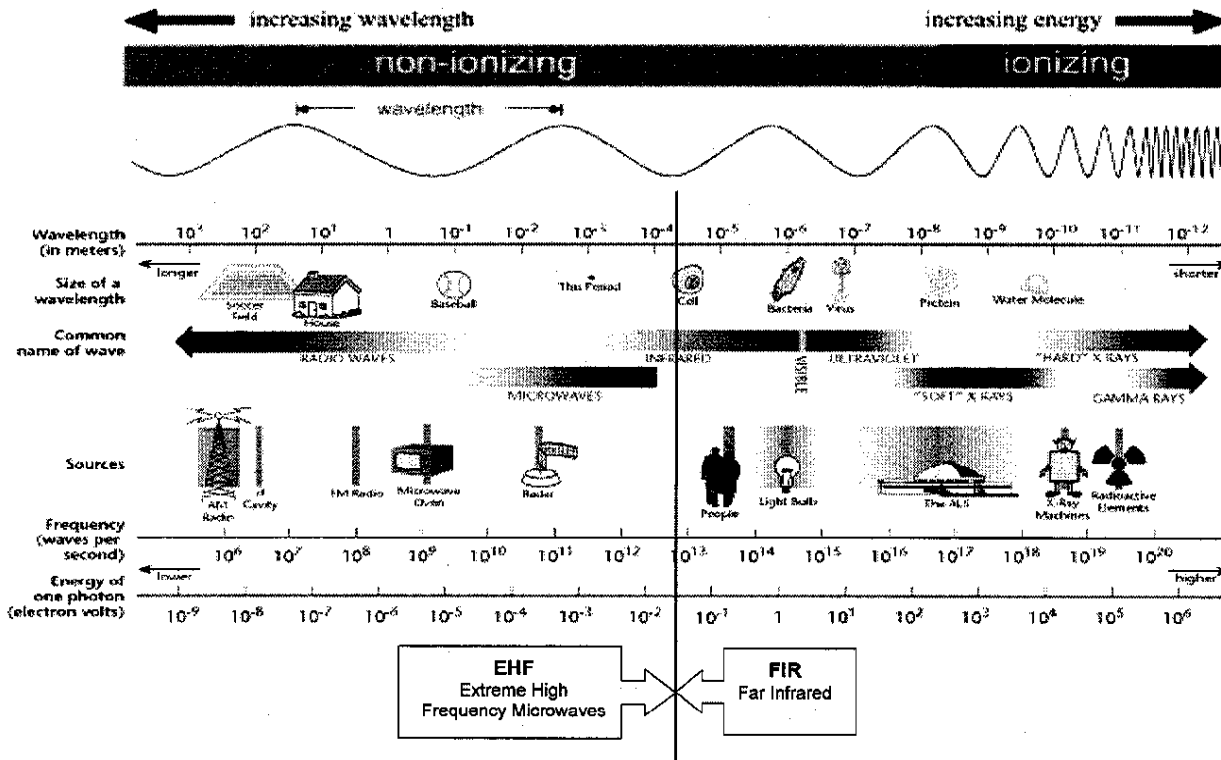


Figure 3-61



3.3.5 Long Distance Viewing (LDV) Hoop – LDV x-ray Hoop Description

(b) (4)



3.3.6 Theory of Operation

3.3.6.1 Backscatter x-ray Subsystem

- An x-ray beam scatters from the target to a detector on the near side creating a photo-like image that is easy to interpret and understand.

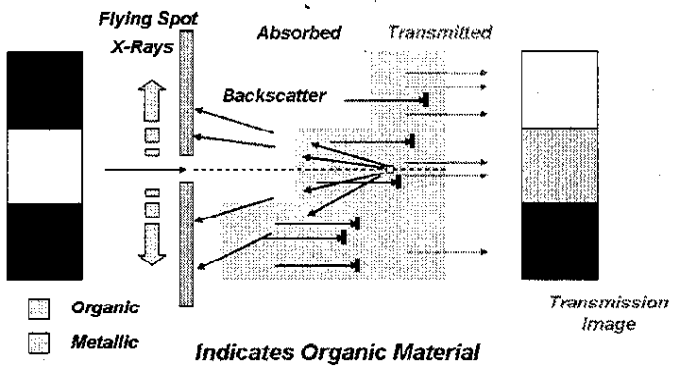
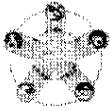
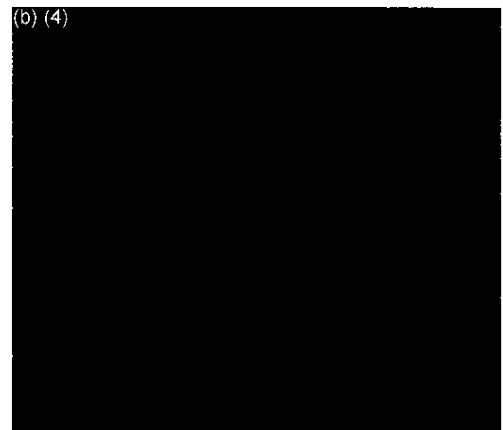


Figure 3-63





3.3.6.2 Capability: Identify Organic Elements & In-Organic Element Shadows

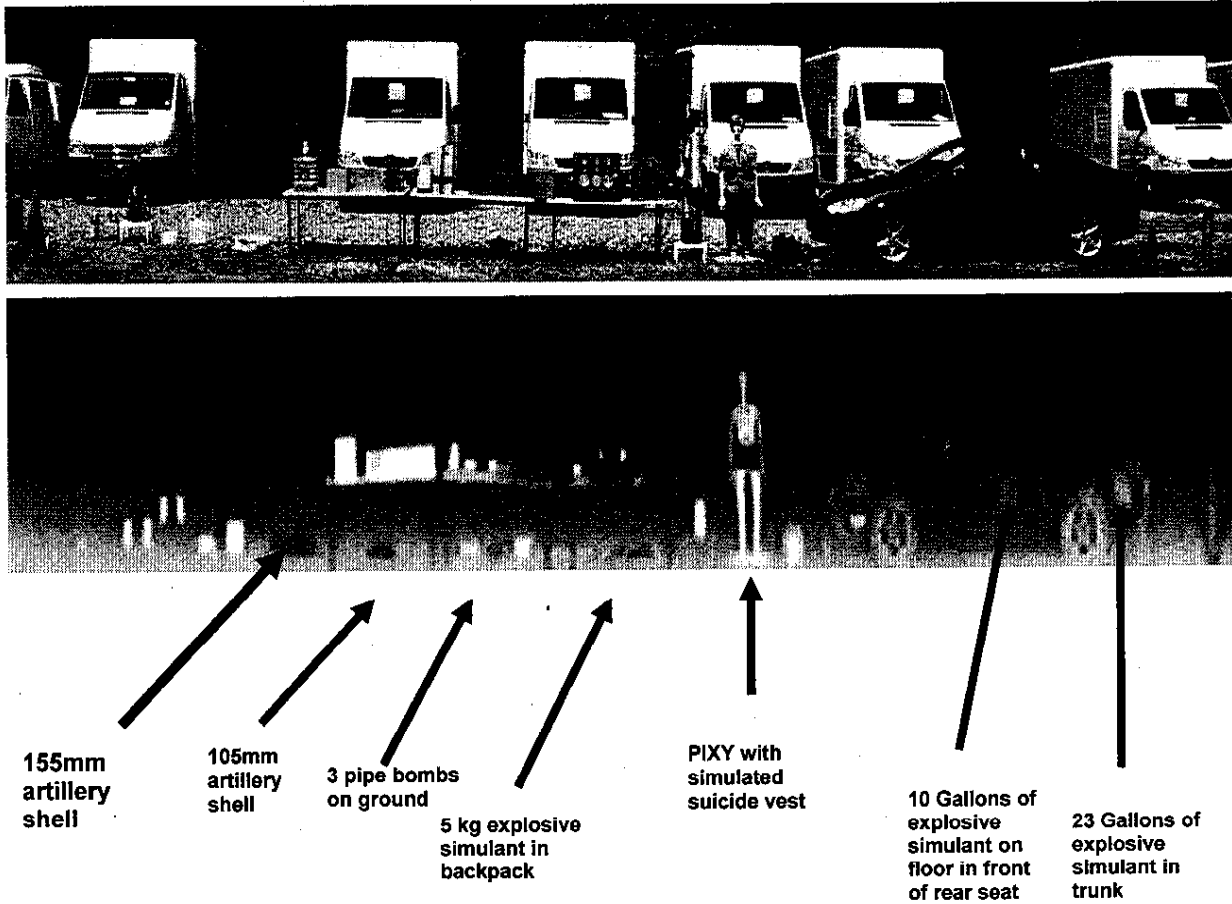
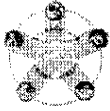


Figure 3-66. Backscatter image at 30 feet (10m)

(b) (4)





(b) (4)



3.3.7 Sensor Statement of Work

3.3.7.1 *Identify Sensor Types Availability*

- Backscatter x-ray Sensor
 - Platform
 - LDV Configured Z Backscatter Van (ZBV)
 - This previously developed prototype resulted from modifications made to a standard ZBV.

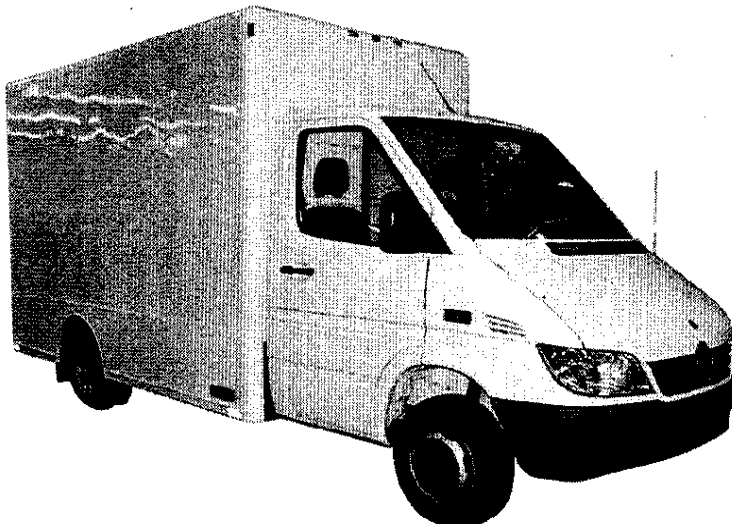
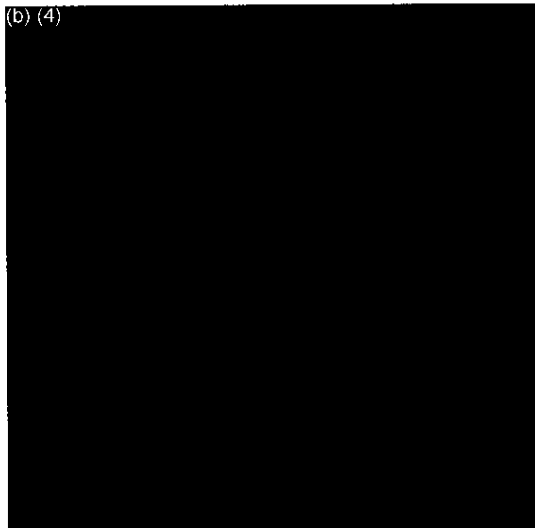


Figure 3-69

3.3.7.2 Specification



- X-ray Source

- (b) (4)
- (b) (4)
- (b) (4)
- Wide Angle 225Kev x-ray Tube
 - Voltage: 225 KeV x-ray Voltage (Unipolar)
 - Power: (cont. Max.): >3000W
 - Focal Spot Size: <3.0 (IEC336)



- Radiation Coverage >5 Deg x > 90 Deg
- (b) (4)
- (b) (4)
- (b) (4)
- Radiation Leakage: <100 mR/h
- (b) (4)

3.3.7.3 Testing Protocol

3.3.7.3.1 Physical

- Operation in a temperature range of 0°F to 122°F
- Operation after being stored in the temperature range of -25°F to 140°F

3.3.7.3.2 Environmental

- Temperature tests will be performed in accordance with MIL-STD-810F
- Low and High temp storage test
- Ambient, Low, and High temp operational tests consisting of scanning 1 personnel wearing various threats
- Each specific configuration (person, threat, threat locations) will be repeated 5 times each to gain statistical sample size

3.3.7.3.3 Transportability

- Center of gravity (CG) measurements
- Road shock and vibration
 - (Munson Test Course (Belgian block, gravel, etc))

3.3.7.3.4 Safety

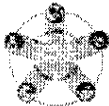
- Testing will be conducted in accordance with Test Operations Procedure (TOP) 6-2-507, Army Regulation (AR) 385-16, and Military Handbook (MIL-HDBK) 454A

3.3.7.3.5 Performance and Human Factors Engineering (HFE)

- MIL-STD-1472F

3.3.7.3.6 Software Performance

- System software failures and incorrect software logic that could cause system hazards will be characterized.



3.3.7.3.7 Threats and Phantoms

- Types
 - 6 Defined Explosives
- Multiple Locations

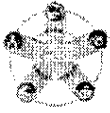
(b) (4)



3.3.7.4 Output

(b) (4)



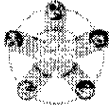


- Image Manipulation
 - Thumbnail
 - Icons
 - Filters
 - Color
 - Window

3.3.7.4.1.1 Experiments to Validate

(b) (4)





3.3.7.5 Baseline Performance



3.3.7.5.2 Derived Confidence Level

3.3.7.5.2.1 Uncertainty Percentage

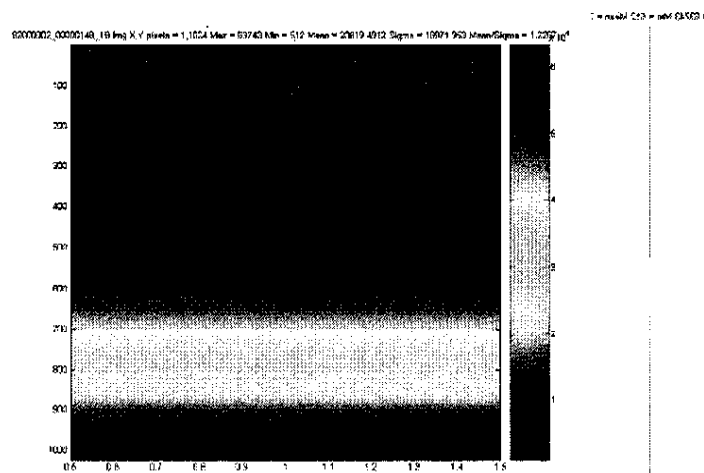
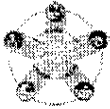


Figure 3.75. FFT – Frequency Domain Analysis



3.3.7.5.2.2 False Positive Rate

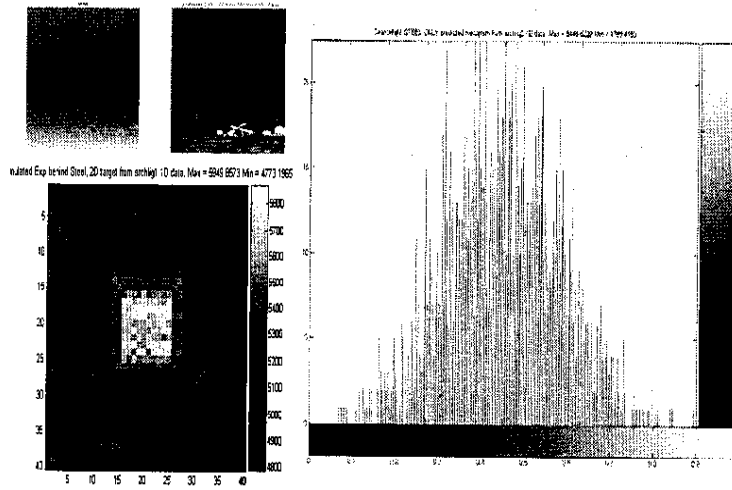
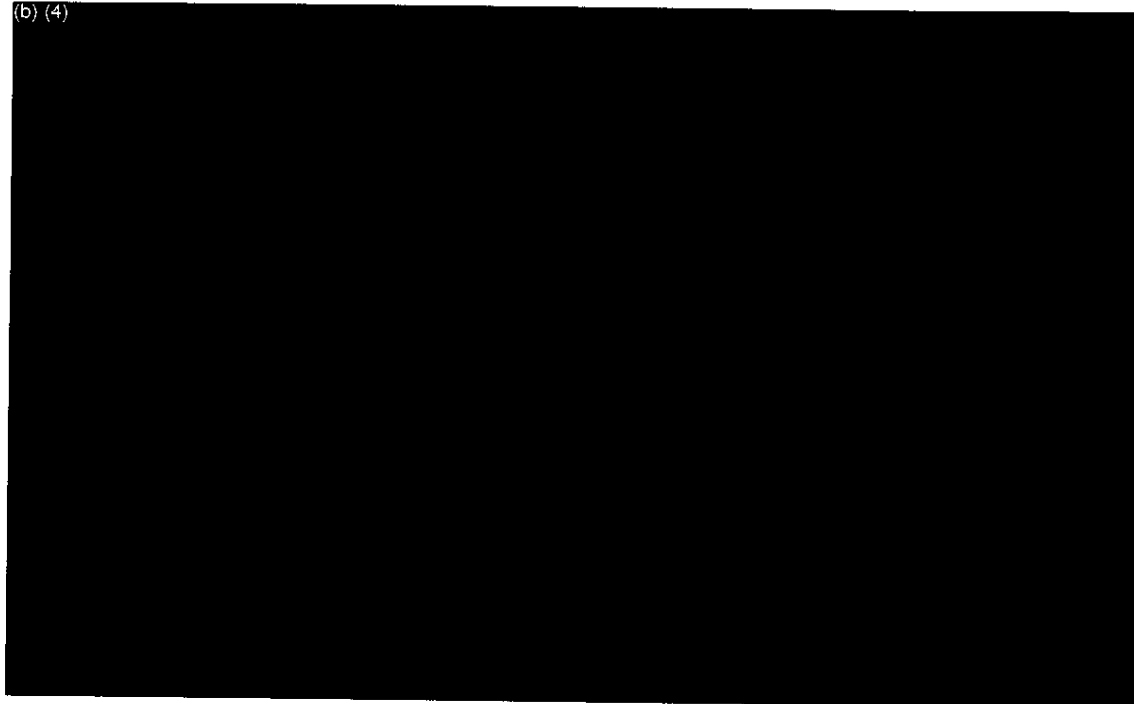
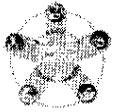


Figure 3-76. Blob Anomaly – Histogram Analysis

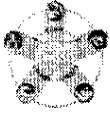
(b) (4)





(b) (4)





(b) (4)





(b) (4)





(b) (4)





3.3.8 Sensor Hardware Interface

3.3.8.1 In-System Characteristics (Operating Envelope)

3.3.8.1.1 Sensor Physical Characteristics

Sensor Physical Characteristics	
Length	45.0 inches
Width	35.0 inches
Depth	24.0 inches
Weight	496.0 lbs
Sensor Power Parameters	
Voltage	240 volts
Current	35 amps
Phase (If A/C)	Single Phase
VA	8583
Watts (Watts Dissipated)	7503 Watts
Duty Cycle	80%
Connection Type	IEC-320 outlet

3.3.8.1.2 Sensor Environmental Characteristics

Expected Thermal Conditions	
Heat – Operating	42.2 C
Heat – Storage	60.0 C
Cold – Operating	0.0 C
Cold – Storage	-32.0 C
Humidity – Operating	10%-95% (Non Condensing)
Humidity – Storage	10%-95% (Non Condensing)
Cooling Requirements	No Additional

Expected Thermal Conditions	
Heat – Operating	42.2 C
Heat – Storage	60.0 C
Cold – Operating	0.0 C
Cold – Storage	-32.0 C
Humidity – Operating	10%-95% (Non Condensing)
Humidity – Storage	10%-95% (Non Condensing)
Cooling Requirements	No Additional



(b) (4)



3.3.9 Sensor Software Interface

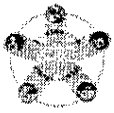
3.3.9.1 Data – Definition

- Image File Data Definition
 - AS&E uses a form of the .TIFF definition derived from the FAA Specifications, it is called the .IMG Format
 - Ultimately any raw format's purpose is to faithfully record both 100% of exactly what the sensor "saw" (the data) and the conditions surrounding the recording of the image.
 - Image files contain the pixel data from an image sensor, the modern equivalent of traditional film, usually at 12 or 14 bits per sensor bucket.
 - An average A4 scan paper size produces 50 kilobytes (KB) of data at 300 ppi (pixels per inch resolution)

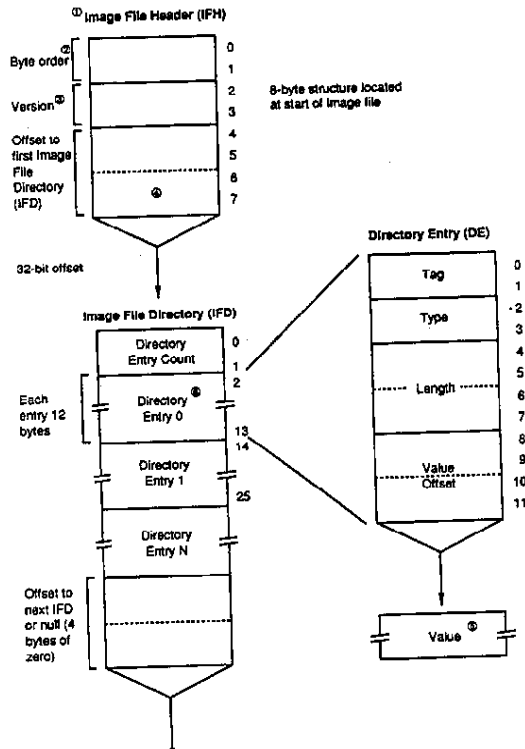
3.3.9.1.1 Data - Structure

3.3.9.1.1.1 Meta Data

- Standard Data Structure
 - Sensor ID
 - Scan Date
 - Scan Time



- Scan Location
- Algorithmic Alarm Level
- Alarm Confidence Level
- Sensor Threat Self Evaluation



3.3.9.1.1.2 Raw Data

- AS&E .IMG Image Format (Similar to .TIF)
 - Header Info
 - Image Data
 - Comments



3.3.9.1.2 Communication/Event Interface

Input Queue

- Is Sensor Ready
- Sensor ON
- Sensor OFF
- Initialize Sensor
- Calibrate Sensor
- Parameters
- Activate Sensor
- Deactivate Sensor
- Send Data
- Send Current Status

Output Queue

- Sensor Ready
- Sensor is ON
- Sensor Initialized
- Sensor Calibrated
- Sensor Activated
- Sensor Deactivated
- Sending Data
- Send Status
- Heartbeat (Status)
- Auto Alarm

Internal States

- Not Ready
- Not Ready – Initializing
- Ready – Not Initialized (Error)
- Ready – Initialized

3.3.9.1.3 Control Interface

3.3.9.1.3.1 Command Set

- **Register Based Command Set**
- **Base Command Set (HEX 0x0000 Base)**
 - Start Scan 0x0001
 - Stop Scan 0x0002
 - Send Data 0x0004
 - Calibrate Sensor 0x0008
 - Sensor Ready 0x0010
- **Specific Command Set (HEX 0x1000 Base)**
 - Activate 0x1001
 - De-activate 0x1002
 - Initialize Sensor
 - (Warm X-ray) 0x1004
 - Normalize Detector 0x1008



3.3.9.1.4 Status Protocol

- Heartbeat Criteria
 - TCP/IP Ping
 - Sensor Status Bits
 - System Controller
 - X-ray Power Supply
 - Data Acquisition
 - Environmental Conditions
 - Heat
- Monitored Parameters
 - X-ray Tube Voltage
 - X-ray Tube Current
 - Shutter Status
 - X-ray Source Wheel Speed

3.3.9.1.5 Output

3.3.9.1.5.1 Display

(b) (4)





(b) (4)



3.3.9.1.6 Reports

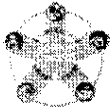
- Uptime (Hours On since last Start)
- X-ray Tube Life (Hours Used)
- Last Used (Date/Time)

3.3.10 Conclusions

- Backscatter Sensor: Sensor Characteristics
 - **Active** Sensor for Remote / Standoff Detection
 - **Non – Intrusive** Sensor on suspect Target
 - Meets the Hardware Specification of a Platform Object
 - Meets Physical and Environmental Operating Parameters
 - Finds Organic anomalies on suspect Target
 - Detects Organic elements used in Explosives
- Backscatter Sensor Inclusion: Meets the BomDetec Mission
 - Automate: Assists in finding threat with *Automated* processes
 - Integrate: Data *Integrates* into platform suspect target alert process
 - Data Fusion: Data *can be fused* with other data for a more precise alert indication

Based on our understanding of the needs of the ultimate user, we believe that a Backscatter Sensor such as that proposed in this report will provide substantial utility to the operators.

This page intentionally left blank.



4 Hardware Integration (AS&E, (b) (6))

4.1 Executive Summary

American Science & Engineering, Inc. (AS&E) proposes to unite multi-sensor technologies to deliver a system that meets all requirements for an integrated delivery mechanism for the BomDetec program. The system will allow for operators to deliver a multi-sensor platform to a location of choice then actively or remotely invoke the multi-sensor inspection platform towards the target site in question and provide an intuitive, intelligent display of data to the operator, allowing him/her to determine if a suicide bomb threat exists.

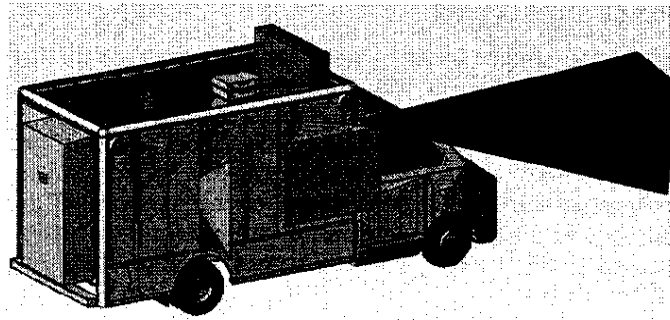


Figure 4-1. Proposed multi-sensor platform

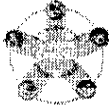
AS&E addressed size, weight, power and performance issues needed by the multi-sensor platform by analyzing the available suite of sensors and their needs when installed into a mobile delivery platform. AS&E has developed a military-qualified vehicle, the ZBV, for the deployment of its sensor – The backscatter x-ray sensor. AS&E based the design of the BomDetec multi-sensor platform on the ZBV as starting point in our studies and analyses. After analysis of the ZBV and other vehicle platforms, the design characteristics of the ZBV appeared to work best in the scenarios needed for the BomDetec platform. The delivery platform is a Mercedes Benz “Sprinter” chassis with a custom, ruggedized, vibration-isolated, environmental container attached to the bed frame of the vehicle.

As a result of this program, a preliminary design has been developed for containing multi-sensor technology for the detection of suicide bombers and IEDs. The multi-sensor platform should be sufficiently versatile to aid in suicide bombers and explosive ordnance detection in a variety of environments.

Specifically,

1. A multi camera intelligent video system will initially identify and track suspect individuals.
2. A radar system will be the first sensor invoked to determine if any metal content is on the suspect.
3. An x-ray imaging system will then be activated to discern if the presence of organic material, such as raw explosive substances, IEDs, or VBIEDs, are located on the suspect.
4. A Terahertz sensor will determine if the organic material has an explosive chemical signature. This data from this combination of sensor will provide the decision analysis subsystem, characteristics that will determine the threat level posed by the suspect.

Our joint conclusion is that possible to design a mobile platform that contains automated and integrated multiple standoff/remote sensor capabilities, mounted in a ruggedized, vibration isolated, environmental container and develop a concept of operations that will allow the system to take acceptable data under a



wide variety of conditions. The data collected will be algorithmically fused allowing the operator to discern the presence of suicide bomber IEDs.

We recommend continuing this program to permit the development of a prototype system.

Our joint team has the ability to plan and execute this program to meet all of HSARPA/BomDetec goals. Our integrated approach will establish a timely and effective product to help resolve situations in treacherous environments.

4.2 Purpose of Program

The scenarios visualized for the BomDetec system are that of a surveillance vehicle having multi-sensor capability installed for screening suicide bombers and vehicles at the entrance to a protected facility, such as a military base, an embassy or check point.

The program united four existing sensor technologies into a common ruggedized surveillance vehicle, intelligent video, backscatter x-ray, Millimeter Wave Radar (MMW Radar), and Terahertz Wave (THz), creating a sensor suite. The sensors will be tested and evaluated independently within the common hardware platform. AS&E, as the system and hardware integrator, gathered information – mechanical, electrical (power signal, control), thermal, and optical – about each sensor, determined the best locations for mounting the sensors and evaluated the interactions of the sensors. The system integration and hardware integration effort lead to a system configuration and preliminary design. The design provides for an integrated, automated solution using standoff/remote sensors, delivering the sensor data to a central location for evaluation and test.

The system will be organized by an intelligent video and data handling system, which will identify and track every person entering the surveillance zone. It will provide a ground-based coordinate system and motion compensated tracking coordinates for the other sensors. It will alert and provide tracking coordinates for each sensor when a person comes in range. An operator will be able to intervene and direct a Pan-Tilt-Zoom (PTZ) camera for zoomed images or direct other sensors for surveillance of a specific person. The three additional sensors will identify metal, conformation and explosives in the surveillance zone. The tracking system will attach these data to the appropriate person in the zone. Millimeter Wave Radar (MMW Radar), will survey the area and identify people with metal objects at distances up to or >50M. At a closer distance (~10M) x-ray backscatter will be capable of imaging both metal conformation and the presence of explosive materials. At still closer distances (~3M), Terahertz radiation will sense and spectroscopically identify explosives on a person. The radar will continue to improve its information as the person approaches, as will the x-ray. At some point the data will exceed a threshold, and the system will identify the person as a “bomber”. Each modality has a specific role, and each provides specific information. Together they will provide a unique, remote (>10M), real-time, chemical sensing and suicide bomber identification system.

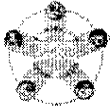
Data from the four sensors will be processed, managed, enhanced and combined in real time. The processed data will be fused to provide the operator with positive identification of a “bomber”. A confirming digital photograph will be presented to the operator along with the sensor identification.

4.3 AS&E Project Scope

4.3.1 Hardware Integration Design

The ultimate goal of the BomDetec program is to develop a system that can detect suicide bombers using IEDs.

- Hardware Integration Goal



- The BomDetec platform must be open architecture to host new sensor types
- The sensor hardware elements will be self contained and follow the physical interfaces described by the BomDetec Platform.
- System Integration Goal
 - The BomDetec system must provide standoff and remote detection using non-intrusive active and passive sensors.
 - The BomDetec system must exhibit 3 major capabilities to achieve this goal: automation, integration, and data fusion.

4.3.1.1 Sensor Selection

- Video: Intelligent Tracking
- Radar: Metallic Material ID
- X-ray: Organic Material ID
- Terahertz: Material Spectroscopy
- FLIR: Material Spectroscopy

4.3.1.2 Sensor Characteristics

- Placement
 - Location and Hardware
- Weight
- Power
 - Signal Conditioning
- ConOps
- Data Processing
- Operator Display
 - Information Display

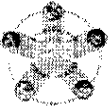
4.3.2 Systems Integration Design

4.3.2.1 Systems Engineering Approach

- System Architecture
 - Open
 - Adaptive
 - Extensible

4.3.2.2 Define Sensor Types

- Active



- Passive

4.3.2.3 Layered Approach

- Integrate Sensors
- Automate Sensor Data Analysis
- Data Fusion of Sensor Elements in the Platform
 - Operator Interface
 - ConOps
- Data Integration, system Control and Data Presentation

4.4 Sensor Hardware Synopsis

4.4.1 Hardware Integration

4.4.1.1 Sensor Types

- Intelligent Video
- Backscatter x-ray
- Radar Beam
- Terahertz Spectroscopy
- FLIR Spectroscopy

4.4.1.2 Sensor Characteristics

- Platform Layout
- Physical
 - Size
 - Weight
- Environmental
- Power



4.4.2 SENSOR – Intelligent Video

4.4.2.1 Vendor: Siemens

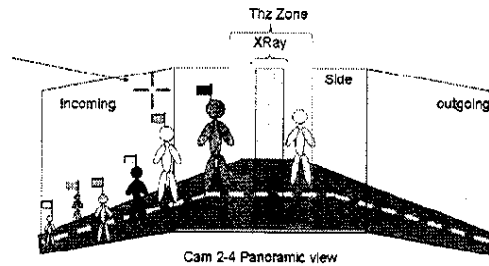


Figure 4-2. Intelligent video sensor

- Sensor Element: Multiple PTZ Cameras
 - 15"x15"x15"
 - 12 lbs
 - 27 Watts
- Sensor Element: Pole Mounting Camera
 - 6"x6"x16"
 - 21 lbs
 - 32 Watts
- Sensor Controller Electronics
 - 19"x10.5"x20"
 - 140 lbs
 - 1210 Watts

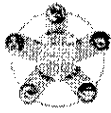
4.4.3 SENSOR – Long Distance Radar

4.4.3.1 Vendor: Raytheon/PPT/Northeastern University



Figure 4-3. Radar sensor

- Sensor Element: Radar Antenna
 - 15.75"Diameter x 23.6" long cylinder
 - 40 lbs



- 0 Watts
- Sensor Controller Electronics
 - 24"x24"x12"
 - 50 lbs.
 - 7 Watts

4.4.4 SENSOR – Backscatter Imaging

4.4.4.1 Vendor: American Science and Engineering

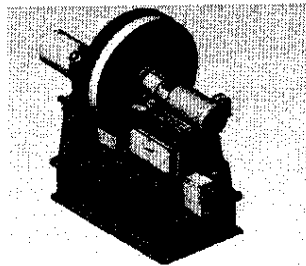


Figure 4-4. Backscatter x-ray sensor

- Sensor Element: LDV X-ray Source
 - 45"x35"x24"
 - 466 lbs
 - 225 KeV
- Sensor Controller Electronics
 - 500 lbs
 - 15000 Watts

4.4.5 SENSOR – Terahertz Spectroscopy

4.4.5.1 Vendor: Rensselaer Polytechnic Institute

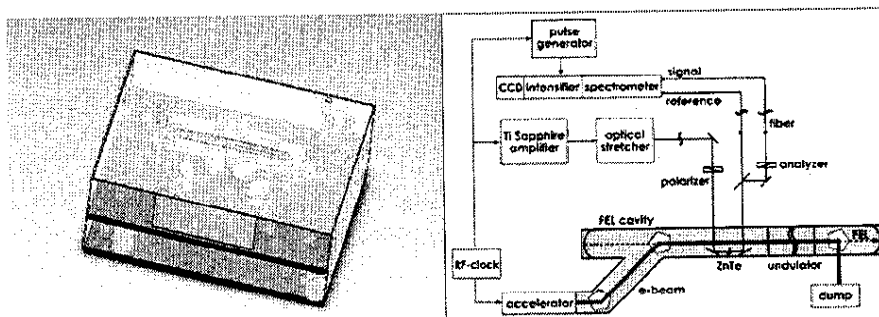


Figure 4-5. Terahertz sensor



- Sensor Element: Terahertz Long distance Generator / Receiver
 - 24"x24"x10"
 - 105.6 lbs
 - Passive Unit
- Sensor Controller Electronics
 - 12"x20"x6"
 - 5 lbs
 - 500 Watts

4.5 Sensor Hardware Platform Integration

4.5.1 Host Vehicle Centralized Sensor Platform

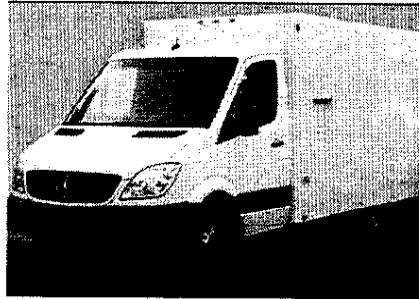


Figure 4-6. AS&E's Z Backscatter Van

- Self Contained Power Plant
- Ample Power for additional Sensors
- Ample Space for Sensors
- Ample Weight Capacity
- Military Qualified
- Environmentally Controlled
- Vibration Damped



4.5.2 ZBV - Exterior Layout

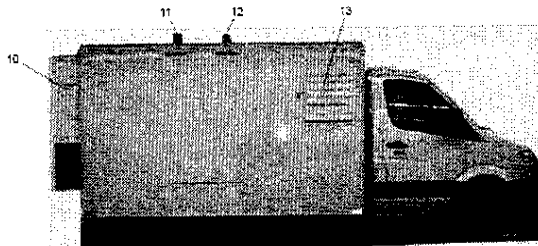
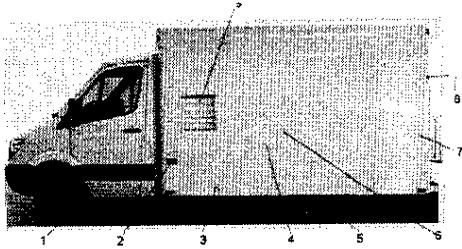


Figure 2-1: ZBV - Major Exterior Components (Right Side Scan shown)

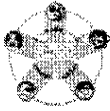
No.	Item
1	Chassis - Cab
2	System ID Label
3	Equipment Coach (Coach)
4	Shore Power conn. (option)
5	Chassis - Wheel Speed Encoder
6	Laptop Remote conn. (option)
7	Forward Scatter conn. (option)
8	Access Panel (door)
9	Generator Air Exhaust Vent
10	HVAC
11	Scanning Warning Beacon
12	X-ray On Warning Beacon
13	Generator Air Intake Vent

Figure 4-7. ZBV Exterior

4.5.3 ZBV - Interior Space and Components Layout

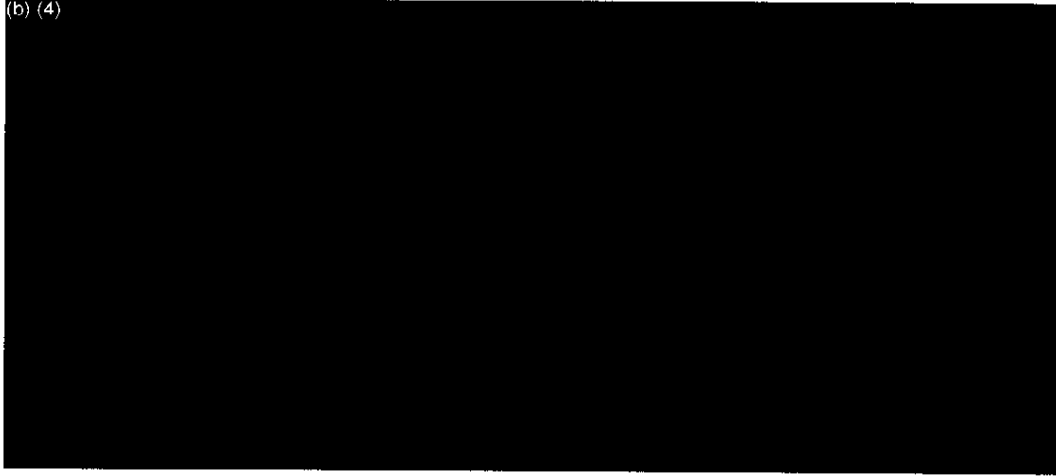
(b) (4)





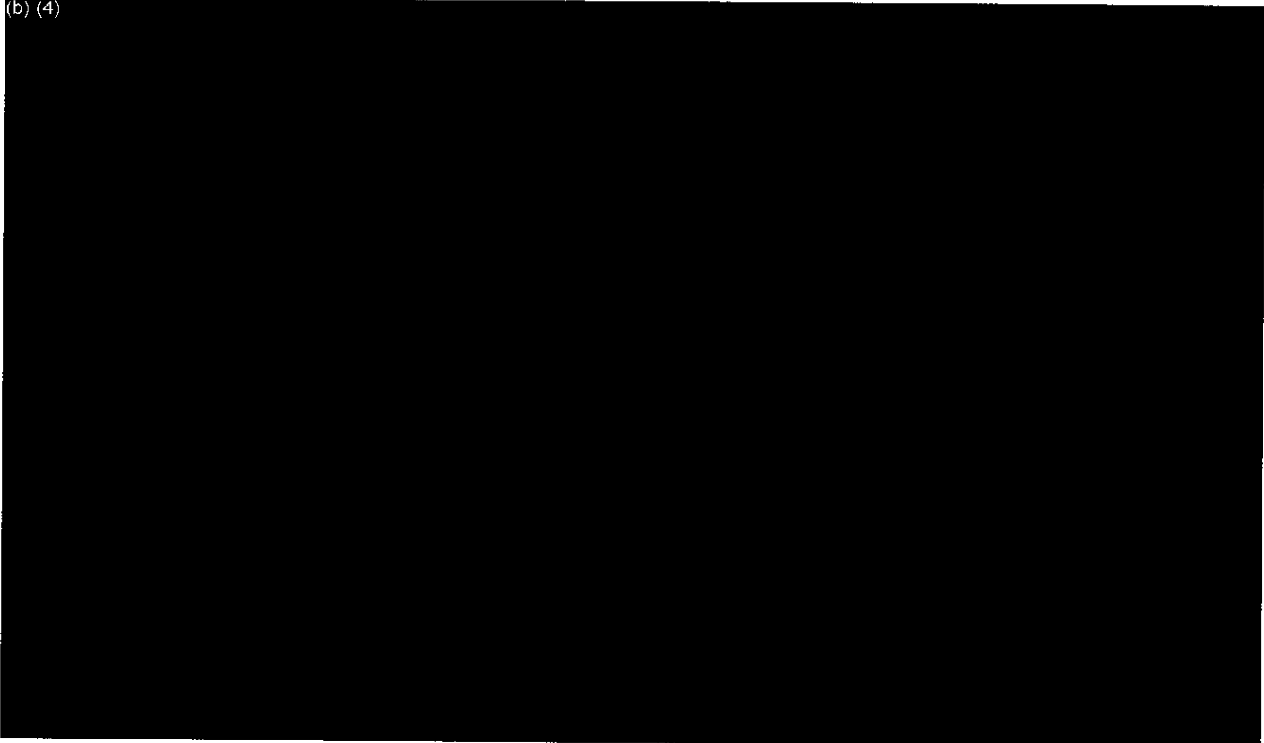
4.5.4 ZBV - Proposed Sensor Equipment Locations

(b) (4)



4.5.5 ZBV - Proposed Sensor Pattern Coverage

(b) (4)



4.5.6 ZBV - Weight Budget

(b) (4)





4.5.7 ZBV - Power Budget

- All sensors input power requirements to be 240 VAC.
- Shielded power cables.
- CE/TUV/UL Approval

4.5.8 ZBV - Power Distribution Block Diagram

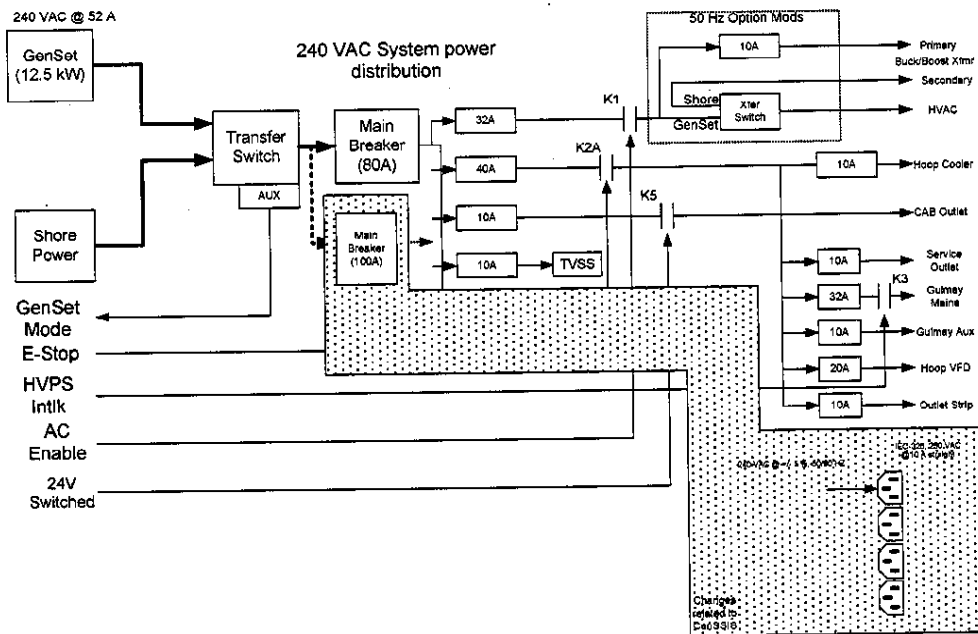
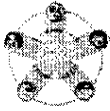


Figure 4-11. Modifications to Lean ZBV Based on 278=2502 Interconnect Diag



4.5.9 ZBV – Physical / Environmental Characteristics

Environmental

See Table 2-11 for specifications.

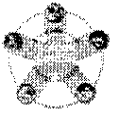
Table 2-11: Environmental Specifications

Category	Specification
Ambient Operating	0°C to 42.2°C (32°F to 108°F)
Storage	-32°C to 60°C (-25°F to 140°F) ^a
Humidity	10–95% relative humidity (non-condensing)

a. The 220 keV X-ray tube must be removed if the ZBV will be stored (non-operating) at temperatures below -10°C (14°F)

Category	Specification
Vehicle Type	Daimler Chrysler (diesel) chassis
Transmission	5-speed Automatic
Fuel	Refer to vehicle OEM manual.
Gross Vehicle Weight	5,000 kg (11,023 lbs.)

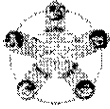
Chassis Type	Suspension	Height	Width (Coach Only)	Width (Mirrors Folded)	Width (Mirrors Extended)	Overall Length (including HVAC)	Coach Length (including HVAC)
International	Standard	260.1-262.9 cm (102.4 -103.5 in.)	204. cm (80.3 in.)	212.1 cm (83.5 in.)	242.6 cm (95.5 in.)	664 cm (261.4 in.)	409.0 cm (161.0 in.)
International - Crew Cab	Standard	260.1-261.9 cm (102.4 -103.1 in.)	204. cm (80.3 in.)	212.1 cm (83.5 in.)	242.6 cm (95.5 in.)	744 cm (292.9 in.)	409.0 cm (161.0 in.)



4.5.10 ZBV – Container Vibration Analysis

(b) (4)

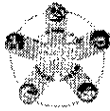




4.5.11 ZBV – Proposed Operator’s Console

(b) (4)





4.5.12 Hardware Objects Power / Thermal Conditions

- Each sensor will receive power through a single IEC-320 outlet (240 VAC @ 10A maximum) each.
- Each sensor will be responsible for its own distribution scheme from this single power input.
- Each sensor will step up or step down the input voltage as required for their sensor
- Each sensor will provide a relay contact closure for an interlock chain which would open to indicate unsafe/fault conditions within their sensor.
- Each sensor must be able to accommodate ZBV operating environment of 0 to 50 deg C
- Each sensor's inrush current must not influence the other operating sensors.

4.5.13 Component Safety Labeling Published Health and Safety Compliances

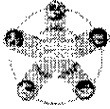
4.5.13.1 System Compliance

Category	Specification
Dose to Cargo	Less than 0.04 micro Sieverts (μ S) per scan, average speed 5 kph at 1.0M distance; less than 0.01 mR
Environmental Dose	Less than 2.5 μ S per hour; less than 0.5 mR in an hour at the exterior surface of the coach wall.
CFR Compliance	Complies fully with all applicable federal health and safety regulations: U.S. Bureau of Radiological Health Standards for Cabinet X-Ray Systems (21 CFR 1020.40); Directive 96/29/Euratom; UK Ionising Radiations Regulations 1989.
ANSI	Complies with ANSI 43.3-1993, section 5.3 as an "open" installation.

4.5.13.2 Safety Labeling

Symbol (colors vary)	Explanation
	Danger - Warning - Caution. Risk of danger or damage. Refer to Field Service Manual. See "Admonitions"
	Earth - ground connection
	Caution. Risk of electric shock.
	Radiation hazard. Risk of radiation exposure. Take recommended precautions. See "Admonitions"
	Ear protection. Risk of damage to hearing. Wear ear protection.
	Caution laser. Risk of damage to vision. Do not look into active source.

Figure 4-16. Safety Labeling



4.6 Hardware Integration Summary

4.6.1 Evaluation

- Physical parameters of all sensor types completed:
 - Physical size
 - Weight
 - Power

4.6.2 Results

- Host vehicle can support the physical size, weight and power requirements of the evaluated sensors
 - Mounted sensors fall within tolerances for vibration and thermal specifications of the host vehicle
 - Sensor placement
 - Optimized for each sensor type
 - Limits potential adverse interactions

4.7 Sensor Systems Integration

4.7.1 Systems Design includes the following:

- | | |
|----------------------|--------------------------------|
| • Analysis | • Function Analysis |
| • Problem Definition | • Function to Physical |
| • Requirements | • Trade-Offs |
| • Block Diagram | • Optimization |
| • ConOps | • Error Budget |
| • Sequences | • Technical Risk |
| • States | • System Level Validation Plan |



4.7.2 Systems Integration

A system is a group of interdependent items that interact regularly to perform a task. But, a system is more than the sum of its parts.

- System Integration must capture and understand numerous complex interactions.
- Provide Systems Engineering Management Plan.
 - Effective communication
 - Up-front planning
- Provide Overall Technical Management
 - Defines what is necessary to manage and control the total technical effort required to produce effective, economical, and efficient technical systems alongside the personnel and business management functions

4.7.3 System Analysis Problem Definition

4.7.3.1 Major System Requirements

4.7.3.1.1 Hardware

4.7.3.1.1.1 Architecture

- Open
- Portable
- Maintainable

4.7.3.2 Integration

- Simple
- Expandable

4.7.3.2.1 Software

4.7.3.2.1.1 Architecture

- Extensible
- Maintainable

4.7.3.2.1.2 Command and Control

- Resource Management
 - Queuing
 - Dispatch



4.7.3.2.1.3 Decision Intelligence

- Integration
- Data Fusion

4.7.3.2.1.4 Automated Results

4.7.3.3 Systems Architecture

4.7.3.3.1 Typical Sensor Interactions

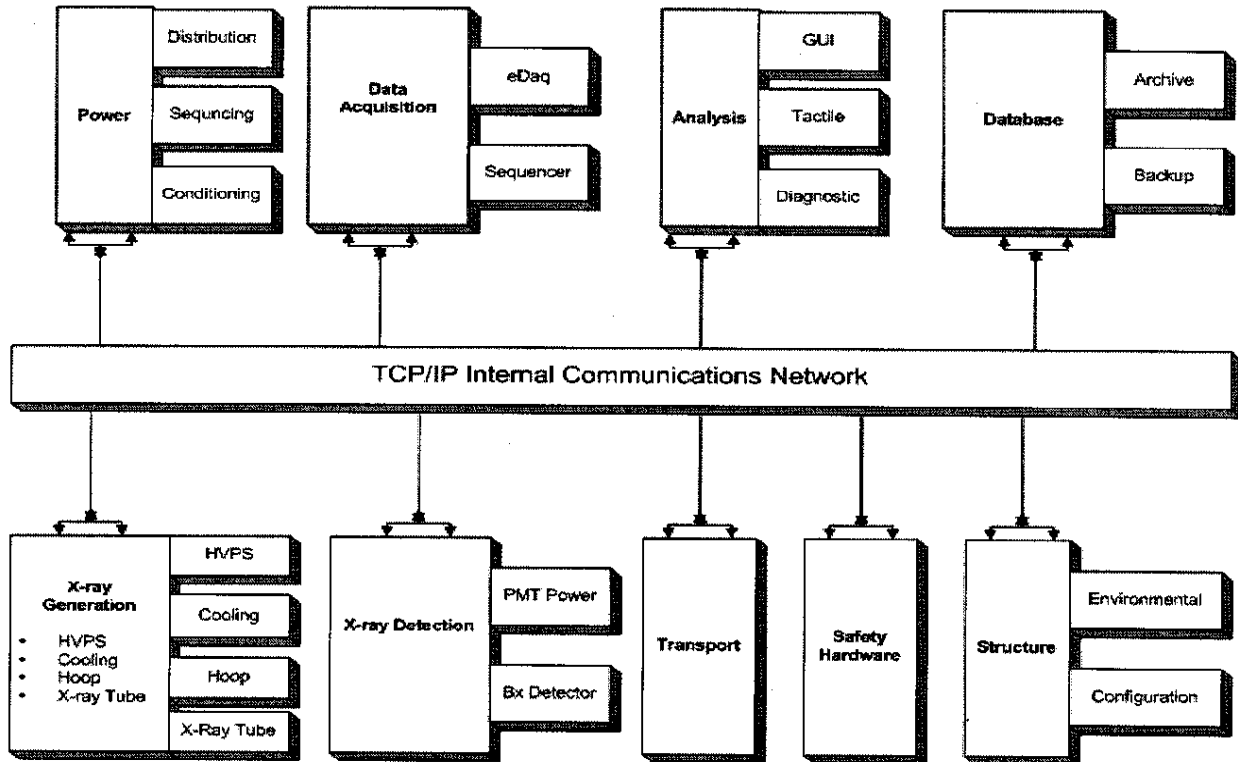
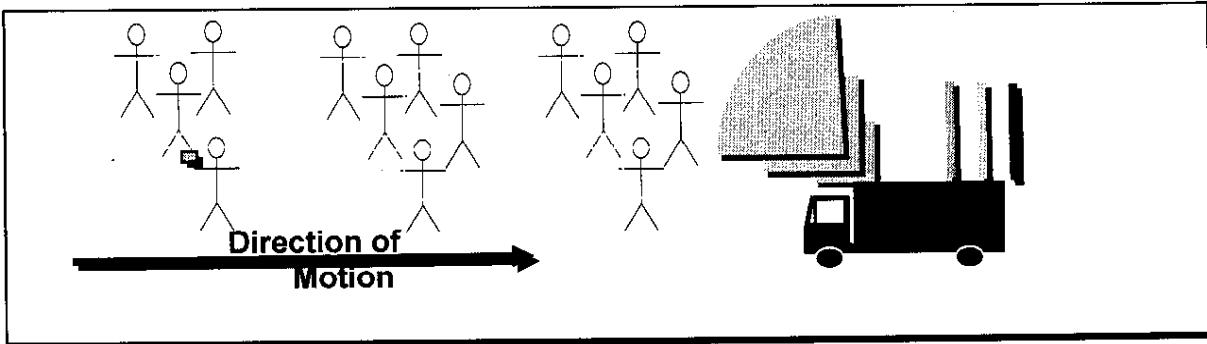
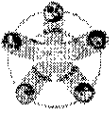


Figure 4-17

4.7.3.3.2 System Concept of Operations (ConOps)

4.7.3.3.2.1 Sensor Invocation

- Video : Initiate Target Event
- Radar : Detect Geometric Anomaly
- X-ray : Detect Organic Anomaly
- THz : Identify Materials
- FLIR : Confirm Materials




 = Bomb

Figure 4-18

4.7.3.3.3 Basic System Sequence

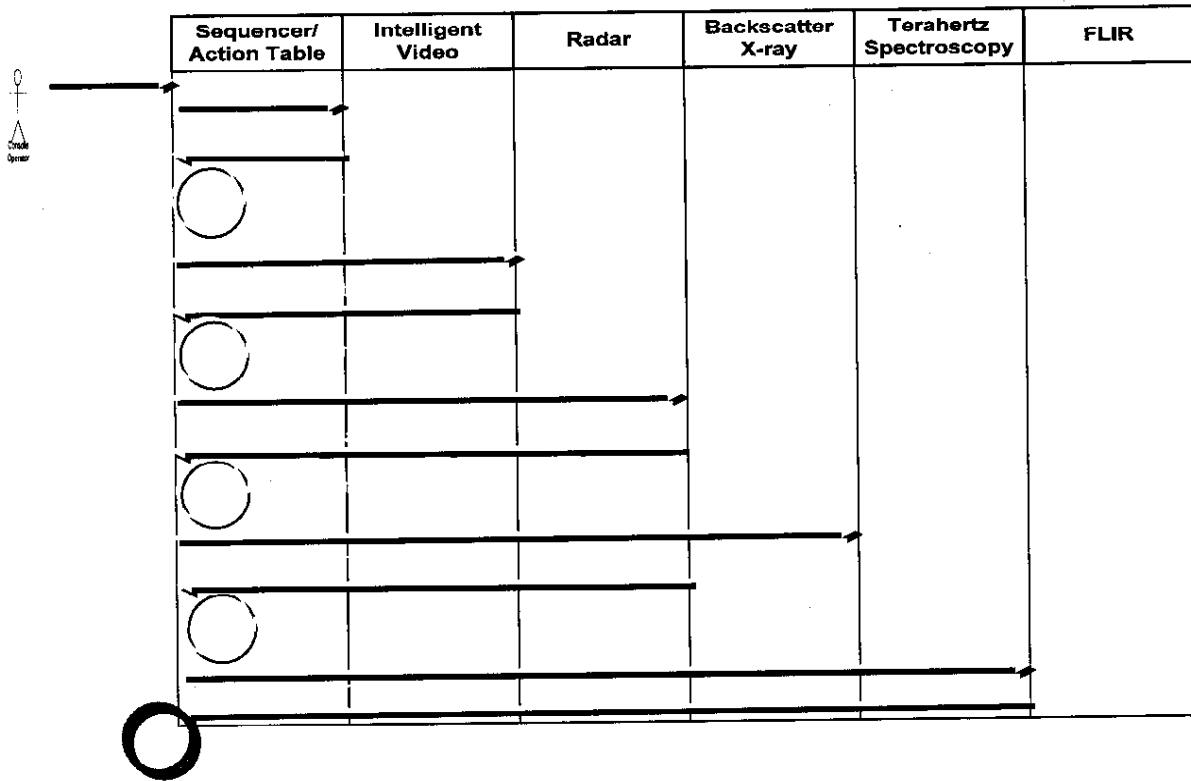
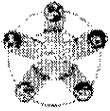


Figure 4-19



4.7.3.3.4 Major System States

There are four states of operation.

1. Standby/Safe Mode: active but not scanning
2. Real Time Operation:
 - Scanning of Individuals
 - System Status
3. Science:
 - Balance output of Sensors
 - Adjust Sensor Parameterizations
4. System Maintenance: add, delete or modify sensors

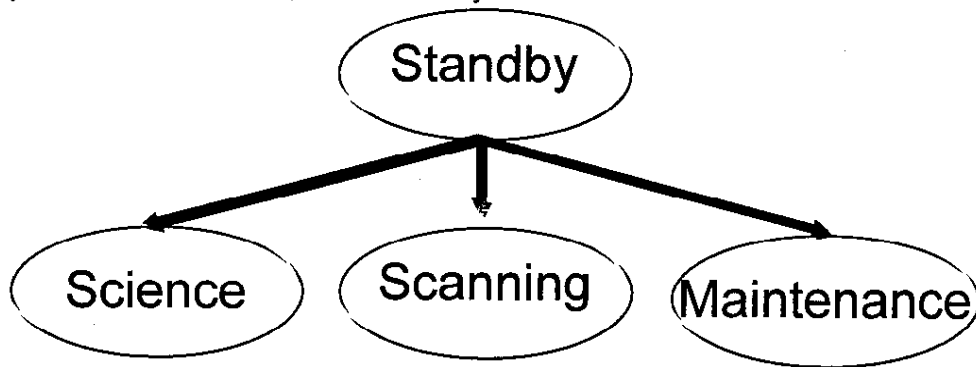
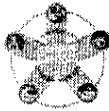


Figure 4-20



4.7.3.4 System Analysis

4.7.3.4.1 Problem Definition: Functional to Physical

4.7.3.4.1.1 Modeling and Prediction

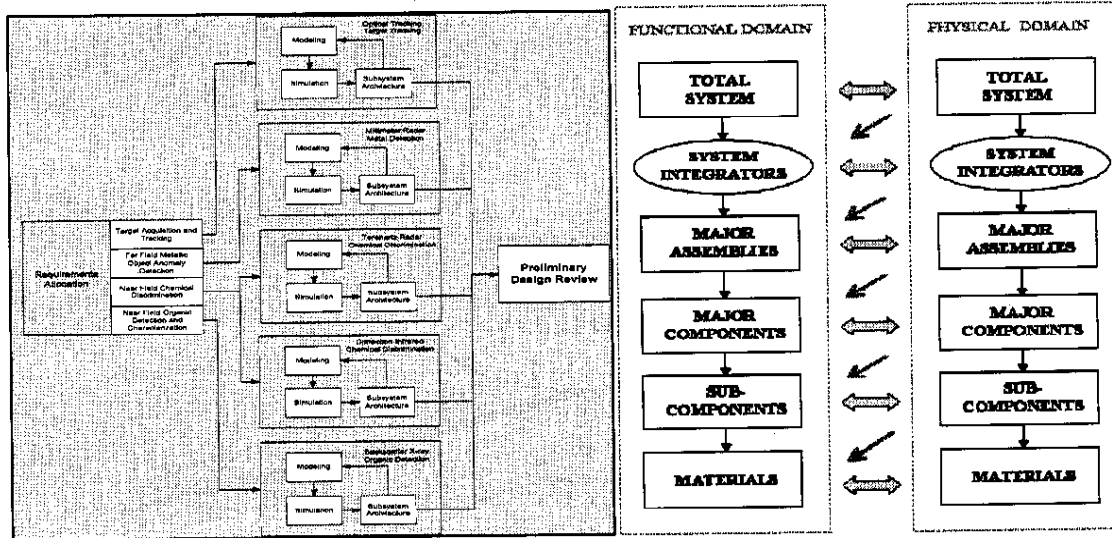


Figure 4-21

4.7.3.4.1.1.1 Tool Chain Architecture

4.7.3.4.1.1.1.1 Define Major Assemblies and Components

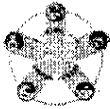
- Modeling Sensor Sub-Assemblies
- HICD - Component Interfaces
 - Sub-Assemblies Boundaries

4.7.3.4.1.1.1.2 Prediction

- Produce-ability
- Change Management (Process and Component)
- Probability
 - MBTF

4.7.3.4.1.1.1.3 System Design Change

- Estimating Cost
- Managing Cost



4.7.3.4.1.1.4 Object Characteristics

- Cost
- Performance
- Reliability

4.7.3.4.1.1.5 Decision Making

- Accurate
- Effective

4.7.3.4.2 System Design - Trade-off

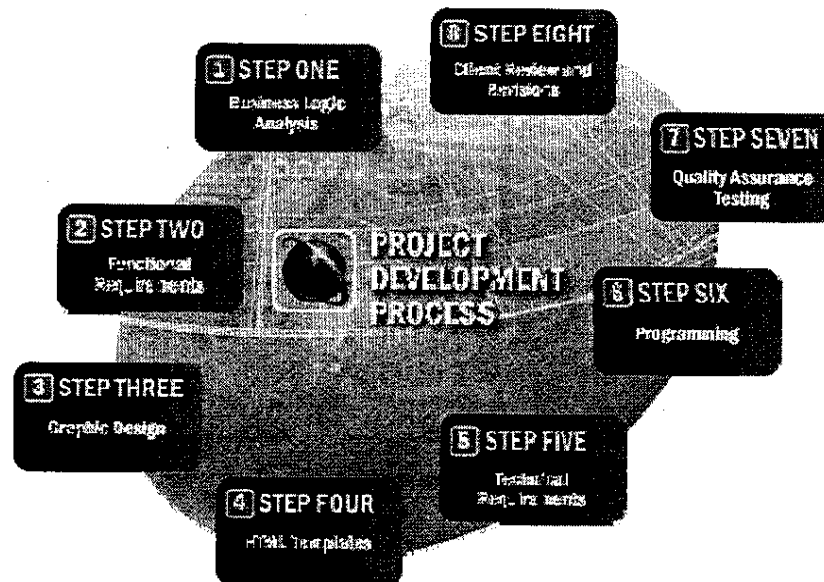


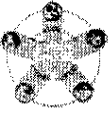
Figure 4-22

4.7.3.4.2.1 Sensor Type

- Purpose
- Range

4.7.3.4.2.2 System Electronics

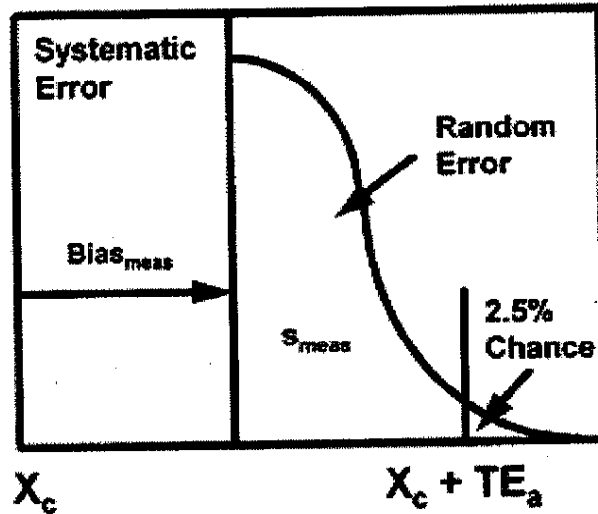
- Purpose
 - System Command, control communications
- Contains Command and Data Handling
- Communication
- Control Electronics



4.7.3.4.2.3 Design Ramifications

- Weight
- Power
- Space

4.7.3.4.3 System Error Budget



$$\bullet TE_a \geq bias_{meas} + 2s_{meas}$$

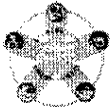
Figure 4-23

4.7.3.4.3.1 Error Budgets Definitions:

- Repeatability
- Reproducibility
- Stability
- Sensor bias

4.7.3.4.3.2 Error Budgets Inclusions:

- Sensitivity
- Standard deviation
- Degrees of freedom



4.7.3.4.4 System Technical Risks

4.7.3.4.4.1 Risk Management



Figure 4-24

4.7.3.4.4.2 Risk Assessment

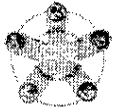
- Weight
- Cost

4.7.3.4.4.3 Risk Mitigation

- Drive Completion of Prototype
- Characterization of Data
- Documentation of Process

4.7.3.4.4.4 Risk Transfer

- Radiation safety Distance
 - Shielding vs. Distance = Weight

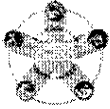


4.7.4 System Level Validation Plan

(b) (4)



- Incorporate review feedback as necessary and study any additional questions raised
- Establish Budget for Phase 2
- Issue Final Report for Study Phase
- Receive Funding
- Design, Build, Test and Deliver Platform
- Customer Support



5 Data Integration, System Control and Data Presentation (Siemens, (b) (6))

5.1 Introduction

This interim report puts the BomDetec work conducted by the SCR Team in the context of the Goals, Approach, Challenges, and Testing, all leading to Conclusions presented at the end of section 5.

5.2 Goals

As a TTA-2 Phase I project, the high-level goal was to:

- “develop novel or innovative technologies and/or systems to develop a sensor suite that can detect whether a person is wearing IEDs (improvised explosive devices) at sufficient distance to prevent him from entering populated or strategically important areas.”

Such “body-worn explosive devices” continue to be “a growing and important threat to both civilians and the military. Being small, IEDs are hidden under the clothing of suicide bombers. Since they are often built out of non-standard parts, these explosives are hard to detect, especially at a safe distance.”

Quantitatively,

- the overall program goal is “a BomDetec Van that will find 100% of Suicide Bombers at >10M,” by program completion.
- “The BomDetec Proposal is to detect the presence of suicide bombers in accordance with the above so that up to several hundred personnel approaching a checkpoint can be effectively screened per hour with the BomDetec system.”

As requested, the focus of Phase I was on establishing feasibility by conducting “the necessary feasibility analysis, research, development, and demonstrations to validate the proposed concepts”. Feasibility of the system was reported at the Preliminary Design Review (PDR) held on October 1, 2007.

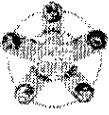
Among the BomDetec sub-goal capabilities targeted by Homeland Security, the following areas were included:

- Providing wide area surveillance and detection at distances greater than 10 meters;
- Maximizing the detector performance to minimize false alarm rates.
- Finding and verifying a platform to integrate the needed components and the above capabilities.
- Establishing the feasibility of the subsystems (platform, data architecture, and algorithms), so that data from the four or more sensors can be processed, managed, enhanced and combined in real time, fused to provide the operator with positive identification of a “bomber”, and presenting a confirming digital photograph to the operator along with the sensor identification.

The above were all achieved by the work described in this report.

Three of the 9 team-proposed deliverables were completed and are described in this report:

- BomDetec software breadboard design
- Data analysis
- Data fusion approach



Along with this interim report, Siemens is submitting a detailed Phase II proposal for its role in building a breadboard of the BomDetec System from the results of our Phase I testing and simulations, and based on the results of other Team members.

5.3 Approach

Initially, our approach was to utilize “four technologies (intelligent video, radar, x-ray, and terahertz) synthesized into one surveillance vehicle system for suicide bomber detection”, enabling possible “bombers” to be identified and continuously tracked starting at a distance >50M. Siemens came to realize that the “intelligent video” was more than an imaging sensor technology, but rather the glue tying together all the system’s physical sensors and providing the platform to handle the massive “suicide bomber detection” task as we’ve come to understand it. In this role, the video, coupled with the SiteIQ platform, provided:

- An organizational basis for the entire system, allowing the data to “travel” with the pedestrians entering the surveillance zone.
- A ground-based coordinate system and motion compensated object tracking coordinates for the other sensors,
- Alerting operators and providing tracking coordinates for each sensor when a person comes in range, and
- Allowing the utilization of additional sensors of various modalities.

So, in the beginning, video was “one of four”, as illustrated in the now-out-of-date Figure 5-1 below, but by the end, we realized, and the full Team agreed, it was more.

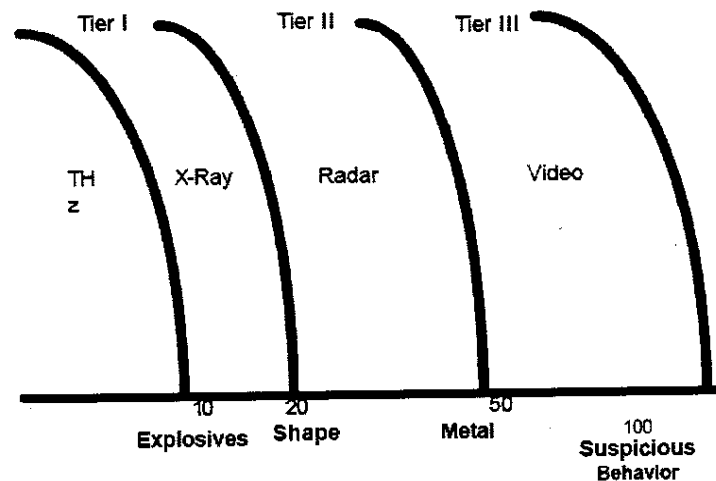


Figure 5-1. Range & Feature Assumptions in the Early “Four-Sensor” BomDetec System Model

Siemens’ personnel traveled to each of the partner installations and worked with the partner personnel to define the sensor data, data transmission protocol, data interpretation algorithms, and sensor hardware and software control system. These data from the partner sensors and knowledge of the Siemens’ intelligent data acquisition and storage, data analysis and fusion, and video sensor control, was the basis for the design of the BomDetec software system, one of our major deliverables.



5.4 Challenges and Roadblocks

From the outset, several challenges, or “roadblocks”, were recognized. They were quite well handled as detailed in subsequent topics in this report. The challenges included:

- How to construct a multi-modality, multi-sensor system
- Providing automated wide-area surveillance
- Determining a platform to meet the system requirement
- Managing resources
- Evaluating the many algorithms and models
- Achieving real-time, robust, high-accuracy performance

5.4.1 How to construct a multi-modality, multi-sensor system

An explosives-detection system usually involves multi-modality multi-sensors, and the environment was known to be of a dynamic nature. The strategic objective of sensor integration and control was to provide a real-time surveillance system that collects data from various sensors, performs data processing and presents information to a human operator.

Multi-sensor systems are not uncommon; however, multi-modality systems are certainly much less common.

5.4.2 Providing automated wide-area surveillance

The challenge for BomDetec was to extend SiteIQ to provide highly automated sensor control and threat analysis of a continuous stream of pedestrians.

5.4.3 Determining a platform to meet the system requirement

As the project started, the challenge was to determine the platform upon which the sensors would attach and bomber detection could be successfully carried out. We evaluated SiteIQ and chose it because it matched key requirements including modularity, ease of integration of multiple sensors, etc.

The SiteIQ “as-is” provides broad-area situational awareness, integrates inputs from sensor network, and generates “alerts” for the human operator, as shown in Figure 5-2 below; however, the BomDetec requirement went well beyond that.



Figure 5-2. SitelQ Capabilities at BomDetec Program Start

5.4.4 Managing resources

There was clearly a need to develop methods for managing resources – sensors, system, and assigned personnel. The system would need to utilize past data on persons, concentrate on unknown persons, etc., to attempt to converge on high-threat/low-threat decisions as quickly as possible, thereby freeing the sensor and computational resources to do the same on other persons.

5.4.5 Evaluating the many algorithms and models

Siemens proposed the need to evaluate many algorithms to determine which would be best. Similarly, there was a need to determine the best models to use for persons, data storage on persons, etc.

5.4.6 Achieving real-time, robust, high-accuracy performance

Achieving real-time, robust, high-accuracy performance in the BomDetec system was identified as a difficult challenge from the beginning.

5.5 System Design Results

The challenges were attacked systematically, leading to the generation of models, simulations, and ultimately to working concepts, design, and testing. This section reviews some of the models.

5.5.1 Reference Model

The objective was to provide a real-time surveillance system that collects data from various sensors, performs data processing and presents information to the operator.

A software system for this application would need three sub-systems: a sensor control unit (SCU), a central control unit (CCU) and a display unit, illustrated in Figure 5-3 below.

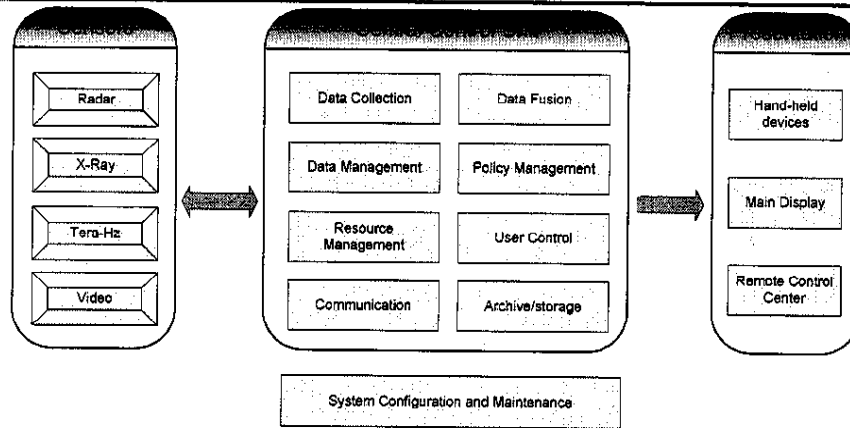
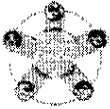


Figure 5-3. System Reference Model

5.5.2 Sensor Communication Model

A sensor communication model was generated as shown in Figure 5-4 below.

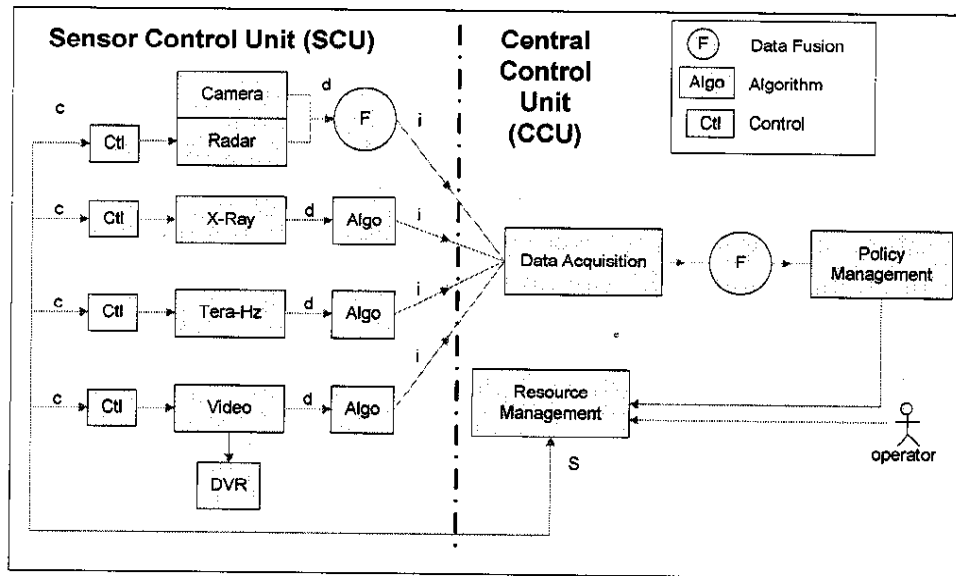


Figure 5.4. Sensor Communication Model

5.5.3 Communication Through Network

The Network Communication Model is shown in Figure 5-5 below, including:

- Communication interface: XML schema and TCP/IP protocol
- Data from the sensor: processed sensor data, status, error, etc.
- Sensor control commands
- Mega data—such as video stream

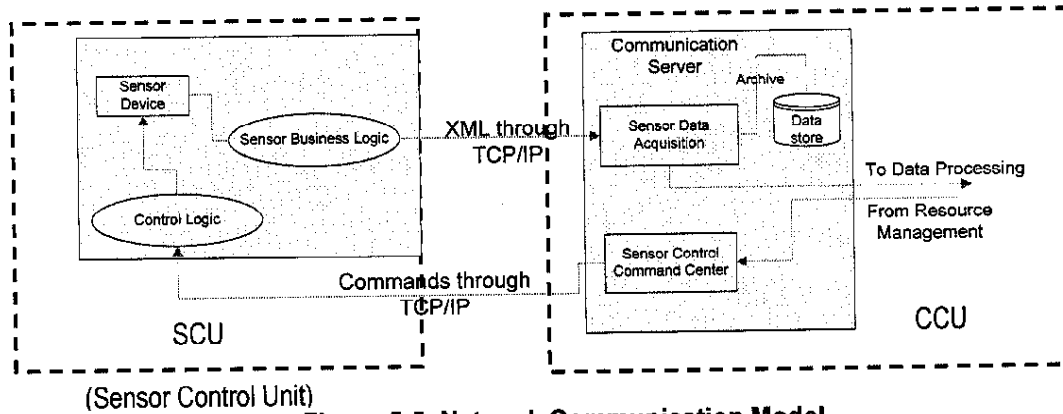


Figure 5-5. Network Communication Model

5.5.4 Data Format

The role of data integration was to provide software framework for receiving and handling data, sending commands, etc. To do this, it was important to document the data and command definitions. Annex A contains the Data and Command definitions documented through Siemens meetings with the other BomDetec Team Members.

5.5.5 Data Fusion

It was recognized that data fusion must be performed at various levels

- Direct fusion of sensor data
- Fusion based on feature vectors extracted from sensor data
- Decision level fusion—each sensor data is processed separately to reach high-level decisions and then combined

Data level fusion is limited

- The sensors all have different physical properties
- Data formats do not agree

Features that can be extracted from the sensors are listed in the table below.

Radar	Backscatter x-ray	Terahertz
range, track, angle	image features such as region, edge, etc.	Spectrum features, such as peak location, signal strength, etc.

The BomDetec system requires a two-task sequence:

- Data Fusion Task 1
 - Perform fusion on dynamically updating data (partial data)
 - Provide fusion results as the input to resource management
- Data Fusion Task 2
 - Organize and register sensor data
 - Present to the operator in the most effective and efficient manner



At the Decision/Feature Level Fusion, features are extracted from the sensor data through data analysis, decisions are made at each sensor level and fused by statistical inference and learning schemes. The fusion of Multi-Modality Data using two-level statistical inference is illustrated in Figure 5-5 below, where the physical properties of an object (metal, chemical, etc.) are described in terms of the object i , property k , at time t .

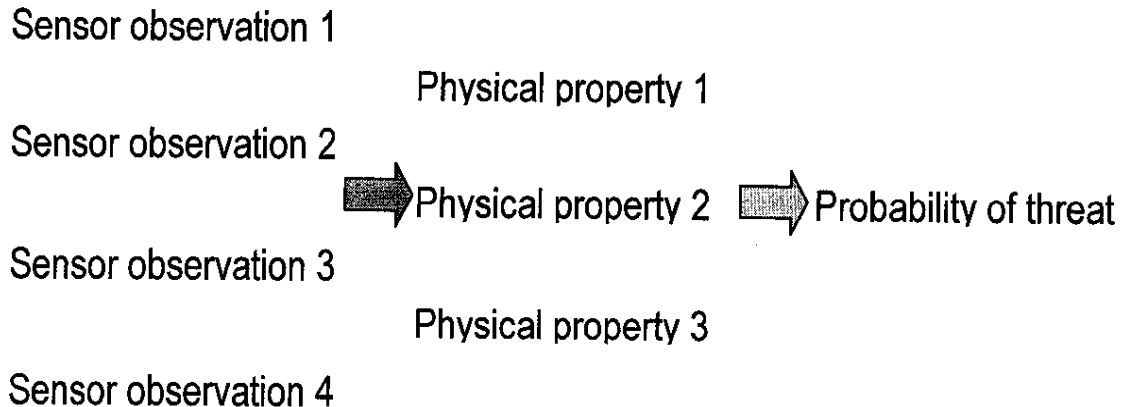


Figure 5-5. Fusion of Multi-Modality Data: Illustrating Two-Level Statistical Inference

The Information Presentation in Data Fusion Task 2 requires registration of location and orientation:

- Video serves as the basis of the unified coordinate system
- Other sensors are triggered according to synchronized location and orientation
- Therefore data is naturally aligned

Both backscatter x-ray and video are image data and therefore it is possible to have data-level fusion—image registration and display. Information presentation interface will be carefully designed to present the sensor data in a most effective and efficient way such that the operator can quickly understand the situation.

5.5.6 Database Schema & Sequence Diagrams

Refer to Annex B for development of the Database Schema and Sequence Diagrams.

5.6 Resource Management Concept Development

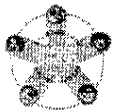
One of the most important parts of this system is the Resource Management Concept.

5.6.1 Active Sensing and the Importance of Resource Management

A fundamental aspect of sensor systems is the limited sensor resource – and determining which sensors should be utilized to evaluate specific pedestrians. Also known as Active Sensing, what is needed is a dynamic decision making process for

- Sensor selection and deployment
- Information analysis and fusion
- Information presentation

The goals of Active Sensing are to:



- Maximize information gain and minimize costs.
- Reduce uncertainty
- Enable alarm generation

The importance of Resource Management can best be understood using a failure example case without or with bad resource management. In these situations,

- The long range sensor will keep generating numerous events
- If, for each event, a PTZ camera is assigned for tracking, soon no PTZ is available for new events.
- Backscatter x-ray and Terahertz sensors would be used upon irrelevant events, and
- Computing power would be exhausted, with slow response.
- The operator would be overwhelmed by emerging events.

5.6.2 Resource Management Process

Resource management is a real-time dynamic process. At any instant, system will evaluate the overall situation to manage available resources—assignment to and revocation from events. (See Figure 5-6 below.)

Guidelines for designing such a process are:

- Resources are assigned to the most relevant event
- Resources for new event are at most times available
- The Resource Management can be overridden by operator

In this way, it is possible for the BomDetec System to efficiently use the limited resources to maximally reduce uncertainty, achieving the goals of Active Sensing.

Information Organization for Events

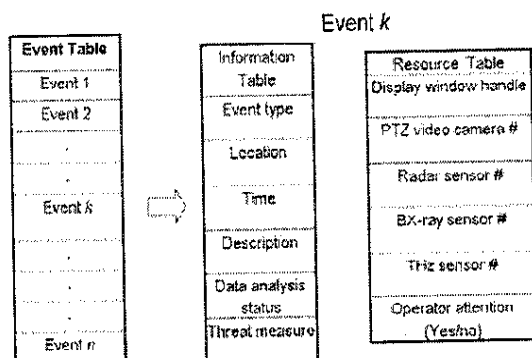


Figure 5-6. Information Organization for Events

The mathematics of the Resource Management process is covered in ANNEX C (Section 5.10.3).

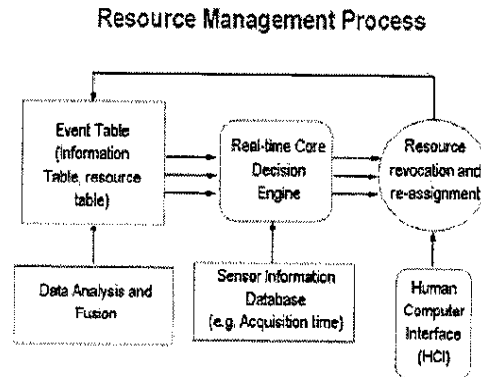
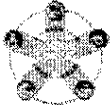


Figure 5-7. Resource Management Process

5.7 Defining Tests of System Feasibility

Following our approach, it was important to test our system-design assertions and verify that the resulting architecture and algorithms would work in conjunction with sensors and other hardware components to achieve the Phase I goals and to demonstrate the feasibility of approach, components, and full-system operation. Siemens conducted tests of Intelligent Video modules as part of its original plan.

In many cases, simulations were more appropriate in Phase I than formal tests. These simulations were important to the Siemens team for developing the major system concepts reported in the conclusions in this report.

5.7.1 Software System (including SitelQ Platform) Simulation

It was important to simulate the software system, including the SitelQ Platform. This includes:

- Evaluation of the SitelQ software system in general.
- Verification of using SitelQ as our software development platform, and
- Confirmation that we will be able to build up a multi-modality sensor system with the software infrastructure.

The functionalities to be simulated included:

- data communication
- sensor setup
- policy enforcement
- resource management

The System Configuration included setting up the SitelQ Platform with PTZ and fixed view cameras, configuring the SitelQ Engine to enable object detection, and defining alarms, zones, and icons for the associated policies.

The simulation system is shown in Figure 5-8.

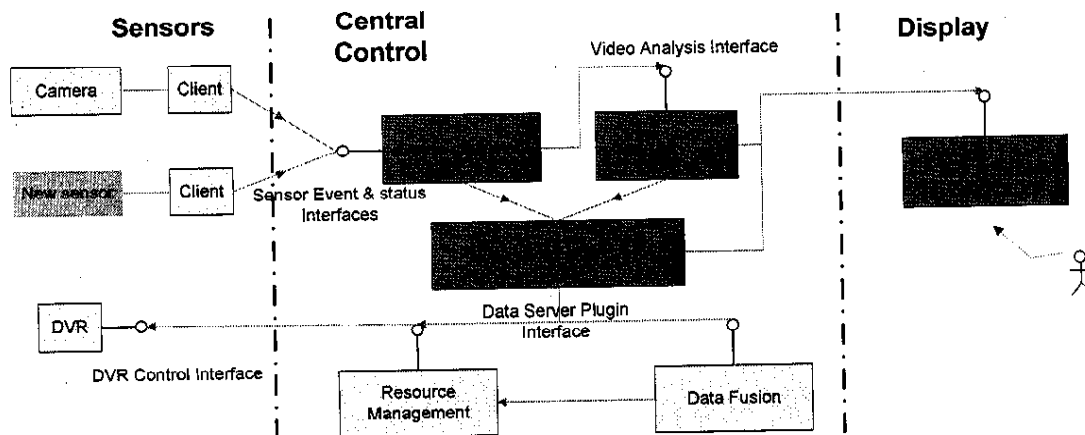
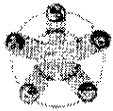


Figure 5-8. Software System Simulation

In this simulation, we added a new sensor (e.g., radar) to the system. New policies and alarms were setup for this new sensor.

5.7.2 Algorithm Testing

We will illustrate algorithm testing in terms of the testing performed on the Detection Algorithms. As an example, we tested two classes of algorithms:

- Part-based Algorithm
 - Search for parts or features
 - Semantically meaningful parts, such as “legs”, “torso”, “head”...
 - And “lower-level” features such as corners, edges, textures, gradient distributions
 - Searching done with multi-scale convolutional filters and histograms
 - Group parts together into pedestrian figures, using
 - The “AdaBoost” algorithm to combine evidence for pedestrian from the parts
 - Rules to reason about occlusion of individuals within clusters of pedestrians & physical obstructions
- Shape-based Algorithm
 - Define pedestrian shape-templates, as in Figure 5-9, using camera and scene geometry
 - Search the image for people
 - Blob detection by background subtraction
 - Fit pedestrian (1 or more) shapes to blob using Markov Chain Monte Carlo (MCMC) methods.

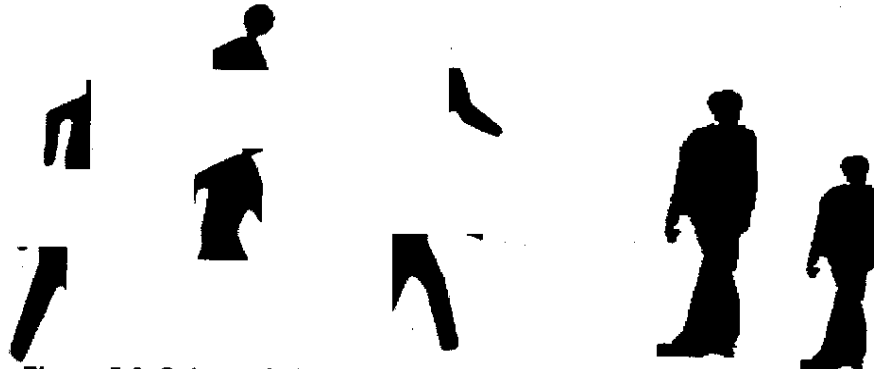


Figure 5-9. Schematic illustrations of “parts” and “shape” detection

Many other algorithms were tested, but the above provides an example of the methodology for determining the testing definitions.

5.8 Test Results

Following earlier use in this report of detection examples, test results are provided. Also, simulation results provided great insight into system performance, and enough information to provide confidence in the feasibility of systems which can be developed based on the Phase I results.

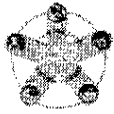
5.8.1 SiteIQ was verified to provide a highly flexible configuration.

As illustrated in Figure 5-10, SiteIQ was verified to provide a highly flexible configuration:

The screenshot displays the Vistascape software interface. On the left, there is a sidebar with various management options: Manage DB, Manage Alarms, Manage Settings, and Utilities. The main window is titled 'Alarm Criteria and Action Administration (Update)' and shows configuration for 'Alarm Region ID: 18' and 'AreaID: 1'. It includes sections for Alarm Criteria (Time Range, Alert Level, Exclude States, Exclude Types), Alarm Region Action Color, and Advanced Alarm Criteria (Speed Range, Width Range, Height Range, Check Object Moving Direction, Check and generate alarm on this). Below these are Alarm Action Settings (Display Active Alarms, Play at sound, View object with live camera, Send Email, Mail Content, Mail Message). A 'Vistascape Object Properties Report' is visible in the top right, showing input object parameters and object ID. The central part of the interface shows a live video feed from a camera, displaying a parking lot with several cars. At the bottom, there is a 'Sensors and Settings' table.

Update	Delete	AreaID	Sensor PCID	Sensor PC Description
Update	Delete	1	129.73.11.100	Radar
Update	Delete	1	129.73.8.72	SCR Proxy
Update	Delete	1	129.73.9.148	Camera

Figure 5-10. Illustrating the highly flexible configuration possible with SiteIQ at the PDR.



5.8.2 Simulations Results for Real-Time Solution, especially regarding Sensor Scheduling

Simulations provided a way to determine the feasibility of Real-Time Solutions, as illustrated for Sensor Scheduling in Figure 5-11 below.

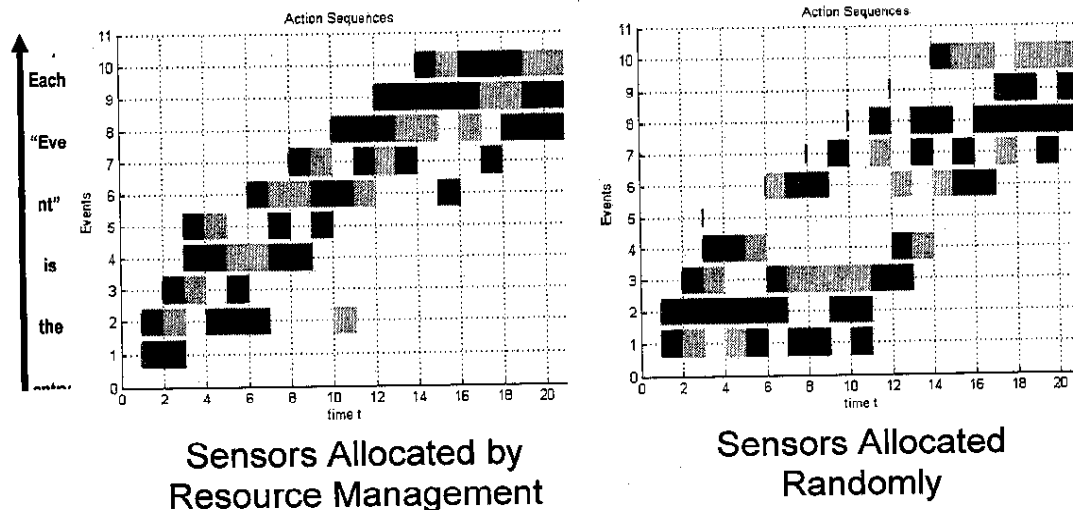


Figure 5-11. Illustrating the feasibility of Real-Time Solutions via Simulation at the PDR.

5.8.3 Simulation Results: Convergence of Threat Levels

While all pedestrians enter the surveillance range with 50% probability of being a suicide bomber or not, the results in Figure 5-12 show that:

- The probabilities diverge to 100% for pedestrian bombers
- And 0% for regular pedestrians.

Further, one can see that “managed” results are faster and hence much better than “random” results.

This point is sufficiently important, that we should restate the Principles of Resource Management and some typical Resource Management Behaviors should be explained.

Again, in the beginning, a pedestrian is assumed to be equally probable being a threat or non-threat. This is the moment of highest uncertainty and lowest information. With each sensor action (measurement), a pedestrian becomes more probable to be either a threat or non-threat. There is reduced uncertainty, based on increased information. An algorithm determines sensor action based on computing the total information gain and to make it maximum. This makes the threat probability of all pedestrians deviate faster from 50% to close to 0 or 100%. The information within a full scene is the sum of information of all pedestrians.

Typical Resource Management behaviors can be illustrated as follows: for a new pedestrian, information is minimal, so the sensor action will greatly reduce uncertainty and gain information; therefore, the algorithm usually assigns a sensor.

For a pedestrian with high certainty of threat or non-threat, there is sufficient information obtained from previous sensor actions, so that more sensor action will not gain much information; therefore, the algorithm usually stops assigning sensors

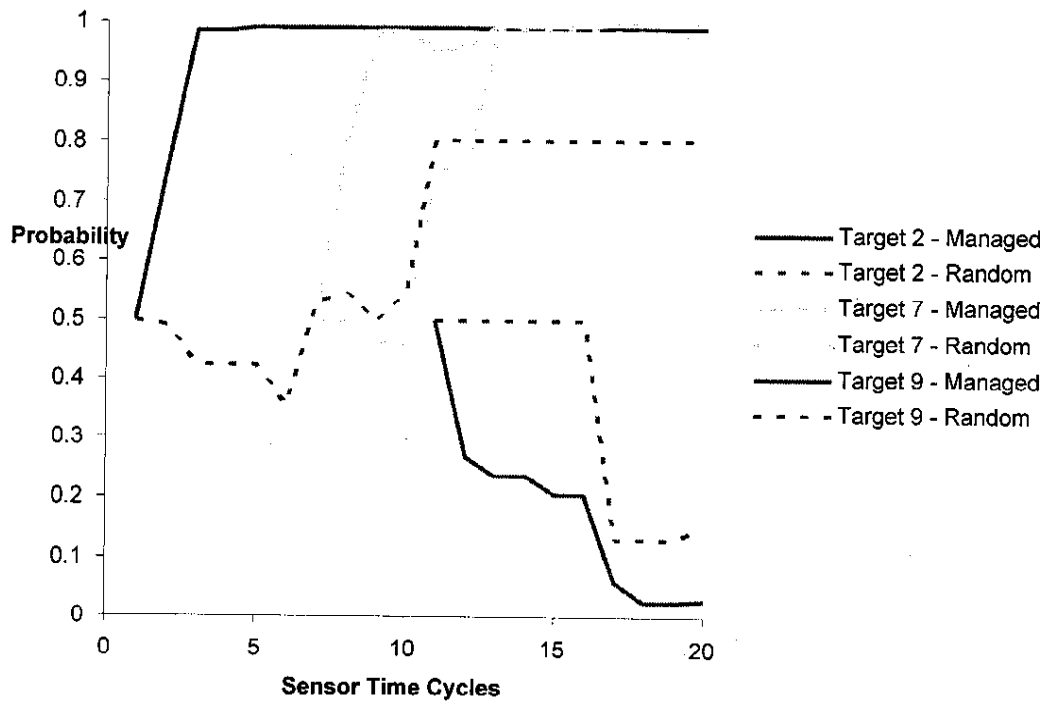
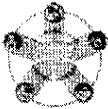


Figure 5-12. Illustrating Convergence of Threat Level Results at the PDR

For a previously measured pedestrian, partial information obtained from previous sensor actions (perhaps some physical property, e.g., metal was detected), so the algorithm will assign a complementary sensor to measure the pedestrian (e.g., chemical). The reason is to maximize information.

An important aspect of the BomDetec system is that it automatically detects and tracks the pedestrians using video tracking as they enter the scene. An operator will occasionally re-initialize tracking on some pedestrian if the tracking algorithm fails to detect or track it. The system performs automatic and dynamic sensor allocation on the tracked objects, as described above.

Occasionally, an operator may identify a suspect behavior and override sensor control, assigning a PTZ video camera to this object to provide a dedicated video stream for the operator. The system performs data analysis and fusion of sensor data and dismisses most of pedestrians as normal. The operator does not need to look at the sensor data.

5.8.4 Pedestrian Detection Results: ROC Curve

We quantitatively evaluate our pedestrian detection results using the receiver operator characteristics (ROC) curve that is common in "detection" engineering.

Our ROC Curve is illustrated in Figure 5-13.

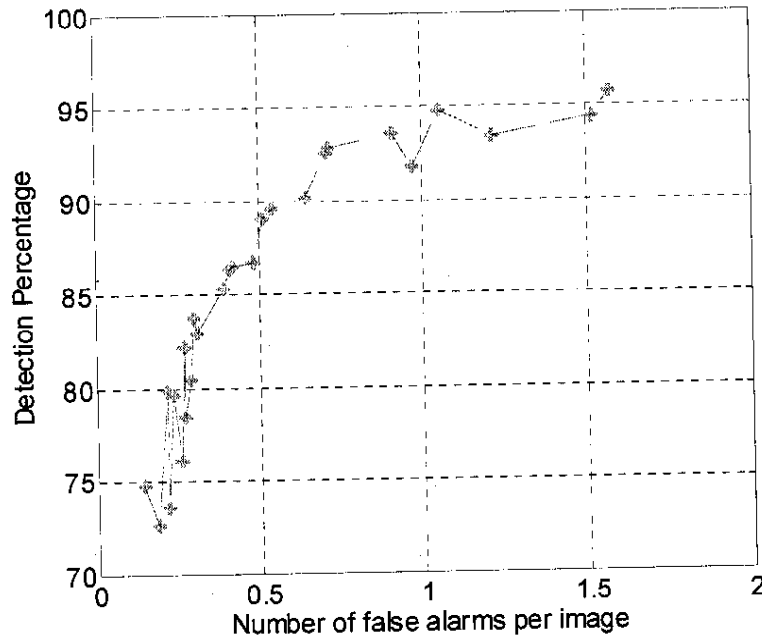


Figure 5-13. Illustrating Detection Results with the ROC Curve.

In this context, the detection algorithm we tested detects over 90% of the pedestrians at the cost of an average of 0.5 false alarms per image, or 95% detection percentage at the cost of 1.5 false alarms per image. These results are comparable to the best pedestrian detectors available [Zhao & Nevatia CVPR 2003] given the complexity of the data (large perspective changes, occlusion and high density crowd).

The detector we tested can serve as a baseline detector for future phases of BomDetec. However, there is still need for improvements in order to best achieve the BomDetec performance we seek, i.e., detecting and tracking of *all* pedestrians in a scene. Our recommendations include:

1. Integrate the detection results temporarily. At any single frame, there might be the risk of miss detection or false alarm. By combining information from multiple frames, however, such risks can be reduced. For example, if a pedestrian is not detected due to partial occlusion, he/she can still be detected once he/she comes out of occlusion. See Figure 5-14 below.
2. Currently our algorithm is not best tuned for the BomDetec scenario. More domain specific priors (camera settings, crowd densities, et al.) will help improve the results.
3. The algorithm runs slowly now (1 frames per second). Programming (software) work is needed to improve it.
4. The algorithm can be improved. For example, the current optimization algorithm (Markov-Chain Monte Carlo) is neither the best nor the fastest.

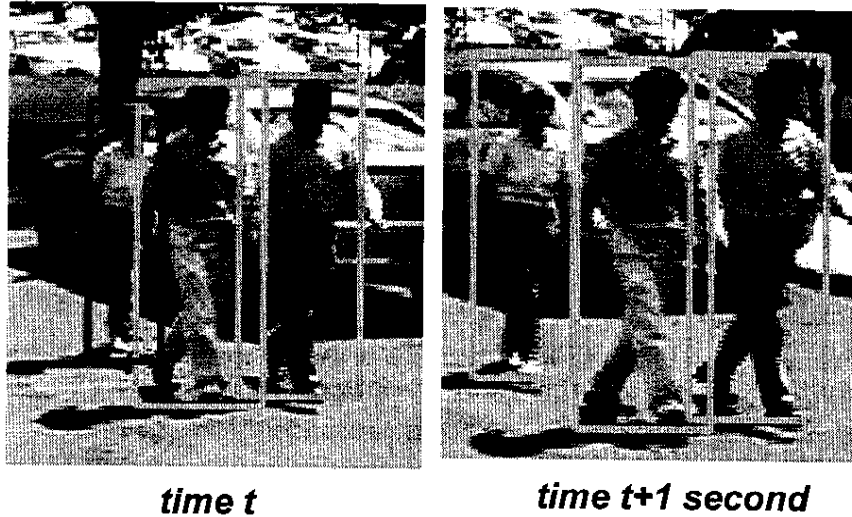
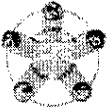


Figure 5-14. Illustrating detection of a pedestrian coming out of occlusion.

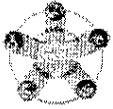
5.8.5 Pedestrian through-put Results based on Operator Workflow Analysis

Siemens conducted an Operator Workflow Analysis to evaluate the performance capabilities of the system, as presented in Figure 5-15.

Time	Distance to Van	System Action		Operator Action	
		Modes: Scan	Present Fusion	Modes: Perception	Analysis Decision
T-24 sec	D-48 meters	Fixed Video tracks new Pedestrian		Observes behavior, appearance	
T-22 sec	D-44 meters	Pedestrian scanned by Radar			
T-20 sec	D-40 meters	Radar derived threat info presented		Operator analyzes radar info If not a threat, Operator can switch to next pedestrian	
T-17 sec	D-35 meters	PTZ Video acquires Pedestrian and presents close-up view to Operator		Operator decides to zoom in with PTZ Video Operator identifies & selects Pedestrian in fixed video feed If not a threat, Operator can switch to next pedestrian	
T-15 sec	D-30 meters			Compares close-up image of Pedestrian and with bomber profile "Flags" Pedestrian as suspicious for scanning by X-Ray / THZ	
T-10 sec	D-20 meters	Prepares for X-Ray / THz scan using motion data from Video		During this time window Operator can switch to Phase 1 Or Phase 3, or view close-up of PTZ Video	
T-0 sec	D-0 meters	X-Ray / THz scan			
T+01 sec	D+02 meters	All data integrated & threat visualization presented			
T+02 sec	D+04 meters			Operator compares Fused Information to Bomber profile	
T+12 sec	D+24 meters			Operator decides Pedestrian is a threat and generates alert	

Figure 5-15. Operator-intensive scenario Workflow Analysis

The pedestrian through-put Results based on this analysis are as follows:



- One operator scenario
 - Can sustain continuous rate with pedestrian spacing of 60m, (30 seconds), or **120** people/hour
- Two operator scenario
 - Each operator specializes on Phase 1 or 3
 - Can sustain continuous rate with pedestrian spacing of 20m (10 seconds), or **360** people/hour
- Four operator scenario
 - operators work Phase 1, which has 3 sub-phases, 1 operator works Phase 3. They could divide the labor by pedestrian or by sub-phase (Experiment needed)
 - Can sustain continuous rate with pedestrian spacing of 5m (2.5 seconds), or **1440** people/hour

5.8.6 CONOPS Demo/Simulation Results

Siemens produced a CONOPS concept demo and simulation and presented it at the PDR. The CONOPS is contained in Section 2.

5.8.7 Tracking results - Overview

We collected several trackers for the BomDetec project. We tested on the following tracker.

1. The mean-shift tracker [Comaniciu et. al. CVPR 2000, ICCV 2001]. This is an efficient tracker utilizing color histogram and greedy gradient ascent search. The advantage of such a tracker is that it uses primitive features such as color so that it is robust to distortions due to non-rigid body motion, rotation and partial occlusions. We have running code for this tracker.

2. Variations of the mean-shift tracker, including variations in the number of color bins per color channel.

We found that the above tracker and its variations seem to be sufficient for Phase I. However, we also collected the following trackers for Phase II (most of which are implemented in C++ and one in MATLAB), and they can be adapted to BomDetec requirements:

1. Variations of the mean-shift tracker, including variations in the number of color bins per color channel (we have running code) and Kalman filter (we have the code, but we did not test it for Phase I because the base-line tracker seems sufficient).
2. Discriminative trackers [Lu & Hager CVPR 2007, Collins et al. ICCV 2003].
3. Multiple-view tracking (including a PTZ master/slave system).
4. Tunable kernel tracking [Parameswaran et. al. CVPR 2007].

To best understand the influence of tracker performance as a result of occlusion, we use data with 3 levels of occlusion:

- no occlusion,
- partial occlusion, and
- severe occlusion (see Figure 5-16 below).

The levels of occlusions are labeled by a human expert but not visible to the tracking algorithms.

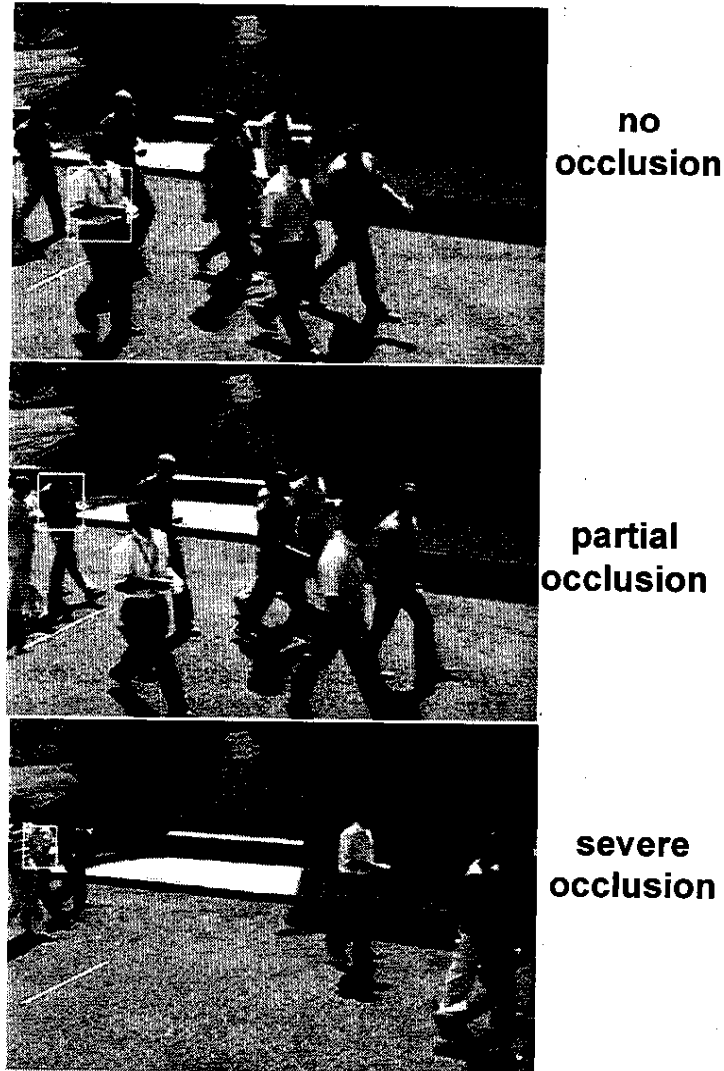
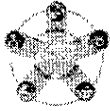


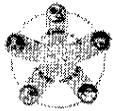
Figure 5-16. Illustrating Levels of Occlusion

Tracking of a pedestrian is being classified into two classes:

1. Succeed, the pedestrian is tracked throughout all frames
2. Partial failure toward end, the pedestrian is lost. The reason we call it partial failure is the tracker usually succeeds in the beginning and only fails in the last few frames, which usually composes only a portion of the whole sequence.

5.8.8 Tracking Analysis – close range

We consider close range to be between 2 and 30 meters, from a camera to a pedestrian to be tracked. We first tested the tracking algorithm with a mean-shift tracker. The algorithm used 5 bits per channel for generating the color histograms. The tracking results are summarized in the following table, e.g., without



occlusion, we achieved a tracking success rate of 91.5% (86 out of 94). The small amount of failure is due to color similarity between foreground (pedestrian) and background. The speed for tracking is about 10 milliseconds per target. That is, we are able to track at most 3 persons per CPU using this algorithm assuming the video rate is 30 frames per second (33 milliseconds per frame). By using multiple-threading algorithms on multiple-CPU as well as better implementation, this number can be significantly improved.

	No Occlusion	Partial Occlusion	Severe Occlusion	Speed
Mean-shift tracker (5-bits/channel)	91.5% (86/94)	83.8% (31/37)	61.5% (16/26)	~10 ms

We then tested a mean shift tracker with 7 bits per channel for color histogram generation. The improved tracking results are shown below. The experiments confirmed our intuition that higher resolution in the color space improves the discriminative power of a tracker. It recognizes foreground and background better. However, this tracker is no longer real-time, and it requires 250 milliseconds per tracked pedestrian. Improvements can be made in the future.

	No Occlusion	Partial Occlusion	Severe Occlusion	Speed
Mean-shift tracker (7-bits/channel)	96.8% (91/94)	86.5% (32/37)	69.23% (18/26)	~250 ms

5.8.9 Tracking Analysis – Long range

We consider long range to be over 30 meters between the pedestrian and tracking camera. We observed that people at 100 meters are too small for any visual tracker using conventional camera setups as illustrated in Figure 5-17 below.

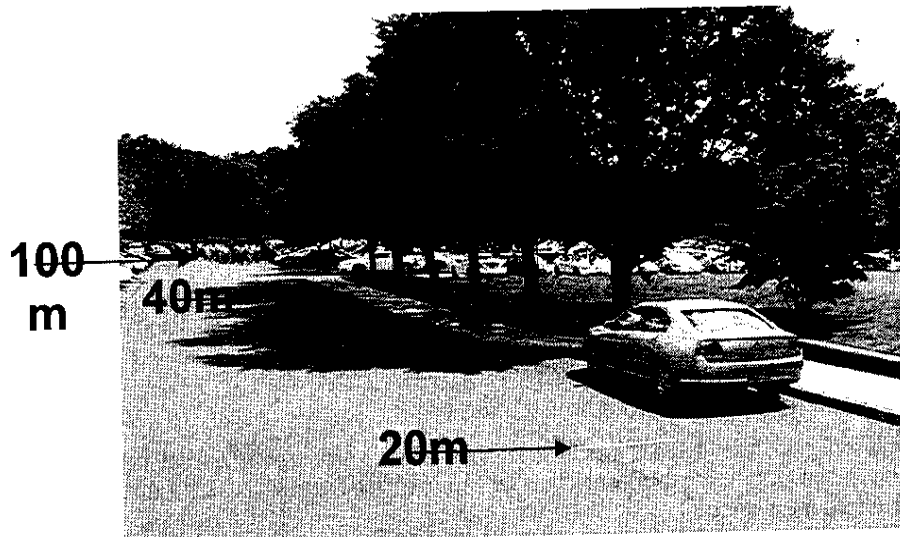
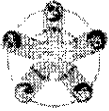


Figure 5-17. Illustrating Long Range Tracking

We propose variable focal-length camera arrays for the task. We tested the mean shift tracker with 5-bits per channel for targets around 40 meters. The tracker performance is summarized in the following table.



	No Occlusion	Partial Occlusion	Severe Occlusion
Mean-shift tracker (5-bits/channel)	88.0% (22/25)	80.0% (4/5)	40.0% (2/5)

5.8.10 The Need for Multiple-View Localization

Another important role of the intelligent video system is to provide a coordinate system for all sensors in the system. The coordinate system provides spatial and temporal information of an event and synchronizes multi-sensor actions. For example, the x-rays should be fired exactly when a pedestrian passes through its sweeping plane.

It is well-known that by using a single camera we cannot estimate the depth of an object. Thus we need at least two cameras, as illustrated in Figure 5-18 below.

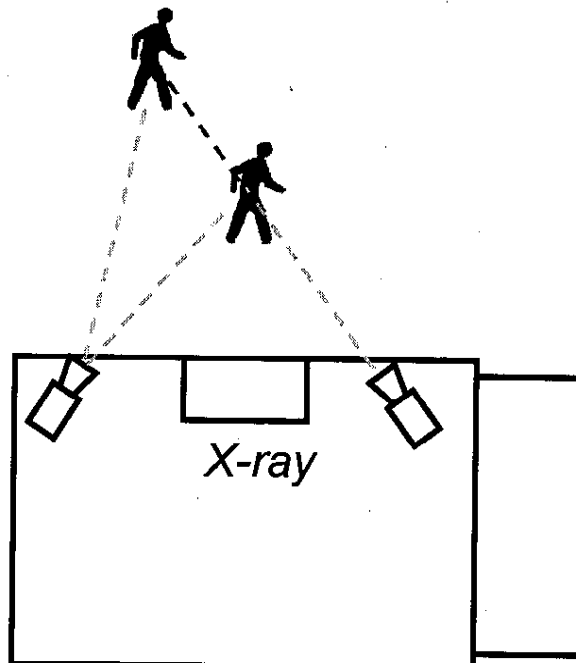


Figure 5-18. Illustrating the Need for Multiple-View Localization

5.8.11 3D Localization Testing

We used a stereo rig with two Firewire (IEEE 1394) cameras as shown in the following Figure 5-19 for 3D localization test. The two cameras have a baseline length of about 70 centimeters.

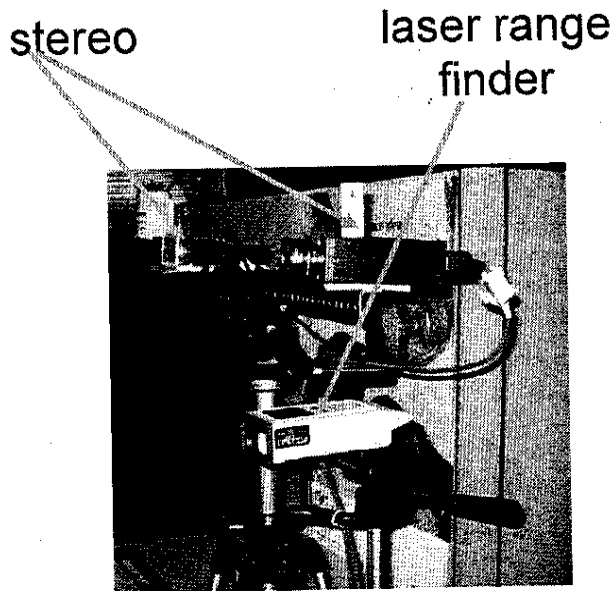
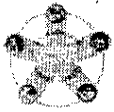


Figure 5-19. Illustrating 3D Position Measurement.

To calibrate the cameras, we used a check-board pattern and the *camera calibration toolbox for MATLAB* (http://www.vision.caltech.edu/bouquet/calib_doc/).

In order to measure 3D, we need to find the corresponding feature point in the right image given a feature point in the left image, where feature points are usually corners. To find corresponding feature points in the two input images, e.g., nose tip projections in the two images, we compare the intensity patterns around two hypothesized corresponding feature points using a method called sum of absolute difference (SAD). The intensity patterns are subtracted pixel-by-pixel, and the summation of absolute values of their intensity differences is used as a measure of successful correspondence. The smaller the SAD, the better the chance of finding correspondence. The search is done over all possible range, in this case, along a line called epipolar line.

After calibration and finding correspondences, triangulation was used for measuring the 3D positions of the feature point in the left image, as illustrated in Figures 5-20 and 5-21 below. First the checker board pattern is used for calibration:



Figure 5-20. Illustrating 3D Position Measurement - Calibration

Then the Sum of Absolute Difference is utilized for finding correspondence:



Figure 5-21. Illustrating 3D Position Measurement – Finding Correspondence

5.8.12 Distance (Depth) Measurement - Results

We use the calibrated stereo rig and collected images for distance (depth) measurement test. The comparison of the ground-truth measurement and the stereo measurement is shown in Figure 5-22. In the figure, we plotted all measurements of all people standing within 10 meters to the stereo rig. By visual inspection we see that the stereo measurement agrees very well with the ground-truth. To further investigate the measurement error, we plot the measurement errors in the right figure. The measurement errors are about 0.3 meters at 10 meters, or 3% error. We discuss the implication of these measurement errors in the next section.

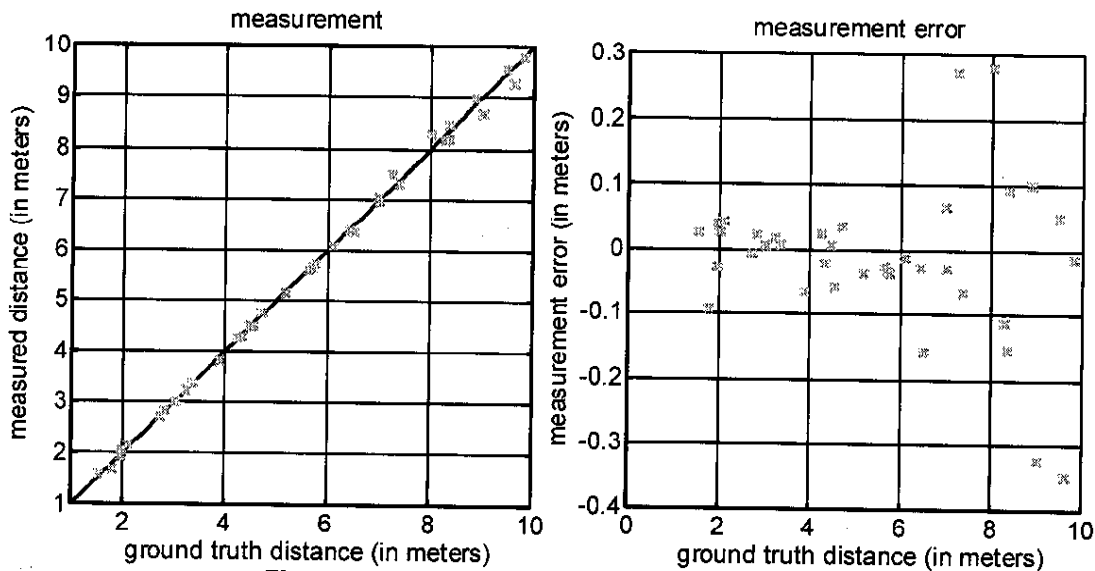
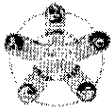


Figure 5-22. Illustrating Distance Measurement

5.8.13 Is the Distance (Depth) Measurement Accurate Enough?

There are two different types of tasks in which accuracy of 3D measurement is critical. The first type is synchronization among different sensors, i.e. telling different sensors when to fire. We believe the accuracy of the above mentioned stereo system is sufficient for this task. Due to temporal resolution of the system (time delays in the system), it is usually not advisable to be stringent on sensor firing time. Instead, it is safe to leave a temporal buffer before and after the exact event time. For example, we may want to fire the x-ray 0.5 seconds before the hypothesized pedestrian passes through the x-ray sweeping plane, and remain scanning 0.5 seconds after the hypothesized pedestrian passes the plane. In this case, the stereo accuracy is sufficient and the amount of synchronization error is usually negligible compared with time delays in the whole system.



The second type task for a video system is to guide point-and-shoot type of sensors such as the Terahertz or the radar. We calculated that under the configuration shown in Figure 5-23, the amount of distance measurement error corresponds to a spot of diameter 10 centimeters on the target at a distance of 10 meters from the sensor. This is sufficient if the pedestrian is facing the sensor considering the typical dimensions of a people. This will be slightly more complicated if the pedestrian is walking with his/her side toward the sensor. In this case, it is advisable that the point-and-shoot sensor takes into account of the stereo measurement error and plan scanning sequence accordingly.

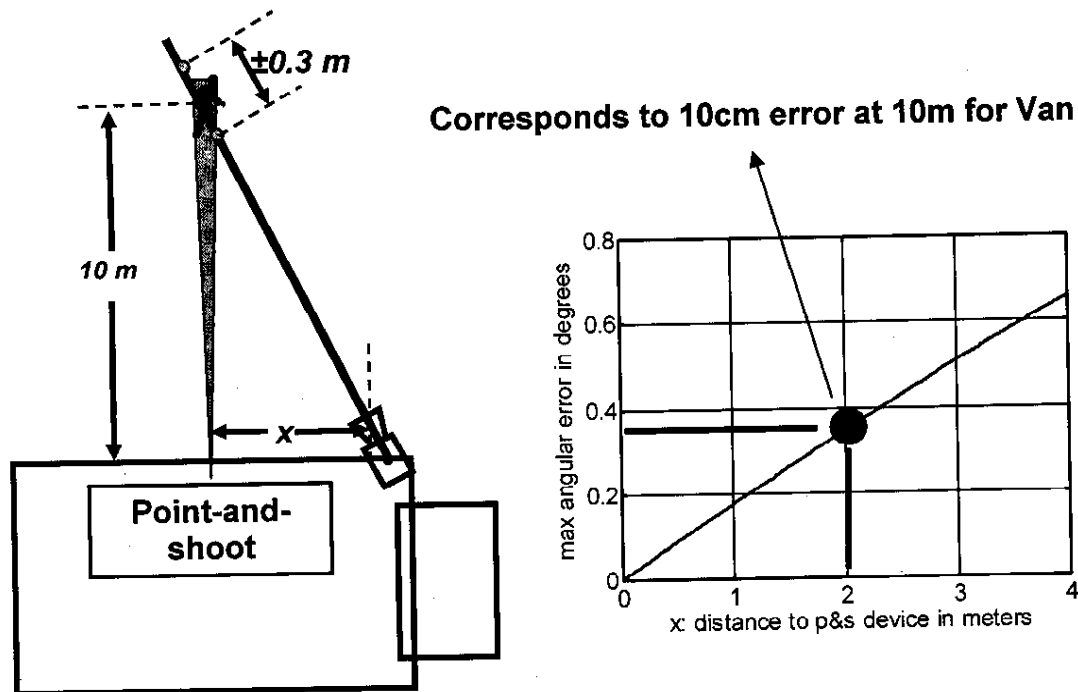


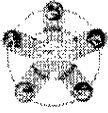
Figure 5-23. Illustrating the correspondence between distance and angular error.

The stereo measurement system we built for Phase I can be improved in many ways,

1. Finding correspondence is still the most computationally intensive and error-prone part. We propose to use background subtraction to limit the search range of a feature point. In this way, we can simultaneously increase the robustness and reduce the computational burdens.
2. The exact sensor placements will be further investigated in Phase II taking into account: stereo measurement accuracy (large base-line placement increases measurement accuracy with less verging angle), angular measurement accuracy (closer to the point-and-shoot sensor, less angular error), et al.
3. The current code is written in MATLAB. For real-time performance, we need to code it in C++.
4. We need to define an easy multiple camera/sensor calibration system. This is critical because we need sensors to communicate using a common coordinate system.

5.9 Conclusions

Conclusions were derived from this work at both a high level, and also for the "Challenges" enumerated earlier in this report.



5.9.1 High-level Intelligent Video Conclusions

At the highest-level of overview, the conclusions for our Phase I work are:

- The range of intelligent video technologies is found to be extensible to address BomDetec tasks: pedestrian detection and tracking, 3D target localization, multi-sensor calibration and mosaicing.
- Intelligent video sensors meet the Hardware Specification of a Platform Object.
- Intelligent video sensors meet Physical and Environmental Operating Parameters.

5.9.2 Multi-modality Conclusions

Multi-modality integration conclusions were generated, including:

- A key characteristic of the BomDetec system is its support of multi-modality sensor technologies.
- Different levels of data fusion can be achieved inside BomDetec through the connections to the Policy Engine and Resource Management. For BomDetec Phase 2, it is feasible to implement a decision level data fusion.
- (Multi-modality) Data Communication and Sensor Control protocols will be based on the SitelQ infrastructure.

Having said that, it is clear that future work is still needed:

- Design and develop registration, calibration and control algorithms for multi-modality sensors.
- Design and develop simulation systems to simulate and benchmark system performance with different sensor configurations.

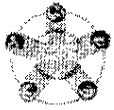
5.9.3 Conclusions on SitelQ as Integration Platform

The Conclusions on SitelQ as an Integration Platform are as follows:

- The software architecture of SitelQ is close to our system reference model approximating its three major subsystems: Sensor Control Unit, Central Control Unit and Display Unit.
- It is feasible to register non-video sensors and set up policies associated with each sensor. SitelQ offers the ability to easily integrate new sensors.
- SitelQ provides possibility and flexibility to integrate external systems or components into SitelQ. Therefore, we can build our own control, data processing, and display components on top of SitelQ.
- Data storage, reporting and system maintenance of SitelQ can be extended to suit our needs.
- SitelQ is now part of the "Siveillance" product line from Siemens Building Technologies, and it includes a modular video analytics platform that addresses a range of indoor video analysis functions as well as traffic video analysis and perimeter intrusion. We anticipate the integration of our Phase 2 video analytics and sensor fusion modules into this platform.
- Significant assistance from Siemens' VistaScape Division will be needed to efficiently make the extensions needed in Phase 2.

5.9.4 Pedestrian through-put based on Operator Workflow Analysis

Conclusions on pedestrian throughput based on Operator Workflow Analysis are:



- Automation of threat detection and analysis is necessary to boost throughput above those using operator-intensive workflow scenario.
- It is not feasible for the operator to do the following:
 - control every sensor action
 - keep track of every pedestrian
 - view the sensor data of every pedestrian even if the data is reduced through data fusion
- Otherwise the operator will soon get overwhelmed by the continuous stream of pedestrians and their data; however,
- On the other hand, there should be a systematic way to optimally deploy limited sensor resources to maximize information gain.

5.9.5 Resource Management Conclusions

The Resource Management conclusions are as follows:

- The need for Resource Management established through operator workflow analysis of the streaming pedestrian urban sidewalk ConOps.
- The feasibility of Markov formalism demonstrated through simulations.
- Resource Management software development and testing will be a significant task in Phase 2.

5.9.6 Pedestrian Detection Conclusions

The Pedestrian Detection conclusions include:

- The tested pedestrian detection algorithm can be adapted and utilized as a baseline detector.

Our recommendations are:

- Add temporal integration to resolve uncertainties and ambiguities
- Future work is needed, including:
 - Adapting to BomDetec scenario (training for the specific camera settings, crowd density, etc.)
 - Increasing speed (currently about 1 fps) thru algorithmic & software improvements.

5.9.7 Tracking at mid/long range (>30m)

People at 100 meters are too small for the trackers, and tracker performance is not as satisfactory as close range. We determined that variable resolution/focal length cameras needed, since many pixels wasted on background (sky, vegetation, etc). A combination of short focal-length and long focal length cameras make people at long range appear as large as short range, so they will be designed into the system and tested in Phase II.

5.9.8 Need for multi-focal length cameras

We concluded that there is a need for multi-focal length cameras. Our recommendations are:

- Short range (2-20 m) tracking can already be applied with fairly good performance
Mid/long range tracking will equal short range tracking using new optical/algorithm design.



- Miss tracked pedestrian can be readily re-detected & re-tracked (with a new ID). Group tracking (versus individual tracking) will help.
- Multiple camera tracking can alleviate occlusion effect.

Future work is needed:

- Improve speed
- Sensor planning
- Algorithmic improvements
- Software integration work

5.9.9 3D Localization Conclusions

Our conclusions on 3D localization are:

- Accuracy of 3D localization at 10 m is sufficient for targeting sensors
- Finding correspondence is the most computationally intensive and error-prone part
- Other cues such as background-subtracted image can help

Future work is still needed:

- Sensor planning
- Easy calibration procedures
- Robust correspondence algorithm development
- Re-engineer research code into integrated software framework.

5.9.10 Achieving real-time, robust, high-accuracy performance

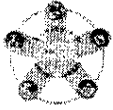
The Phase I system does not operate in real time, so this will be an important goal for the Phase II system.

5.10 Annexes

5.10.1 ANNEX A - Data and Command Definitions

This section contains the Data and Command definitions documented through Siemens meetings with the other BomDetec team members.

- Video: Data Definition
- Terahertz: Data Definition & Command Definition
- Radar: Data Definition & Command Definition
- X-ray: Data Definition

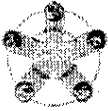


Video: Data Definition; page 1 of 2

Category	Name	Description	Unit	Size
Raw data	Image Radar	Image that is pointed in the same direction as the radar	pixel	TBD (i.e. 1024x768 RGB compressed)
	WideAngleView	Image that combines images from multiple fixed cameras into a panoramic view of the scene	pixel	either 3x1280x1024 RGB or a combined panorama image of yet undetermined size
	PTZViews	Detailed views from the individual PTZ cameras	pixel	1024x768 RGB
Feature/Event	PeopleTracks	world position, speed, orientation and probabilistic uncertainty of these values	bytes	2 3-d float vectors + 1 float value + 2 3x3 float matrices = > 100 bytesper track
Processing Outcome	Initiation and Tracking of People	People entering the scene are detected and tracking is initiated. The position and identity information is transmitted to the the CCU using the SiteIQ xml format via TCP/IP		

Video: Data Definition ; page 2 of 2

Performance	Radar and Wide-Angle Cameras	These cameras are pointing in fixed directions thus they should be able to give a consistent frame rate of ≥ 25 fps.	ms	
	PTZ Cameras	Depending on the distance in positional space there is some delay in focusing in on new targets. Frame rate ≥ 20 fps. Evaluation in progress.	s	
	Detection and Tracking Algorithms	Depending on the number of tracks the response time will change. We will enforce a minimum response rate based on the tracking accuracy that is necessary to accurately aim the x-ray and t-hz sensors. Goal is to achieve 20 fps for up to 20 people. Frame rate can be adjusted by lowering the tracking accuracy for faraway (= low-priority) targets.		
Status / Error	All Cameras	general status and error information		
	PTZ	current position/orientation		
	Tracking Algorithm	information about computation load/delay/number of people lost		



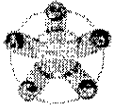
Tera-Hz: Data Definition

Category	Id	Name	Description	Unit	Size
Raw data	1	waveform	THz time domain signal	Byte	10k (tentatively)
	2	spectrum	FFT of wave form	Byte	10k
	3				
Feature/Event	4	Peak positions	Peak frequencies in spectrum	THz	Array of real (1k)
	5	Peak intensities	Peak intensities in spectrum	Byte	Array of real (1k)
	6	Target distance	Measured distance by from time of flight of THz beam. It should have finer resolution than other sensors.	m	1
Processing Outcome		FFT	Sent to CCU		10k
	11	Spectrum comparison	Comparison of FFT data with built in explosive library		
	12	Possibility of possession of explosive material	Lower possibility of the possession of explosives	byte	1
Performance	13	Alert	High possibility of the possession of explosives	Byte	1
	14	Time1	Sensor reaction and data acquisition	sec	2
	15	Time2	FFT, comparison	sec	1
Status / error	16	ready	Sensor is ready to run	byte	1
	17	scanning	Sensor is scanning	byte	1
	18	error	Error in THz sensor	byte	1

Table 1: Descriptions of sensor outputs

Tera-Hz: Command Definition

command	Operation	description
start	Start scanning	Start scanning of THz sensor.
stop	Stop scanning	Abort THz sensor scanning
Associated commands	Start scanning command initiate several commands inside of THz sensor:	(Internal commands) Move to initial position, set mirror position, start scan
Echo a received command	possible	
Other information	THz sensor needs frequently updating position and orientation (angle (θ,φ)) data. Position data needs to be specific to the portion of the target. For example, if the target seems to have explosive around the chest, the position data needs to be the position of the chest, rather than head or shoulder.	
Other information	Processing of raw data. THz sensor need further processing in CCU. A comparison of library data to raw data sent to CCU to extract peak position/intensity pattern to generate alert.	



Radar: Data Definition

- Raw data will be processed by a pre-processing unit within the sensor unit.
- Output from the Radar unit contains threat declaration.
- Data will include multiple object tracks within 10 degrees
- Each track contains dynamic data that will update in sub-seconds

	Category	Name	Description	Unit	Size	
Radar	Raw data		Processed by Radar Pre-processing unit			
	Feature/Event	Range		Object range information		
		Angle		Object angle		
		Track		Detected object track		binary
	Processing Outcome	threat		Detected threat declaration		
	Performance			Radar response in milliseconds	ms	
				Pre-processing is done within seconds	s	

Radar: Command Definition

- "Heartbeat" signal can be sent regularly for notification of status

	id	Operation	command
Radar	1	Start	Start Operation
	2	Stop	Stop Operation
	3	Steer	Steer to certain angle

Table 2: Descriptions of sensor control



Backscatter x-Ray: Data Definition

	Category	Description	Unit	Size
X-Ray	Raw data	The Sensor data produced by the X-ray inspection system is a binary file. It is a proprietary format but is similar to TIFF. The metadata that the system can include is configurable but is at a minimum: <ul style="list-style-type: none"> • Date and Time • Operator Name • Comment 	KB	1500
	Feature/Event	The Backscatter X-ray image produced will allow an operator to detect a Low Z Atomic number element anomaly in suspect target. This detected anomaly is then interpreted to be a threat (Explosive) or not by the operator by using SW tools available to operator.		
	Performance	The X-ray Sensor needs time for the X-ray generation subsystem to begin generating x-rays, this takes around 10 seconds. A minimal time frame is needed to scan a suicide bomber (Around 1 second). So the duration of command reception and data sending is ~10 seconds. But the operator may need 30 seconds or so to manipulate and analyze the image to determine if a threat is present.	sec	10

5.10.2 ANNEX B - Database Schema and Sequence Diagram

5.10.2.1 Database Schema

The central data repository of BomDetec consists of tables that store data on the following topics:

- Object Tracking
- Threat and Alarm Criteria
- Sensor Registration and Configuration
- Reporting

SQL Agent jobs and stored procedures will be used for database routine maintenances and data manipulation.

5.10.2.1.1 Object Tracking

Sensors send data concerning the type and characteristics of the objects they track to the central database. The data is then stored in the above tables. The data is also copied for long term storage to the archive database. The data contained within the ObjectLocation is regularly pruned by SQL Agent job.

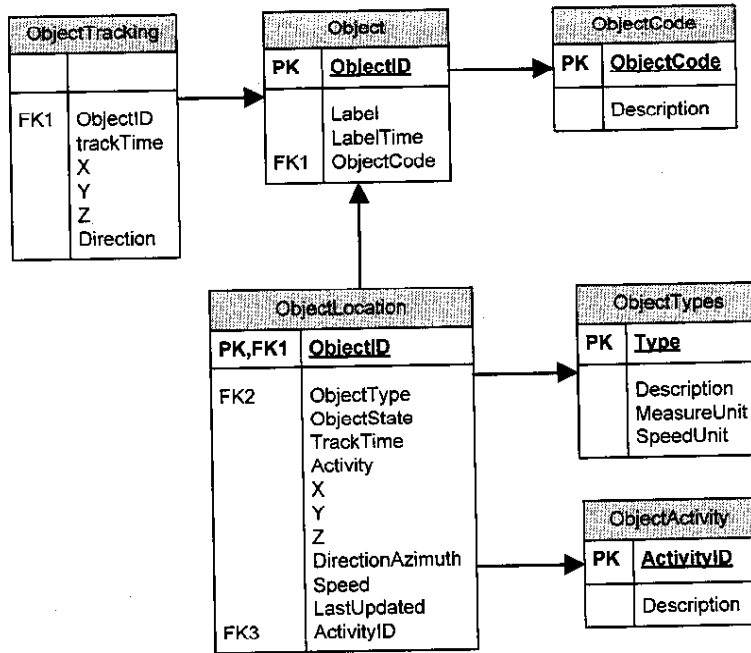
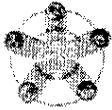


Figure 5-24

5.10.2.1.2 Threat and Alarm Criteria

When an alarm occurs, a record of the alarm occurrence is stored in the Alarms table and the active criteria in place when the alarm occurred are recorded in the AlarmDefinition_Map table. Threat levels are predefined while confidence levels are provided by each sensor.

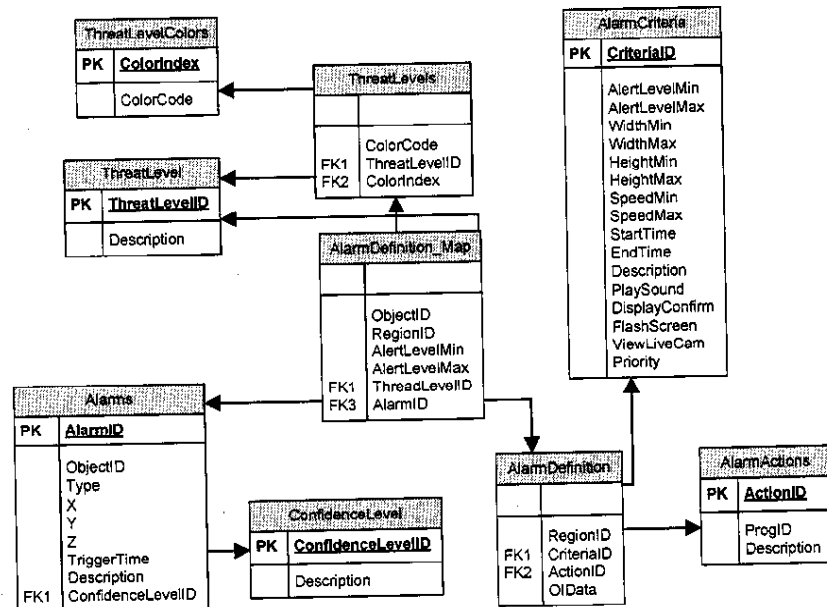
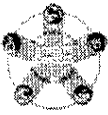


Figure 5-26



5.10.2.1.3 Sensor Registration and Configuration

The Sensors table contains a record for each sensor such as fixed camera, PTZ camera, Radar, X-Ray and Terz. One or more instances of the sensors may run on a single computer. The SensorIP column of the Sensor table contains the IP address of the machine on which the sensor software is installed. SensorID is a unique identifier to identify each registered sensor.

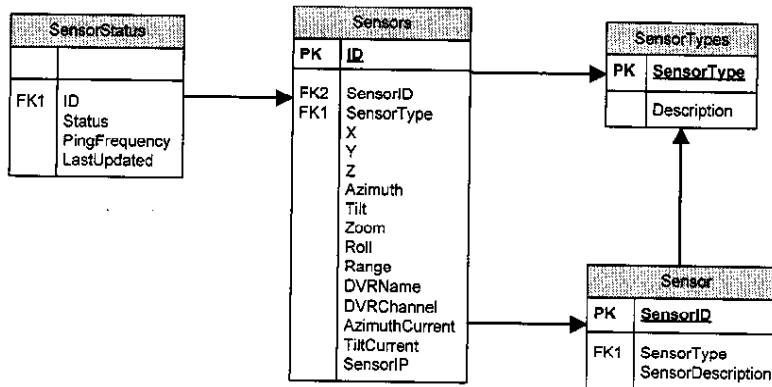
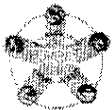


Figure 5-27

5.10.2.1.4 Reporting

Reports are generated from the following tables: AlarmSummaryReport, ObjectSummaryReport, ObjectDetailReport, SensorProblemReport, ThreatSummaryReport, ActionSummaryReport, etc.



5.10.2.2 Sequence Diagram

5.10.2.2.1 Sequence Diagram 1 – Normal Operation Mode Module-Level Data Flow

In normal operation scenario, each sensor sends event data (in XML) to the Data Server of the Central Control Unit. The Data Server then performs first level data analysis, i.e. sifts out invalid data package. The processed data is then stored in the Central Data Storage. With a decision level data fusion, the Policy Engine evaluates predefined rules with the input event data and if a threat level and its confidence score meet certain alarm criteria, the associated alarm will be triggered. And the alarm will be reflected on the display. At the same time, information about the tracked object, threat and alarm is stored in database for reporting purpose. Resource Management coordinates its internal sensor control command list based on their priorities and sends control commands to the sensor units.

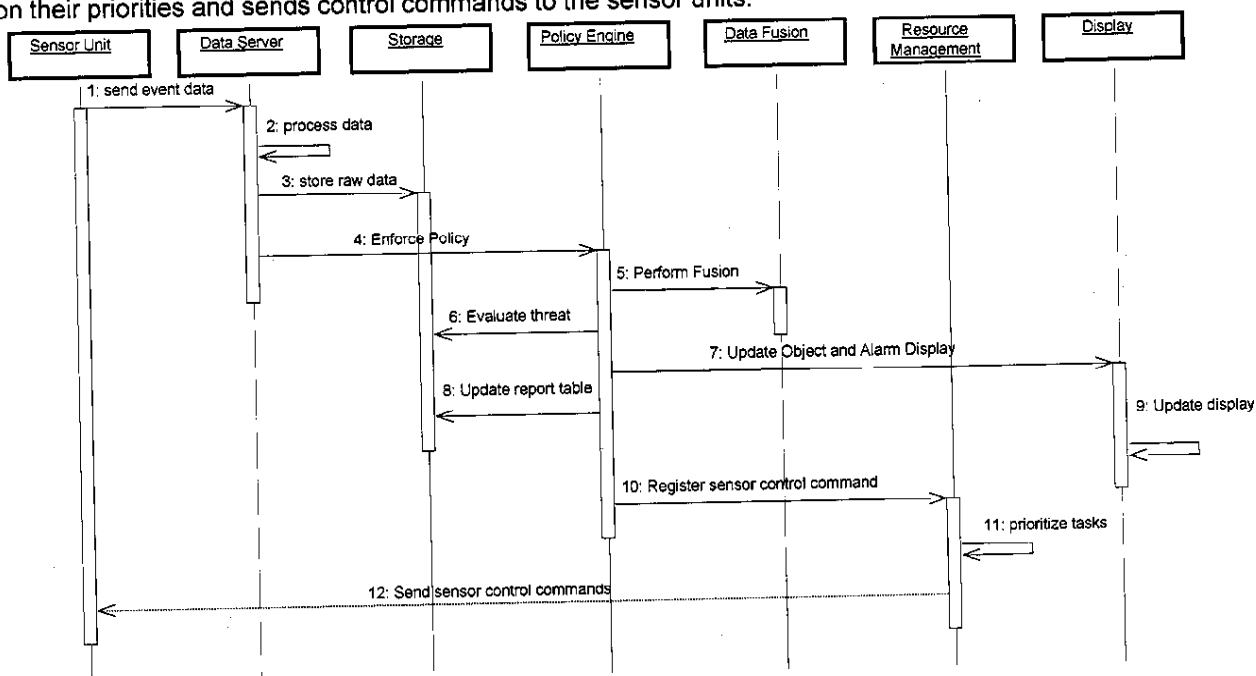
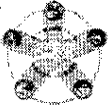


Figure 5-28



5.10.2.2.2 Sequence Diagram 2 – An example of Data Fusion

In this example, a radar sensor detects a threat and sends this information to the Central Controller. Policy Engine evaluates the threat with the policy database. If a decision can not be made, it creates a track for further tracking. When another threat is detected on the same object by the X-Ray sensor, the Policy Engine evaluates it again with the policy database. At the same time, track information for this object is updated and forwarded to the Data Fusion Module. Based on threat levels and their confidence scores, the Data Fusion Module sends result back to the Policy Engine. Then alarm criteria are evaluated with the fusion result. An alarm will be issued if the fusion result meets any alarm criteria.

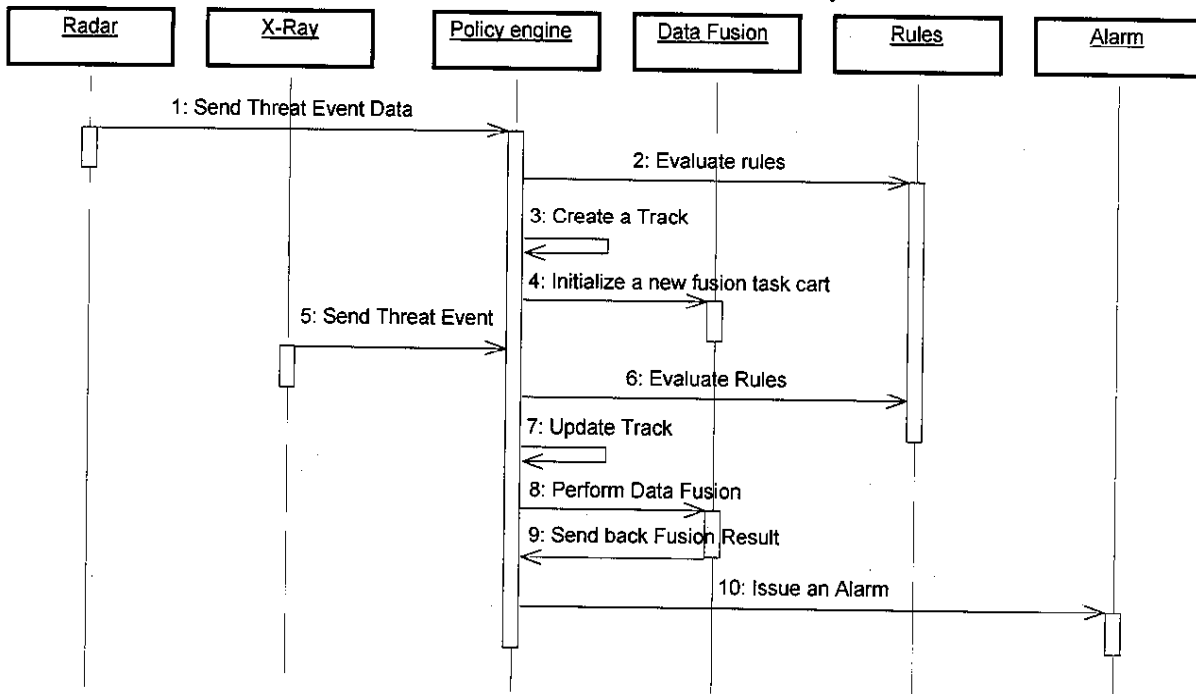
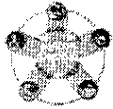


Figure 5-29



5.10.2.2.3 Sequence Diagram 3 – Operator Interaction

The display of BomDetec system allows the operator to issue special commands such as to start tracking on a person. In this case, the command is handled by the Resource Management Module. First, the command is added into the control command list based on its priority. When executing this control command, the Resource Management checks sensor status from the Central Database. If the sensor is ready to receive new commands, the Resource Management module issues the command to the Sensor Unit.

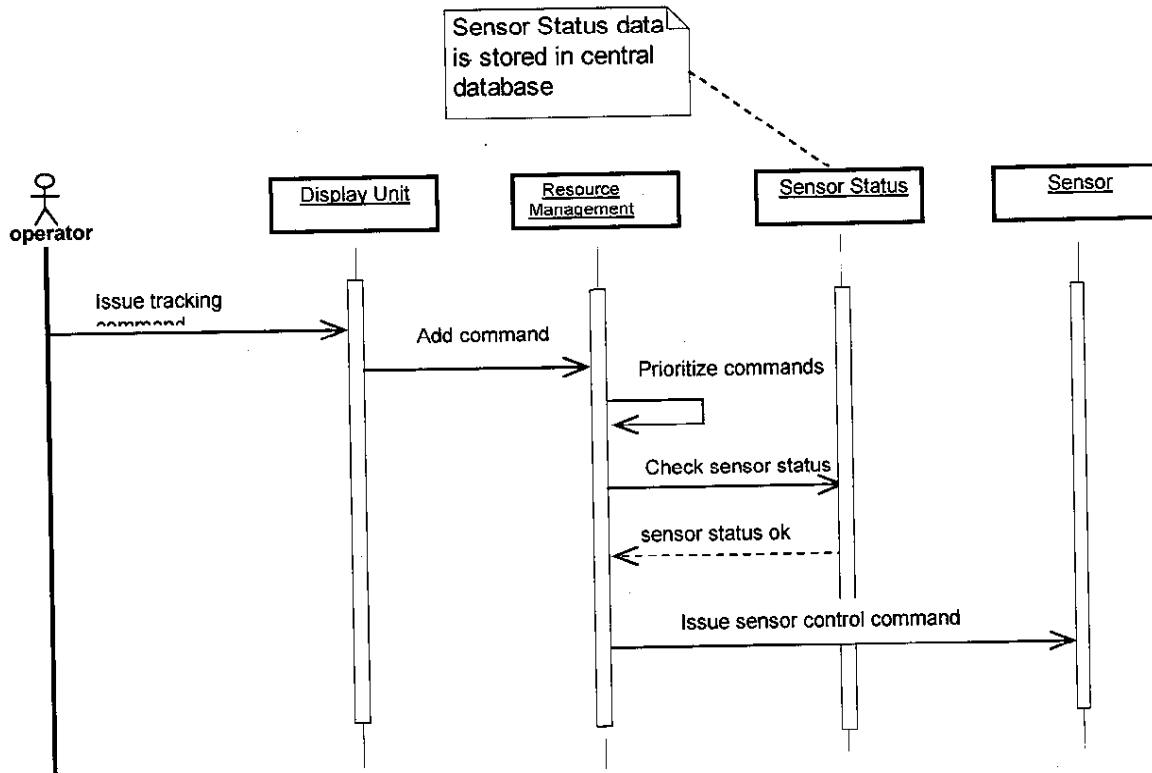
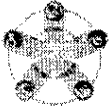


Figure 5-30

5.10.3 ANNEX C – Resource Management: A Dynamic Multi-Modality Sensor Control and Data Fusion Framework for Target Classification

5.10.3.1 Abstract

As described in Section 5, the BomDetec System requires Resource Management. Simulations have clearly shown that operators can not track all the pedestrian traffic, choosing sensor activities, but rather an automated Resource Management System is required. This realization is important for the continuing development of the BomDetec System. This annex provides the theoretical framework for multi-modality sensor management and data fusion for the such a multi-target classification system for BomDetec. To achieve the optimal solution for sensor management in a dynamic environment, the system will dynamically assign and re-assign sensor resources to targets to reduce the ultimate objective function of the system, i.e., the uncertainty of the whole target set. The proposed framework takes into consideration a two-level hierarchical state estimation from a sequence of actions and observations. The



ultimate goal is the higher level state estimation while the lower level state estimation provides so-called "partial information" in varying degrees among those lower level states. The information gain metric has the option to adapt to more complicated situations by introducing a sensor-action cost function and a mutual information weight function, which can be chosen according to the expected practical situation.

5.10.3.2 Introduction

Dynamic Resource Management has become increasingly important in the development and construction of modern multi-sensor system. It occurs in many applications to perform perception activities with constraints of sensor resources.

In a real-time and dynamic multi-events detection and recognition system with multiple sensor modalities, autonomous sensor management becomes a complicated issue. The challenges of the problem can be stated as: it is under highly dynamic environment; there are insufficient sensor resources; there are complicated situation of different modalities with various features; sampling intervals of different modalities are different, need to synchronize; it is a real time detection with limited resources (including computation resource) needs to be considered; it needs to recognize a large number of different kinds of threats, etc.

In a typical application scenario, multiple objects (such as pedestrians) are moving towards a site under surveillance. Among with there will be potential threats. A group of multi-modality sensors are available to measure the various physical properties of each object. Based on the sensor results the system will classify them into, i.e., threats or non-threats. The number of objects is dynamically changing. With limited sensor resources, the application needs to finish the classification task before each of the objects reached the site. Therefore the optimal and dynamic deployment is the core function of the system.

This invention proposes a multi-modality multi-target dynamic sensor management algorithm in a threat detection and identification problem. The framework of dynamic sensor Resource Management has two main iterative processes, namely active sensor selection and dynamic fusion. They are two interactive component processes as shown in Figure 5-31.

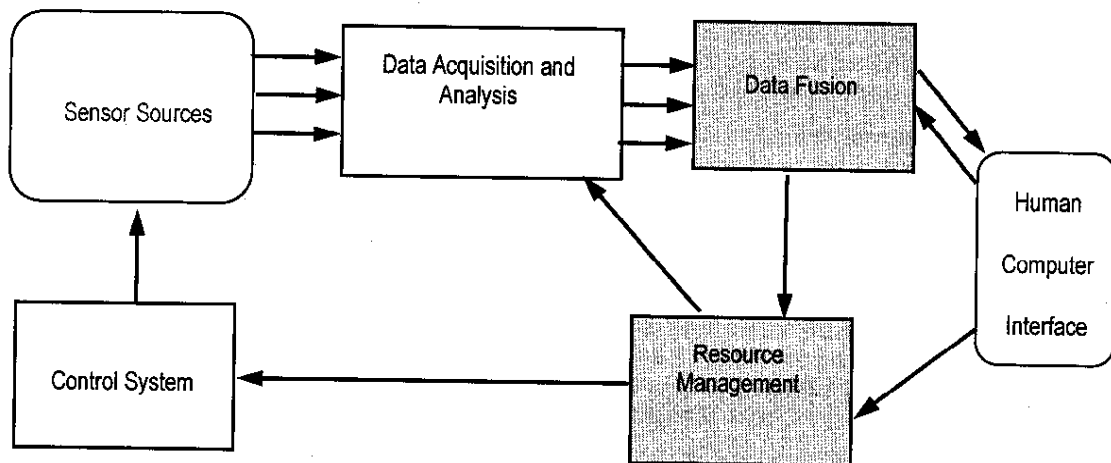


Figure 5-31. General Approach in Sensor Management and Data Fusion

The proposed framework is based on the principle of maximal reduction of target uncertainties with respect to threat detection and identification. A Markov decision process (MDP) model can be utilized as the framework for handling dynamic and uncertain situations. The proposed algorithm takes into account a two-level hierarchical state estimation from a sequence of actions and by making the optimal decision



on the sensing actions with constraints of sensors. The ultimate goal is the higher level state estimation while the lower level state estimation provides so-called "partial information" in varying degrees among those lower level states. The information gain metric has the option to adapt to more complicated situations by introducing a sensor-action cost function and a mutual information weight function, which can be chosen according to the expected practical situation.

5.10.3.3 Proposed Method

The multi-modality sensor system includes a set of information sources (sensors), a sensor selection strategy, a set of observed evidences that responds to the sensor actions, a fusion mechanism, a detection criterion, and a set of events/targets that operators aim to recognize. The framework has two main iterative processes: active sensor selection and dynamic fusion. They are the two interactive component processes that form the process of active sensor management.

Assume for object system i , the K -dimensional state vector is estimated for the recognition of each event (an event is a suspicious threat target, and it will be under consideration). Each component of the state vector is a continuous random variable, and will be understood along time from measurements for each event. We denote the state variable vector as x_{it} , for each target i at time t . Among them, the k^{th} system state component is denoted as x_{it}^k , where $k=1, \dots, K$, $i=1, \dots, N_t$. We assume N_t targets/events at time t ($t=0, 1, \dots, T$), which may vary with time. We derive the distribution of x_{it}^k from its initial uncertainty. For each target/event at time t , the goal is to evaluate the probability of object i being a threat, and that event can be defined as the detection state variable Ω_{it} . Ω_{it} is a discrete random variable whose probability is denoted as $P(\Omega_{it})$.

A sequence of sensor actions is taken to obtain the measurements of targets/events. Action vector a_{it} of target i at time t is defined as $a_{it} = [\alpha_1, \alpha_2, \dots, \alpha_M]^T \in Z^M$, where M is constant indicating the number of modalities in use and α_m is the number of sensors used in the m^{th} type of modalities. If no sensor is assigned to target i , the action vector a_{it} will have all zero components. Typically, in the case of a target being deployed with one sensor, the action vector has one 1 component and all 0s on other components. The cost of the action vector, $C(a_{it})$, is defined as the longest cycle of all its modality components with non-zeros, multiplied by number of its modality components with non-zeros.

Denote o_{it} as the observation vector of target i at time t , which is the result of action a_{it} at time t for target i . Depending on the total number of non-zero components in action a_{it} , the dimension of observation o_{it} is varying. Typically in case of one sensor assignment, the observation o_{it} is with one dimension. Each observation may be related to one or more states and provides updating information to their distribution, which will be discussed later.

In our system, the current state distributions of targets/events are estimated by taking a certain sequence of sensor actions. It can be viewed as a discrete time stochastic process with states x_{it} . The state estimation procedure possesses the property of Markov processes: the conditional probability distribution of future states $x_{i,t+1}$ depends only upon current states $p(x_{i,t})$ and action taken $a_{i,t}$, but not on any past states, i.e., it is conditionally independent of the past states given current states.

With the knowledge from distribution of $x_{i,t}$ and new observation $o_{i,t}$, the distribution of $x_{i,t+1}$ related to $o_{i,t}$ will be updated. This *posteriori* or conditional probability of the current instant will serve as the *a-priori* probability at the next instant. The result of sensor action and estimation is the continuous update of the *a-priori* probability distribution of $x_{i,t}$ and Ω_{it} .

The iterative processes, active sensor selection and dynamic fusion, are briefly introduced as below.



5.10.3.3.1 Active Sensor Selection

By deliberately choosing sensors, active sensing attempts to identify a set of sensors that achieve the optimal trade-off between the benefit and cost of the sensors. The benefit is that the evidence collected from the sensors may provide informative knowledge for the decision-making, e.g., it may change the choice of an optimal action, reduce the uncertainty of the hypothesis state, etc. The cost could include both physical and computational cost.

Therefore, the active sensor selection is an optimization problem. The optimal sensory action set could be a sensory action set that maximizes the benefit given a budget limit or a sensory action set that represents the best trade-off between the benefit and the cost.

5.10.3.3.2 Dynamic Fusion

After deciding the optimal sensory action set, the next step is to fuse the information for further decision-making. In the fusion step, the posterior probability of state is estimated from the evidence collected from the selected sensor sets with the dynamic inference technique. From a Bayesian point of view, the task is to compute the *posteriori* probability $p(state_t | evidence_{1:t}, decision_{t-1})$ from a *priori* probability $p(state_{t-1} | evidence_{1:t-1}, decision_{t-2})$ recursively, where $evidence_{1:t}$ is the set of evidence collected from the activated sensors in the optimal sensor set up to time step t , and $decision_{t-1}$ is the optimal decision at time step $t-1$. Also, $p(evidence_t | state_t)$ is the likelihood, and $p(state_{t-1} | evidence_{1:t-1}, decision_{t-2})$ is previously inferred at time step $t-1$. In our problem, the evidence is what we observe from the sensors, i.e., o_t , and the decision is our optimized sensor action.

5.10.3.4 Proposed Approach Described in Markov Decision Process

In event recognition with respect to threat detection and identification, we assume our goal is to minimize the uncertainty of the detection state variable Ω_t , and we dynamically assign sensor resources to achieve this goal. Since entropy is usually used to describe information uncertainty, the ultimate optimal function can be represented as the minimization of entropy:

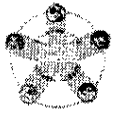
$$\min_{A_{t-1}} H(\Omega_t | O_{t-1}, A_{t-1}),$$

$$\text{subject to } \sum_{i=1}^{N_t} a_{it} \leq c_t, \text{ at each time } t.$$

If we denote Ω_t as the detection state set of all current events, $\Omega_t = \{\Omega_{1t}, \Omega_{2t}, \dots, \Omega_{N_t t}\}$, A_{t-1} as the action sequence before time t , $A_{t-1} = \{a_{t-1}, a_{t-2}, \dots, a_0\}$, and O_{t-1} as the corresponding observation sequence $O_{t-1} = \{o_{t-1}, o_{t-2}, \dots, o_0\}$. The action at time t is a_t which comprises action of each target, a_{it} , $i = 1, \dots, N_t$. The observation o_t is similarly defined.

The initial distribution of all targets are assumed to be uniform, therefore, the above goal is equal to optimize the mutual information of events Ω_t and observation O_{t-1} corresponding to actions A_{t-1} .

$$\max_{A_{t-1}} I(\Omega_t; O_{t-1} | A_{t-1}) = \max_{A_{t-1}} (H(\Omega_0) - H(\Omega_t | O_{t-1}, A_{t-1})) = \min_{A_{t-1}} H(\Omega_t | O_{t-1}, A_{t-1})$$



For each target i , similarly, $A_{i,t-1}$ is denoted as the action sequence before time t ,

$A_{i,t-1} = \{a_{i,t-1}, a_{i,t-2}, \dots, a_{i,0}\}$, and $O_{i,t-1}$ as the corresponding observation sequence

$O_{i,t-1} = \{o_{i,t-1}, o_{i,t-2}, \dots, o_{i,0}\}$.

The maximization of mutual information from the initial time to the current time is considered as maximal incremental gain of information at each time step.

$$\max_{a_t} I(\Omega_t; o_t | a_t) = \max_{a_t} (H(\Omega_t) - H(\Omega_t | o_t, a_t)), \quad \forall t \geq 0$$

When we consider the situation of individual *independent* events, the above mutual information can be the sum of individual mutual information. Events with groups of targets need to consider correlation within groups of targets.

$$\max_{a_t} I(\Omega_t; o_t | a_t) = \max_{a_t} \left(\sum_{i=1}^{N_t} I(\Omega_{ii}; o_{ii} | a_{ii}) \right)$$

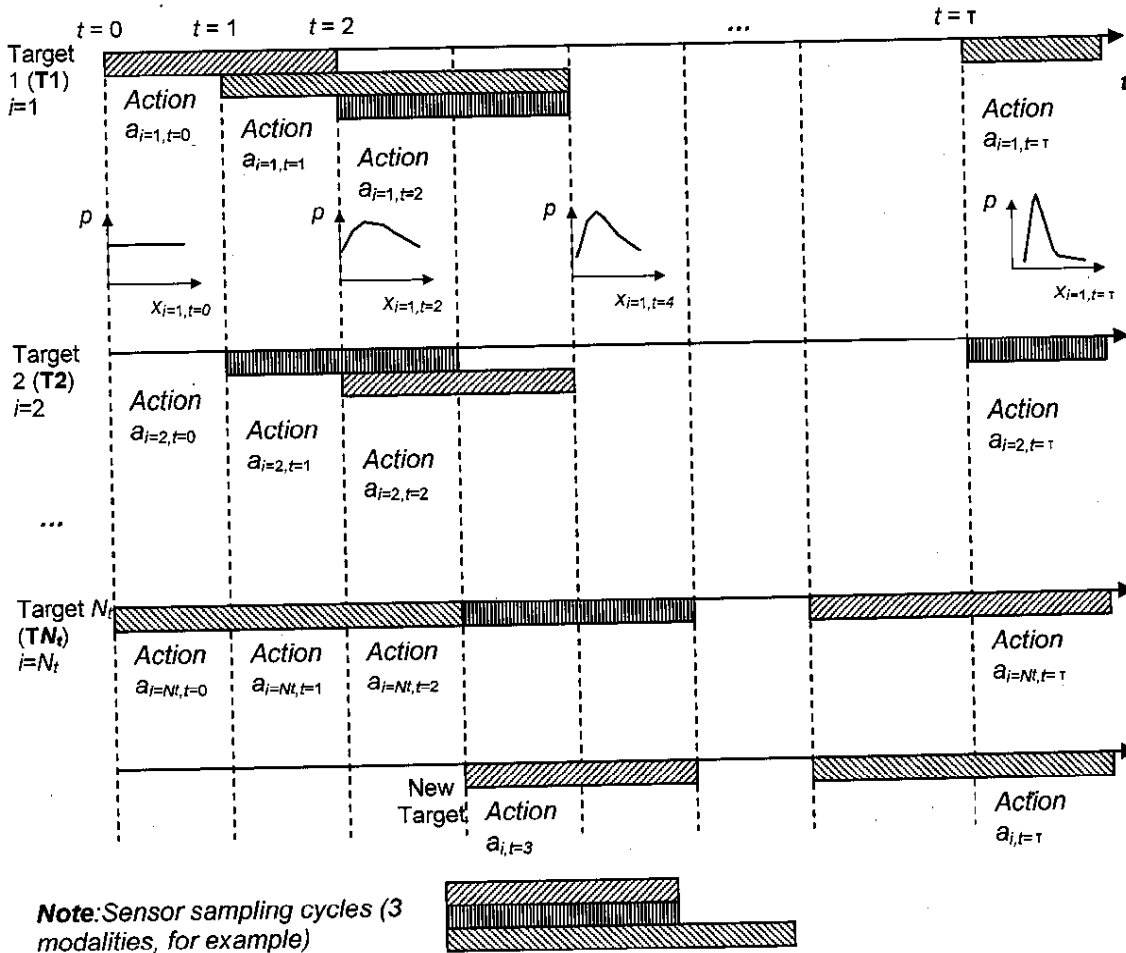


Figure 5-32. Resource Management scheme



Our scheme is to maximize the mutual information gain from the next observation at each time step. Since the sensor acquisition time is different, the unit time information gain is inversely proportional to the sensor action duration, which is defined by the cost function $C(a_{it})$ of each action. Thus our Resource Management method is to solve the optimal action taken at each time t so that the objective function of total mutual information gain rate at time t is maximized.

$$a_t^* = \arg \max_{\substack{a_t = \\ [a_{1t}, a_{2t}, \dots, a_{N_t}]^T}} \sum_{i=1}^{N_t} \frac{u_i(t) I(\Omega_{it}; o_{it} | a_{it})}{C(a_{it})},$$

subject to $\sum_{i=1}^{N_t} a_{it} \leq c_t$ at each time t ,

where $u_i(t)$ is a priority function which is used to give various weights to the information gains according to some rules. In our application, the method prioritizes the uncertainty reduction of targets which are more likely threats than non-threats, although they may have the same uncertainty values.

The time horizon can be divided into stages ($t=0, 1, \dots, T$) with the same intervals. The sensor resources are allotted to the targets once at one time stage. The state vectors of the targets under observation are updated with the dynamic fusion mechanism once the evidences are collected. The whole Resource Management scheme can be illustrated in the following plot.

In the multi-modal detection and recognition system, each target will be understood with multiple state variables. The multi-state variable distribution at time t can be represented as $p(x_{it})$ for target i . By taking sequential actions, the target states can be estimated and reduced uncertainty. Considering each target, the multi-state distribution $p(x_{it})$ is written as follows if assume we have K state components.

$$p(x_{it}) = p(x_{it}^1, x_{it}^2, \dots, x_{it}^k)$$

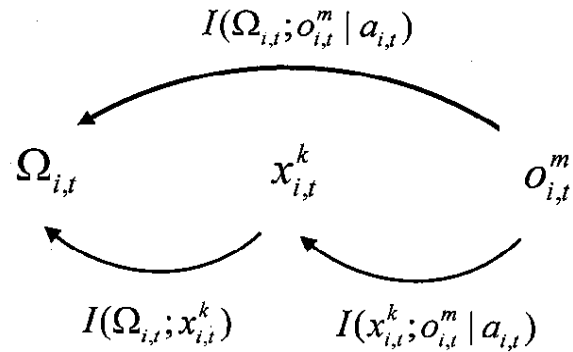
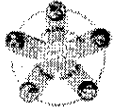


Figure 5-33. Three random variables and related mutual information

The uncertainty of events/targets depends closely on how well we understand the state variables with low variance. It also depends on whether the state variables are in easy discrimination regions determined by threat and non-threat distributions.

The proposed algorithm takes into consideration of a two-level hierarchical state estimation from a sequence of actions and observations. The ultimate goal is the higher level state estimation whereas the lower level state estimation can provide partial useful information in varying degrees among those lower level states. The figure below shows the relationships of the two level states.



On average, uncertainty of the states x_{it} will be reduced when we obtained observations o_{it} , given action a_{it} . It can be represented by the mutual information, $I(x_{it}^k; o_{it}^m | a_{it})$, between x_{it}^k and o_{it}^m . At the same time, uncertainty of the detection state Ω_{it} will also be reduced on average when we obtain a certain state value, x_{it}^k . It can be represented by the mutual information, $I(\Omega_{it}; x_{it}^k)$, between Ω_{it} and x_{it}^k . The mutual information $I(\Omega_{it}; x_{it}^k)$ varies choosing different k , i.e., different components of state x_{it} . In other words, we need to prioritize the state x_{it}^k which contributes most to the detection state estimate. The relationship between $\rho(\Omega_{it})$ and $\rho(x_{it}^k)$ can be illustrated by the above figure.

The optimizer a_i^* can be obtained, if it maximizes the total mutual information gain per cycle between stages of all targets. It is the **active sensor selection** process.

$$a_i^* = \arg \max_{a_i = [a_{i1}, a_{i2}, \dots, a_{iN_t}]^T} \sum_{i=1}^{N_t} \frac{u_i(t) I(\Omega_{it}; o_{it} | a_{it})}{C(a_{it})}$$

Subject to resource constraints at time t ,

$$\sum_{i=1}^{N_t} a_{it} \leq c_t$$

and $\sum_{m=1}^M a_{it}(m) \leq 1$, for $i=1, \dots, N_t$.

If we denote the information gain rate, in terms of cycles, of target i under the assignment $a_{it}(m)$ with nonzero value as G_{im} , the above whole information benefit can be rewritten as

$$a_i^* = \arg \max_{a_i = [a_{i1}, a_{i2}, \dots, a_{iN_t}]^T} \sum_{i=1}^{N_t} \sum_{m=1}^M G_{im} a_{it}(m)$$

where $G_{im} = \frac{u_i(t) I(\Omega_{it}; o_{it} | a_{it})}{C(a_{it})} \Big|_{a_{it}=(0, \dots, 0, 1, 0, \dots, 0)}$, with 1 at the m^{th} position,

where $a_{it}(m)$ is 1 if a sensor in modality m is assigned to target i ; otherwise, $a_{it}(m)$ is 0 if no sensor in modality m is assigned to target i .

The constraints for the above objective function, similarly, can be shown as

$$\sum_{i=1}^{N_t} a_{it}(m) \leq c_t(m), \text{ for } m=1, \dots, M.$$

and $\sum_{m=1}^M a_{it}(m) \leq 1$, for $i=1, \dots, N_t$.



6 BomDetec Phase I Conclusion (NEU, John Beaty)

All of the deliverables for the BomDetec Phase I program have been provided. These include monthly technical and progress reports, a report on laboratory and field evaluation criteria and results for each sensor and the system configuration and design review elements contained in this report. The BomDetec website has archived the material for future reference. This website is username and password protected and available to all members of the team including DHS. The site itself has the web address:

<http://censsis-db3.ece.neu.edu/BombDetec/contract.html>

A concept for flexible hardware and software platforms for the detection of suicide bombers were developed. The hardware platform (American Science & Engineering ZBV) was re-engineered to hold multiple sensors considering their space, power, thermal, and mechanical requirements. Similarly, the integrative software platform (Siemens Corporate Research) was conceptually designed, considering the control, acquisition, interpretation and presentation of the BomDetec sensor data. The base concepts were verified by simulations, paving the way for a ground-up system design in Phase II. This design would accommodate additional and/or different sensors. Each sensor in the initial suite of proposed sensors was evaluated and as appropriate incorporated into Phase II.

At the conclusion of Phase I of the BomDetec program, two observations can be made:

1. It is clear that a multi-sensor approach to the suicide bomber detection issue is the appropriate approach – “there is no silver bullet”. Engineering based on the current system understanding and testing each sensor’s performance will focus R&D in appropriate areas.
2. Likewise, it is clear that building a flexible hardware and software platform to accommodate new sensors in the continuing challenges in a measure-countermeasure environment is also an appropriate approach.

In summary, the conceptual system design work is ready to be started in Phase II of the program and the team is eager to commence this important phase of the effort. The white paper describing this work will be delivered to DHS in mid-November 2007.

This page intentionally left blank.